

# MASTER THESIS

## APPLICABILITY OF THE PUSHOVER METHOD FOR THE SEISMIC ASSESSMENT OF URM STRUCTURES IN GRONINGEN

A CASE STUDY OF A LOW-RISE APARTMENT BUILDING

F.J. (FALKO) NOORTMAN

February 20, 2019





# APPLICABILITY OF THE PUSHOVER METHOD FOR THE SEISMIC ASSESSMENT OF URM STRUCTURES IN GRONINGEN

A CASE STUDY OF A LOW-RISE APARTMENT BUILDING

by

F.J. (FALKO) NOORTMAN

In partial fulfilment of the requirements for the degree of

**Master of Science**  
in Structural Engineering

at the Delft University of Technology  
Faculty of Civil Engineering and Geosciences

Thesis committee: prof. dr. ir. J.G. Rots TU Delft  
dr. ir. K.C. Terwel TU Delft  
dr. F. Messali TU Delft  
ir. F.H. Middelkoop Royal HaskoningDHV





## ABSTRACT

---

In Groningen, seismic activity has increased due to the extraction of gas in the area. A large-scale research campaign has been launched with the aim to assess and safeguard structures in the region. However, an accurate assessment of these buildings turned out to be a challenge, due to the nonlinear behaviour of the masonry and the dynamic nature of a seismic load. A Nonlinear Time History (NLTH) analysis takes into account both these factors, but the computational demand of such a method is considerable. Another method that is widely used to analyse the seismic response of a structure is the Modal Response Spectrum (MRS) method. The computational demand of this method is considerably less compared to NLTH, but nonlinear material behaviour is only taken into account in an indirect manner via a behaviour factor, and the results are considered to be too conservative. A third method is the Nonlinear Pushover (NLPO) method. It takes nonlinear material behaviour into account and compared to NLTH, NLPO is computationally more efficient. Furthermore, an advantage is that it separates capacity from demand. Even though the NLPO method is commonly applied worldwide, its validity still needs to be proven for the Groningen case.

Another aspect which requires attention is the different computational discretisation methods that can be used to execute an NLPO analysis, namely: the Macro Equivalent Frame Method (EFM) and the Continuum Finite Element Method (FEM). Macro EFM models describe the behaviour of piers and spandrels using macro elements, while FEM models start from behaviour at a smaller scale, subdividing piers and spandrels into multiple elements. Macro EFM models are commonly used. However, it is largely debated for which building types the macro EFM method can be applied. One of the building typologies for which the applicability of the NLPO method and EFM are of interest is the low-rise URM apartment building typology. A significant amount of such structures can be found in the province of Groningen, according to ARUP and NAM (2018). Two main objectives are defined based on the aforementioned information which can be described by the following research questions:

- *To what extent can the nonlinear pushover method be used for the seismic assessment of low-rise URM apartment buildings in Groningen?*
- *To what extent is the equivalent frame method applicable as computational discretisation method for the pushover analysis of low-rise URM apartment buildings in Groningen?*

Both objectives were studied by looking into a single case study, consisting of a low-rise URM apartment building. The behaviour of the structure is characterised by a weak and strong direction, in which the weak direction is characterised by a relatively low stiffness and lateral capacity compared to the strong direction. The seismic response of the structure is determined according to the MRS, NLPO and NLTH methods. Furthermore, the NLPO analyses are executed using two different computational discretisation methods, namely continuum FEM and macro EFM. DIANA is used as a FEM solver for the MRS, NLPO and NLTH analyses and 3MURI is used for the EFM model. Moreover, a modal and uniform lateral load pattern are taken into account for the NLPO analyses. The conclusions which are drawn from the case study can generally be applied to low-rise URM apartment buildings in Groningen. However, it must be noted that significant alterations in geometry and building materials might influence the results. Furthermore, modelling assumptions have been applied, and it is important to note that the possible influence of these assumptions, may partially limit the extent of the conclusions. Moreover, several limitations are inherent to the studied methods, and cannot be accounted for somehow.

All analyses are performed by incrementally increasing the seismic load until one of the near collapse limit state criteria according to NPR 9998 is met. Furthermore, three target displacement methods are evaluated: the capacity spectrum method according to NPR 9998, the regular N2-method, included in the Eurocode 8, and an adaptation of the N2-method which is developed specifically for URM structures by Guerrini et al. (2017). The performance of the structure according to each of the methods is studied subsequently, by looking into the force-displacement behaviour, displacement profile and damage at failure, failure mechanisms and the maximum admissible seismic load.

Two significant disadvantages of macro EFM were identified when comparing the results of the NLPO analyses using 3MURI and DIANA. First, the fact that out-of-plane behaviour is not taken into account in 3MURI could significantly influence the behaviour of a structure in terms of base shear capacity, which is especially true when structures are characterised by an extremely low total length of piers in the in-plane direction. Furthermore, DIANA allows for a more gradual softening behaviour, which helps the post-peak force redistribution. As a consequence, the maximum admissible seismic load according to DIANA could be higher. However, despite the two aforementioned disadvantages of the macro EFM method as implemented in 3MURI, all other relevant results of both methods are similar. The fact that the two identified disadvantages of 3MURI can only result in more conservative results, suggests that macro EFM, as implemented in 3MURI, is a suitable computational discretisation method for the seismic assessment according to the NLPO method for low-rise URM apartment buildings in Groningen. However, it should be taken into account that the conservativeness of 3MURI could lead to a significantly larger amount of required retrofitting, in comparison with DIANA.

The applicability of the NLPO method is reviewed by comparing the results of the MRS, NLPO and NLTH methods. Similar behaviour of the structure according to the NLPO and NLTH method was captured, which suggests that the NLPO method is a suitable analysis method for the studied typology. The maximum admissible seismic load using the target displacement method according to NPR 9998 is in-line with the NLTH analysis. However, the governing load case made use of a uniform load pattern, which returns a structural behaviour different than that obtained by NLTH analyses, as can be seen from the force-displacement behaviour as presented in Figure 1. If only the capacity curve according to the modal load pattern would be considered, then the allowable seismic load according to NLTH is similar to that of NLPO using the target displacement method of Eurocode 8. Furthermore, from the results of the case study can be concluded that the choice of target displacement method has a significant influence on the maximum admissible seismic load. For the case study, NPR 9998 is more conservative in the strong direction, and Eurocode 8 is more conservative in the weak direction. Regarding the MRS method, very conservative results were found. A reason that was found for these conservative results is that the prescribed behaviour factor by NPR 9998 is too low for the case study when compared to that derived from the NLPO analysis. However, even with a larger behaviour factor, the results according to the MRS method would still be conservative in the weak direction.

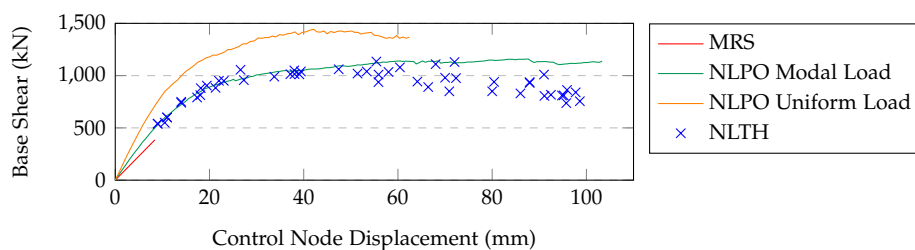


Figure 1: Comparison Force-Displacement Behaviour According to DIANA - Weak Direction



## ACKNOWLEDGEMENTS

---

Undertaking this nine-month long thesis project has been a truly challenging experience which would not have been possible without the support of many people. First of all, I would like to thank my graduation supervisors and committee members Erik Middelkoop, Francesco Messali, Karel Terwel and Jan Rots. I would like to thank Erik Middelkoop for giving me the opportunity to conduct this project at Royal HaskoningDHV, guiding me through my thesis when I faced dead-end trails and answering many of my questions. Furthermore, I would like to thank Karel Terwel for both his practical and academic approach, guidance and critical questions during the meetings, which significantly contributed to the overall process of my work. Next, I would like to thank Francesco Messali for his extensive knowledge on earthquake engineering, computational modelling and the Groningen case in general. Moreover, he was also always available for me to discuss my models, explain several concepts and provide feedback to my work. Ultimately, I would like to thank Jan Rots for inspiring me to write my thesis about the pushover method, his knowledge, guidance and role as chairman of my graduation committee.

Throughout the project, I have been assisted by several colleagues from Royal HaskoningDHV. Their support has been of great value, for which I am grateful. Furthermore, they provided me with a pleasant working environment, which also had a considerable contribution to my work.

A good support system is essential if one wants to succeed with such a complex task as finishing an MSc thesis. I was lucky to be surrounded by friends who made the process a lot easier. Furthermore, I would not have been here without the support of my family. Finally, and most importantly, I wish to thank my girlfriend Daniela for her endless support and encouragement.

*Falko Noortman  
Rotterdam, February 2019*



# TABLE OF CONTENT

---

1	INTRODUCTION	1
1.1	Context of Study	1
1.2	Objectives	2
1.3	Report Structure	3
<b>I LITERATURE STUDY</b>		
2	STRUCTURAL BEHAVIOUR OF URM STRUCTURES	7
2.1	Mechanical Behaviour of Masonry	7
2.2	Behaviour Components of URM Structures	10
2.3	Numerical Modelling Strategies	15
2.4	Material Models	18
3	SEISMIC ANALYSIS METHODS	27
3.1	Modal Response Spectrum	27
3.2	Nonlinear Pushover	32
3.3	Target Displacement Methods	35
3.4	Nonlinear Time History	41
<b>II CASE STUDY</b>		
4	STRATEGY	47
4.1	Building Stock and Typologies Groningen	47
4.2	Characteristics of the Studied Building	49
4.3	Comparison Strategies	53
4.4	Limitations of Case Study	59
5	MODEL AND SETUP	61
5.1	DIANA Continuum FEM Model	61
5.2	3MURI Macro EFM Model	70
5.3	Model Checks	72
<b>III RESULTS</b>		
6	COMPARISON OF PROCEDURES	79
6.1	Comparison Results of Continuum FEM and Macro EFM Analyses	79
6.2	Comparison Results of MRS, NLPO and NLTH Analyses	87
7	CONCLUSIONS	95
7.1	Conclusions	95
7.2	Recommendations	98
<b>IV APPENDICES</b>		
A	DERIVATION EQUATION OF MOTION	101
B	PROCEDURES FOR NONLINEAR ANALYSIS	105
C	DRAWINGS CASE STUDY	109
D	MODEL PROPERTIES	113
E	MASONRY STATE PARAMETER	121
F	RESPONSE SPECTRA	123
G	RESULTS: MODAL RESPONSE SPECTRUM ANALYSIS	127
H	RESULTS: NONLINEAR PUSHOVER ANALYSIS	135
I	RESULTS: NONLINEAR TIME HISTORY ANALYSIS	153

## LIST OF FIGURES

---

Figure 1.1	Seismic Activity versus Reservoir Compaction . . . . .	1
Figure 2.1	Stress-Strain Curves Masonry . . . . .	7
Figure 2.2	Tensional Stress-Strain Curves . . . . .	8
Figure 2.3	Typical Shear Bond Behaviour . . . . .	9
Figure 2.4	Failure Surface for Masonry under Bi-Axial Compressive Stresses . . . . .	9
Figure 2.5	Mechanisms of Lateral Force Resistance . . . . .	10
Figure 2.6	Out-of-Plane Behaviour One-way Spanning Walls . . . . .	12
Figure 2.7	Out-of-Plane Behaviour Two-way Spanning Walls . . . . .	13
Figure 2.8	Influence of Floor Stiffness on Seismic Behaviour Walls . . . . .	13
Figure 2.9	Computational Strategies for Modelling Masonry . . . . .	15
Figure 2.10	Equivalent Frame Method Idealisation . . . . .	16
Figure 2.11	Three-Dimensional Equivalent Frame Model in 3MURI . . . . .	17
Figure 2.12	Tensile Behaviour of Engineering Masonry Model . . . . .	18
Figure 2.13	Flexural Behaviour of Engineering Masonry Model . . . . .	19
Figure 2.14	Shear Behaviour of Engineering Masonry Model . . . . .	20
Figure 2.15	Macro-element used in 3MURI . . . . .	20
Figure 2.16	Scheme Rocking Behaviour . . . . .	21
Figure 2.17	Scheme Shear Sliding . . . . .	22
Figure 2.18	Failure Mode Interaction Surface Contour Graph . . . . .	24
Figure 3.1	Elastic Acceleration Response Spectrum for 1995 Earthquake in Kobe . . . . .	28
Figure 3.2	Example of Design Spectrum . . . . .	28
Figure 3.3	Influence Soil Conditions on Spectrum . . . . .	29
Figure 3.4	Schematic Representation of Pushover Analysis Procedure . . . . .	34
Figure 3.5	Transformation Spectrum to Acceleration-Displacement Format . . . . .	35
Figure 3.6	Stiffness Relation of Equivalent SDF System . . . . .	36
Figure 3.7	Graphical Representation of Target Displacement . . . . .	37
Figure 3.8	Example of a Bi-Linearised Capacity Curve . . . . .	39
Figure 3.9	Capacity Curve Assessment . . . . .	40
Figure 3.10	Variation of Modal Damping Ratios with Natural Frequency . . . . .	43
Figure 3.11	Soil Structure Interaction Representation Methods . . . . .	44
Figure 4.1	Building Classification Steps . . . . .	47
Figure 4.2	Geometric Layout Classification . . . . .	47
Figure 4.3	Structural Layout Classification . . . . .	48
Figure 4.4	Material Walls and Floors Classification . . . . .	48
Figure 4.5	Front View of Building . . . . .	49
Figure 4.6	Top View First Floor . . . . .	50
Figure 5.1	Walls Configuration in DIANA . . . . .	62
Figure 5.2	Nonlinear Line Interfaces on the Fourth Floor . . . . .	62
Figure 5.3	Force-Elongation Behaviour of Anchors . . . . .	63
Figure 5.4	Coordinate System Ribbed Floor . . . . .	63
Figure 5.5	Concrete Beams in DIANA model . . . . .	64
Figure 5.6	Applied Line-Masses in DIANA . . . . .	64
Figure 5.7	Governing Eigenmodes according to DIANA . . . . .	66
Figure 5.8	Foundation Strips and Piles in DIANA . . . . .	67
Figure 5.9	Connection Pile and Foundation Strip . . . . .	68
Figure 5.10	Soil-Block and Soil-Column in DIANA . . . . .	68
Figure 5.11	Walls Configuration in 3MURI . . . . .	70
Figure 5.12	Equivalent loads in 3MURI . . . . .	71

Figure 5.13	Governing Eigenmodes according to DIANA . . . . .	72
Figure 5.14	Governing Eigenmodes according to 3MURI . . . . .	73
Figure 5.15	Shape Governing Eigenmode per Load Case . . . . .	73
Figure 5.16	Deformations according to DIANA . . . . .	74
Figure 5.17	Internal Distributed Forces according to DIANA . . . . .	75
Figure 5.18	Wall Numbering System . . . . .	76
Figure 6.1	Shape Governing Eigenmode per Load Case . . . . .	81
Figure 6.2	Pushover Curves . . . . .	81
Figure 6.3	Comparison Material Model DIANA and 3MURI . . . . .	83
Figure 6.4	Displacement Profile . . . . .	84
Figure 6.5	Comparison Force-Displacement Behaviour - Longitudinal Direction . . . . .	87
Figure 6.6	Comparison Force-Displacement Behaviour - Transverse Direction . . . . .	88
Figure 6.7	Comparison Inter-Story Drifts at Failure . . . . .	90
Figure 6.8	Crack Widths at Failure - Wall L1, L2, L3, L4, L5 & L6 . . . . .	90
Figure 7.1	Walls Configuration in DIANA . . . . .	95
Figure 7.2	Comparison Force-Displacement Behaviour According to DIANA - Longitudinal Direction . . . . .	96
Figure A.1	Single Degree of Freedom System . . . . .	101
Figure B.1	Commonly used Iteration Methods . . . . .	106
Figure C.1	Top View Ground Floor . . . . .	109
Figure C.2	Front View - Section AA . . . . .	110
Figure C.3	Side View - Section BB . . . . .	111
Figure D.1	Equivalent loads in 3MURI . . . . .	118
Figure E.1	Numbered Stress-Strain Curve . . . . .	121
Figure E.2	Numbered Shear Stress-Strain Curve . . . . .	122
Figure F.1	Response Spectra Derived from NLTH Analyses . . . . .	123
Figure F.2	Outer Envelope of Derived Response Spectra . . . . .	123
Figure F.3	Influence Non Linear Soil Properties on Response Spectrum . . . . .	124
Figure F.4	Comparison Real and Scaled Spectrum for $PGA = 0.39 g$ . . . . .	125
Figure G.1	Response Spectra derived from NLTH analyses . . . . .	128
Figure G.2	Governing Modes Part of DIANA Model . . . . .	128
Figure G.3	Cumulative Modal Mass Participation . . . . .	129
Figure G.4	Wall Numbering . . . . .	130
Figure G.5	Distributed Forces - Transverse Direction - Wall T2 . . . . .	130
Figure G.6	Distributed Forces - Longitudinal Direction - Wall L2 . . . . .	133
Figure H.1	Pushover Curves . . . . .	135
Figure H.2	Example Transformation Capacity Curve . . . . .	138
Figure H.3	Bi-Linearisation of Equivalent SDoF Pushover Curve . . . . .	138
Figure H.4	Comparison Capacity and Demand according to NPR 9998 . . . . .	139
Figure H.5	Comparison Capacity and Demand according to Eurocode 8 . . . . .	141
Figure H.6	Comparison Capacity and Demand according to Guerrini . . . . .	142
Figure H.7	Maximum Inter-Story Drift vs Control Node Displacement . . . . .	145
Figure H.8	Displacement Profile . . . . .	146
Figure H.9	Interstory Drift per Floor at Failure . . . . .	146
Figure H.10	Wall Numbering . . . . .	147
Figure H.11	DIANA Damage Parameters at Failure - Uniform Load Distribution . . . . .	148
Figure H.12	3MURI Damage Parameter at Failure - Uniform Load Distribution . . . . .	148
Figure H.13	DIANA Damage Parameters at Failure - Modal Load Distribution . . . . .	149
Figure H.14	3MURI Damage Parameter at Failure - Modal Load Distribution . . . . .	149
Figure H.15	DIANA Damage Parameters at Failure - Uniform Load Distribution . . . . .	150
Figure H.16	3MURI Damage Parameters at Failure - Uniform Load Distribution . . . . .	150
Figure H.17	DIANA Damage Parameters at Failure - Modal Load Distribution . . . . .	151
Figure H.18	3MURI Damage Parameter at Failure - Modal Load Distribution . . . . .	151

Figure I.1	Incremental Dynamic Analysis Curve . . . . .	153
Figure I.2	Maximum Inter-Story Drift during IDA . . . . .	154
Figure I.3	Hysteresis Plots for Signal 2 . . . . .	155
Figure I.4	Capacity Curves according NLTH Analyses . . . . .	155
Figure I.5	Displacement Profile at Exceedance of NC Limit State Criteria . . . . .	156
Figure I.6	Inter-Story Drifts at Exceedance of NC Limit State Criteria . . . . .	156
Figure I.7	Roof Displacement for Signal 2 (PGA = 0.26) . . . . .	157
Figure I.8	Normalised Displacement Profile at Studied Time Steps . . . . .	157
Figure I.9	Damage Parameters at Failure - Signal 2 (PGA = 0.26) - $t = 2.48$ s . . . . .	158
Figure I.10	Damage Parameters at Failure - Signal 2 (PGA = 0.26) - $t = 2.95$ s . . . . .	159
Figure I.11	Crack Widths - Signal 2 (PGA = 0.26) - $t = 10.50$ s . . . . .	159

## LIST OF TABLES

---

Table 1.1	Overview Studied Analysis Methods . . . . .	2
Table 3.1	Calibrated Parameters for Proposed Equation . . . . .	38
Table 4.1	Overview Materials Building . . . . .	51
Table 4.2	Representative Soil Composition . . . . .	51
Table 4.3	Overview Additional Permanent and Variable Loads . . . . .	52
Table 4.4	Limit State Criteria per Analysis Type . . . . .	54
Table 4.5	Values of $\gamma_n$ according to NPR 9998:2018 . . . . .	56
Table 4.6	Differences in Seismic Analysis Methods . . . . .	57
Table 5.1	MRS Analysis Parameters . . . . .	65
Table 5.2	NLPO Analysis Parameters . . . . .	67
Table 5.3	NLTH Analysis Parameters . . . . .	69
Table 5.4	Equivalent Loads in 3MURI . . . . .	71
Table 5.5	Surface Loads in 3MURI . . . . .	72
Table 5.6	Mass of Structure according to DIANA and 3MURI . . . . .	75
Table 5.7	Internal Load Distribution . . . . .	76
Table 6.1	Mass of Structure according to DIANA and 3MURI . . . . .	79
Table 6.2	Participating Modal Mass of the Governing Eigenmodes . . . . .	80
Table 6.3	Natural Period of the Governing Eigenmodes . . . . .	80
Table 6.4	Overview Characteristics Capacity Curves . . . . .	82
Table 6.5	Maximum Admissible Seismic Load according to the NLPO Method . . . . .	85
Table 6.6	Maximum Admissible Seismic Load according to Codes . . . . .	91
Table 6.7	Behaviour Factor according to NLPO Analysis . . . . .	92
Table 6.8	Maximum Admissible Seismic Load when Neglecting Uniform Load Pattern for NLPO . . . . .	93
Table 7.1	Maximum Admissible Seismic Load according to Codes . . . . .	97
Table D.1	Material Properties Masonry - Nonlinear DIANA Model . . . . .	113
Table D.2	Concrete Material Properties - Nonlinear DIANA Model . . . . .	114
Table D.3	Material Properties Ribbed Floor - Nonlinear DIANA model . . . . .	114
Table D.4	Material Properties Foundation Piles - Nonlinear DIANA Model . . . . .	114
Table D.5	Material Properties Nonlinear Interface Elements - Nonlinear DI- ANA Model . . . . .	115
Table D.6	Applied Densities in DIANA . . . . .	115
Table D.7	Material Properties Masonry - Linear DIANA Model . . . . .	116
Table D.8	Material Properties Interface Elements - Linear DIANA Model . . . . .	116
Table D.9	Material Properties Masonry - 3MURI Model . . . . .	117

Table D.10	Material Properties Dummy Walls - 3MURI Model . . . . .	117
Table D.11	Material Properties Concrete - 3MURI Model . . . . .	117
Table D.12	Material Properties Ribbed Floor - 3MURI . . . . .	118
Table D.13	Equivalent Loads acting on the Ground Floor . . . . .	119
Table D.14	Equivalent Loads acting on Floor 2,3 and 4 . . . . .	119
Table D.15	Equivalent Loads acting on the Roof . . . . .	119
Table E.1	Definition of Head and Bed Joint Failure Status Parameter . . . . .	121
Table E.2	Definition of Shear Failure Status Parameter . . . . .	122
Table G.1	Calculation of Parameters for Location-Specific Spectrum . . . . .	127
Table G.2	Properties Pier 4th Floor Part A . . . . .	131
Table G.3	Design Checks MRS - Wall T2 . . . . .	132
Table G.4	Design Checks MRS - Wall L1 . . . . .	133
Table H.1	Overview Characteristics Capacity Curves . . . . .	136
Table H.2	Overview Mass per Floor . . . . .	137
Table H.3	Example Effective Mass Calculation . . . . .	137
Table H.4	Effective Mass and Transformation Factor per Load Case . . . . .	137
Table H.5	Maximum Admissible Seismic Load according to 0.6 % Drift Limit .	143
Table H.6	Maximum Admissible Seismic Load according to 1.5 % Drift Limit .	143
Table H.7	Natural Periods of Idealized Equivalent SDoF System . . . . .	144
Table I.1	Maximum Admissible Seismic Load according to NLTH Method . .	154

## LIST OF ACRONYMS

---

ADRS	Acceleration Displacement Response Spectrum
DI	Dynamic Instability
DL	Drift Limit
IDA	Incremental Dynamic Analysis
MDoF	Multiple Degree of Freedom
MRS	Modal Response Spectrum
NAM	Nederlandse Aardolie Maatschappij
NC	Near Collapse
NLKA	Nonlinear Kinematic Analysis
NLPO	Nonlinear Pushover
NLTH	Nonlinear Time History
PGA	Peak Ground Acceleration
SD	Strength Degradation
SDoF	Single Degree of Freedom
SSI	Soil Structure Interaction
UC	Unity Check
URM	Unreinforced Masonry

# NOMENCLATURE

---

## GREEK SYMBOLS

$\alpha_{comp}$	Maximum Occurred Strain
$\epsilon$	Strain
$\epsilon$	Convergence Criterion
$\gamma$	Shear Strain
$\Gamma$	Transformation Factor
$\kappa$	Compressive Strength Reduction Factor
$\kappa$	Ratio between Horizontal and Vertical Force
$\lambda$	Slenderness
$\lambda$	Unloading Factor
$\mu$	Friction Coefficient
$\mu$	Ductility Factor
$\omega_n$	Natural Frequency
$\rho$	Correlation Coefficient
$\sigma$	Axial Stress
$\sigma_{rf}$	Maximum Occurred Stress
$\phi$	Friction Angle
$\tau_{max}$	Shear Strength
$\zeta$	Viscous Damping
$\zeta$	Damping Ratio

## LOWERCASE SYMBOLS

$a_0$	Mass Proportional Damping Coefficient
$a_1$	Stiffness Proportional Damping Coefficient
$c$	Cohesion
$d$	Width Compressive Zone
$d_t$	Target Displacement
$d_r$	Inter-Story Drift
$e$	Eccentricity
$f_c$	Compressive Strength
$f_t$	Tensile Strength
$f_{tu}$	Tensile Strength Unit
$f_{cmo}$	Mean shear Strength
$f_{vd}$	Allowable Shear Stress
$f_{v,lim}$	Shear Strength Limit
$h$	Crack Bandwidth
$k$	Spring Stiffness
$k_{1d}$	Compressive Zone Coefficient
$k_{1r}$	Ratio Effective Height and Width

$k_{1s}$	Slenderness Coefficient
$k_{2r}$	Ductility Coefficient
$l_c$	Effective Length
$m$	Mass
$q$	Behaviour Factor
$r_p$	Peak Modal Response
$S_d$	Design Spectrum
$S_e$	Elastic Response Spectrum
$S_{ead}$	Elastic Acceleration Displacement Response Spectrum
$S_{MS}$	Design Acceleration in the Short Period Range
$S_{M1}$	Design Acceleration in the Long Period Range
$S_{nlad}$	Nonlinear Acceleration Displacement Response Spectrum
$S_{ve}$	Elastic Vertical Ground Acceleration Response Spectrum
$t$	Thickness
$u_g$	Ground Accelerations
$x$	Displacement
$\dot{x}$	Velocity
$\ddot{x}$	Acceleration

## UPPERCASE SYMBOLS

$D$	Width
$E$	Young's Modulus
$E_d$	Design Load
$E_d$	Characteristic Load
$G$	Shear Modulus
$G_{fc}$	Compressive Crack Energy
$G_{fs}$	Shear Crack Energy
$G_{ft}$	Tensile Crack Energy
$H$	Height
$I$	Moment of Inertia
$M$	Bending Moment
$N$	Axial Force
$R_d$	Design Resistance
$T_c$	Corner Period
$T_n$	Natural Period
$V$	Shear Force
$V_b$	Base Shear

## INTRODUCTION

### 1.1 CONTEXT OF STUDY

One of the richest gas fields in Europe can be found in Groningen, a province located in the north of the Netherlands. A Dutch petroleum company, the Nederlandse Aardolie Maatschappij (NAM), started extracting gas from the field in 1963. This extraction of gas resulted in depletion of the pressure within the reservoir causing the reservoir to compact. This compaction increases the friction in pre-existing faults, and this friction can lead to seismic activity. In Figure 1.1 can be seen that higher magnitude earthquakes occur for a bigger reservoir contraction. From this figure can also be seen that the magnitude of the earthquakes increases by time and Muntendam-Bos and de Waal (2013) concluded that the risk of even higher magnitude increases if the gas extraction continues. Even though the earthquakes are of a relatively low magnitude, some caused considerable damage to the affected buildings, because these buildings were not designed to withstand a seismic load.

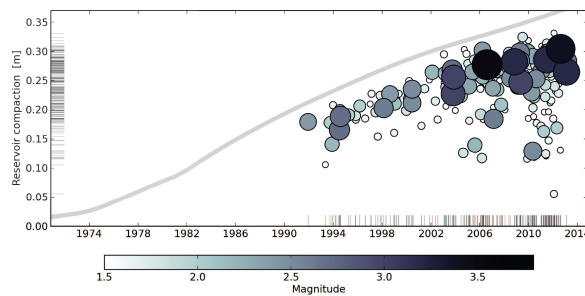


Figure 1.1: Seismic Activity versus Reservoir Compaction.  
Source: Bourne and Oates (2014)

VIA Groningen, a collaboration between the companies Royal HaskoningDHV and Visser & Smit Bouw, was commissioned to analyse the seismic capacity of these masonry structures and provide retrofitting measures where necessary. However, an accurate assessment of these buildings turned out to be a challenge, due to the nonlinear behaviour of the masonry and the dynamic nature of a seismic load. A Nonlinear Time History (NLTH) analysis takes into account both these factors, but the computational demand of such a method is considerable. Another method that is widely used to analyse the seismic response of a structure is the Modal Response Spectrum (MRS) method. The computational demand of this method is considerably less compared to NLTH, but nonlinear material behaviour is only taken into account in an indirect manner via a behaviour factor, and the results are considered to be too conservative. A third method is the Nonlinear Pushover (NLPO) method. It takes nonlinear material behaviour into account and applies an equivalent lateral load pattern in a quasi-static fashion, producing a capacity curve which is subsequently compared to a demand in terms of an acceleration-displacement response spectrum. Compared to NLTH, NLPO is computationally more efficient, and an advantage is that it separates capacity from demand. Even though the NLPO method is commonly applied worldwide, its validity still needs to be proven for the Groningen case. Aspects which differ the Groningen case from other areas in the world are the type of earthquakes, namely shallow short duration earthquakes, and the fact that the structures were not designed to withstand seismic loads. A comparison between the different procedures is required, to gain insight about which method is the most applicable in the various cases that can be found in Groningen.

One of the building typologies for which the applicability of the NLPO method and macro EFM are of interest is the low-rise unreinforced masonry (URM) apartment building typology. A significant amount of such structures can be found in the province of Groningen, according to ARUP and NAM (2018). The NLPO method is an analysis method that could be considered for such buildings because the structures are of considerable size, which makes an NLTH analysis time-consuming. Furthermore, the NLPO method is found to be less conservative than the MRS method. Thus, especially for structures of a considerable size, it is possible to reduce the amount of required retrofitting significantly when applying the NLPO method, compared to the MRS method. Moreover, the stiffness of the low rise apartment blocks is often of a different magnitude in the longitudinal and transverse direction. Thus a study of such a structure is deemed useful, to see in what extent the NLPO method is applicable in a relatively weak and relatively strong direction of the building.

Another aspect which requires attention is the different computational discretisation methods that can be used to execute an NLPO analysis, namely: the Macro Equivalent Frame Method (EFM) and the Continuum Finite Element Method (FEM). Macro EFM models describe the behaviour of piers and spandrels using macro elements, while continuum FEM models start from behaviour at a smaller scale, subdividing piers and spandrels into multiple elements. Macro EFM models are commonly used. However, it is largely debated for which building types the macro EFM method can be applied. Especially the applicability of macro EFM on complex structures is under discussion. Continuum FEM models are commonly used for MRS, NLPO and NLTH, but such models require a considerable computational effort, compared to EFM, as stated by Siano et al. (2017). A comparison between the continuum FEM and macro EFM is deemed useful.

## 1.2 OBJECTIVES

Two main objectives are clarified in this report which can be described by the following research questions:

- *To what extent can the nonlinear pushover method be used for the seismic assessment of low-rise URM apartment buildings in Groningen?*
- *To what extent is the equivalent frame method applicable as computational discretisation method for the pushover analysis of low-rise URM apartment buildings in Groningen?*

Both objectives are studied by looking into a single case study, which a low-rise URM apartment building. All research is based on the Groningen case, taken into account conventional structures, soil properties and seismic activity in the area. All analyses are performed according to the methodology as described in NPR 9998:2018. An overview of the studied methods is shown in Table 1.1.

Table 1.1: Overview Studied Analysis Methods

	MRS	NLPO	NLTH
Continuum FEM	✓	✓	✓
Macro EFM	X	✓	X

### 1.3 REPORT STRUCTURE

The content of this report is divided into three parts: Literature Study, Case Study and Results. A short elaboration of the subject-matter of each of the parts is presented hereafter.

#### LITERATURE STUDY

An extensive literature review is preliminarily executed to provide the reader with an overview of the existing knowledge of the seismic behaviour of unreinforced masonry structures. First, the material behaviour of masonry and failure mechanisms of URM structures are elaborated. Computational strategies for modelling the aforementioned material properties and failure modes are described secondly. Two different computational discretisation methods are studied: the continuum finite element method and the macro equivalent frame method. The material models which are applied in the case study for these computational discretisation methods are elaborated subsequently, which is the engineering masonry model for the continuum FEM model and the 3MURI macro element model for EFM. The last step of the literature study is to elucidate the commonly used analysis methods for determining the seismic response of a structure. These studied methods are the MRS, NLPO and NLTH method. Furthermore, three target displacement methods are evaluated: the capacity spectrum method according to NPR 9998, the regular N2-method, included in the Eurocode 8, and an adaptation of the N2 which is developed specifically for URM structures by Guerrini et al. (2017)

#### CASE STUDY

The second part of this reports consists of a description of the case study. The goal of the case study is to acquire results, which are used to achieve the aforementioned main objectives of this study. First, the building stock in Groningen is studied, and these buildings are subdivided based on their typology. A structure is chosen afterwards, based on the prerequisites for a pushover analysis and the building stock in Groningen. Second, comparison methods are prescribed on how the conclusions can be drawn based on the results of the studied analyses. Furthermore, the limitations of the strategy are also presented. The last step of this part is a description of the model set-up in DIANA and 3MURI. It should be noted that an NLTH analysis has already been performed of the studied structure by an engineer within Royal HaskoningDHV. The model used for this analysis is used as a basis for all performed analysis in DIANA. It is mentioned in the report which parts of the case study are not the work of the author of this document. Ultimately, several model checks are presented of the DIANA and 3MURI model.

#### RESULTS

The third part is comprised of the comparison of the procedures and the conclusions which are drawn based on the results. First, a comparison between the equivalent frame method and the continuum finite element method as a computational discretisation method for the NLPO method is presented. Second, the output of the analyses is used for the evaluation and comparison of the different methods for analysing the seismic response of a low-rise URM apartment building. Ultimately, the conclusions, discussion and recommendations for further research are presented.

#### APPENDICES

All chapters which can be found in the appendices fulfil a supporting role for this study. It is not required to read the appendices to understand the synopsis of this report, but clarifications of the methodologies and conclusions can be found. However, it should be noted that the chapters related to the response spectra and the results of the studied analyses are of vital importance for this study.



Part I

LITERATURE STUDY



## STRUCTURAL BEHAVIOUR OF URM STRUCTURES

This chapter provides an overview of the existing knowledge of the structural behaviour of unreinforced masonry (URM) structures. The mechanical behaviour of masonry is elaborated first, where the attention first lies with the behaviour on a micro level. The step is made afterwards to the behaviour on a macro level. This means that the mechanical properties of the components of masonry are elaborated first, and the composite behaviour of the masonry is presented subsequently. This composite behaviour in its part is linked to the local and global failure mechanisms of URM structures. The failure mechanisms are divided over in-plane and out-of-plane behaviour. Computational strategies for modelling the aforementioned material properties and failure modes are described afterwards. Two different computational discretisation methods are presented: the continuum finite element method and the macro equivalent frame method.

### 2.1 MECHANICAL BEHAVIOUR OF MASONRY

URM structures are made out of brick units which are connected by mortar joints. The behaviour of a masonry structure strongly depends on the type of brick, the composition of the mortar, the dimensions of the bricks and the way bricks are assembled as formulated by Mosalam et al. (2009). In general, the behaviour of brick and mortar is quite similar. Both perform sufficiently well under compression, but their tensional capacity is considerably lower. Typical stress-strain plots for a masonry material are shown in Figure 2.1.

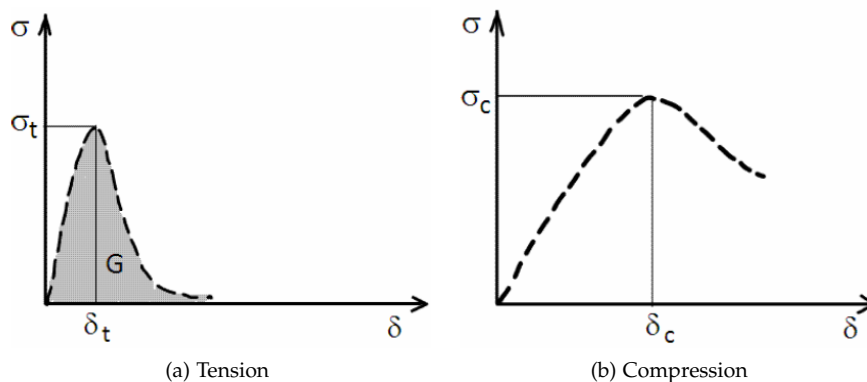


Figure 2.1: Stress-Strain Curves Masonry.  
Source: Angelillo et al. (2014)

It should be noted that the graphs are only qualitative since usually the values of the tensile strength  $\sigma_t$  and the compressive strength  $\sigma_c$  differ by at least one order of magnitude. Angelillo et al. (2014) states that the ratio between the compressive and tensile strength is usually larger than ten, but it could be as big as a hundred. It is difficult to relate the tensile strength of the masonry units to its compressive strength, due to the ratio being influenced by its shape, material, manufacture process and volume of perforations. The behaviour of masonry due to a compression, tension or shear load is described in the following sections, where the distinction is made in its capacity due to an in-plane or out-of-plane load. This distinction has to be made, due to the anisotropic behaviour of masonry caused by the geometry of the joints.

## 2.1.1 COMPRESSIVE BEHAVIOUR

Masonry behaves essentially as an elastic material in compression up to approximately ninety per cent of its strength. Micro-cracks are developing during this elastic phase, but the deformations return to their initial stage after unloading. After this elastic phase, the material behaviour becomes inelastic where the deformations become irreversible. The material shows hardening after some initial crushing. Loading the material beyond its compressive strength leads to a parabolic softening curve. The compressive strength in the direction normal to the bed joint is regarded to be the most relevant structural material property. Thus extensive research on the determine the compressive strength in this direction has been performed. It is commonly accepted that a RILEM test can be performed to determine this strength. A description of this method is elaborated by Wesche and Ilantzis (1980). Compression tests in the direction parallel to the bed joints have received less attention. Tests from Hoffmann and Schubert (1994) show that the ratio between the compressive strength parallel and normal to the bed joints range from 0.2 to 0.8.

## 2.1.2 TENSILE BEHAVIOUR

The tensile behaviour of masonry can also be divided into two phases, as was done for its compressive behaviour. An elasto-plastic phase occurs first until the tensile strength  $\sigma_t$  of the masonry is reached. After this phase, the micro-cracks start to develop into macro-cracks. Due to this, softening behaviour can be observed around the fracture zone. This results in a decrease of the mechanical strength under a continuous increase of the deformation, according to Angelillo et al. (2014). Research has been performed on the tensile capacity parallel to the bed joints by Backes (1985). The distinction can be made between two types of failure, depending on the material properties of the joints and units, see Figure 2.2. The first type of failure (a) occurs with a stepped crack through the head and bed joints. The second type (b) of failure occurs trough head joints and units vertically. Failure due to a perpendicular tensile load is generally caused due to a low tensile bond strength between the mortar and the unit. Tests have also been performed by van der Pluijm (1992) to study the tensile failure behaviour. The focus of these tests was to study the tensile bond strength and the fracture energy. These tests showed an exponential tension softening curve with a fracture energy ranging from 0.005 to 0.02 Nmm/mm<sup>2</sup>. The tensile bond strength ranged from 0.3 to 0.9 Nmm/mm<sup>2</sup>. Tensile failure between mortar and brick units is called Mode I failure.

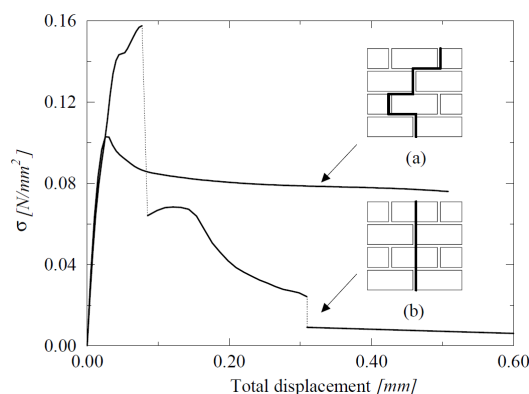


Figure 2.2: Tensional Stress-Strain Curves.  
Source: Backes (1985)

## 2.1.3 SHEAR BEHAVIOUR

Shear behaviour of masonry is directly correlated to the properties of mortar and the roughness of the connection with the bricks. Borri and Maria (2012) found that the shear resistance of masonry elements is linearly proportional to the tensile strength of the mortar parallel to the bed joints. Tests to study the shear behaviour of URM structures have been performed by van der Pluijm (1993). The shear stress on a masonry wall was incrementally increased during these, while the compressive stresses were kept constant. Three different compressive stresses have been studied, as shown in Figure 2.3. From the diagram can be concluded that higher compressive stresses result in higher maximum shear stresses and shear fracture energies. The fracture energy ranges from 0.01 to 0.25 Nmm/mm<sup>2</sup>. This type of failure is called Mode II failure.

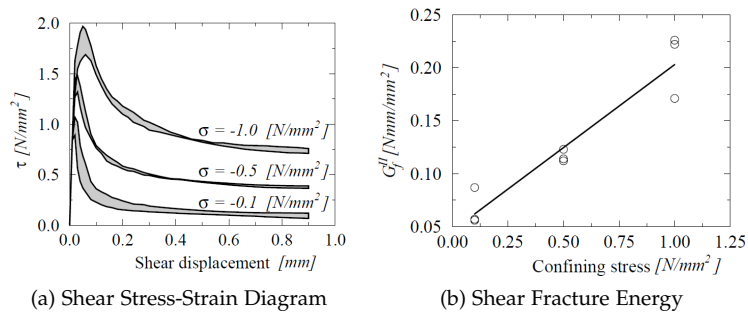


Figure 2.3: Typical Shear Bond Behaviour.  
Source: van der Pluijm (1993)

## 2.1.4 BI-AXIAL BEHAVIOUR

The bi-axial behaviour cannot be completely described from the aforementioned uniaxial loading conditions, according to Lourenço (2017). The behaviour of masonry cannot be defined by the principal stresses only, but the orientation of the units with respect to the principal stresses has to be taken into account. Tests were performed by Page (1982), on masonry walls where not only the magnitude of the principal stresses was varied, but also the orientation of the units with respect to the principal stresses. The failure surface which was determined after one of these tests is shown in Figure 2.4. The first point of interest from this figure is that the compressive capacity in a direction increases if a compressive stress is applied perpendicular to the direction in which the capacity is determined. Another point of interest is that the compressive capacity strongly depends on the direction of the principal stresses with respect to the orientation of the joints.

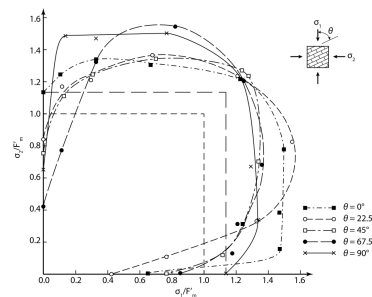


Figure 2.4: Failure Surface for Masonry under Bi-Axial Compressive Stresses.  
Source: Page (1981)

## 2.2 BEHAVIOUR COMPONENTS OF URM STRUCTURES

The local failure mechanisms which can occur due to a seismic load acting on URM structures are elaborated hereafter. The components of a URM structure which are presented are the walls and floors. The distinction is made between in-plane and out-of-plane failure concerning the walls. Failure of the foundation is not taken into account in this study.

### 2.2.1 IN-PLANE FAILURE

Three different in-plane failure mechanisms can occur in URM walls according to Angelillo et al. (2014) and Petrovčič and Kilar (2013): diagonal cracking, shear sliding and rocking. These failure modes are illustrated in Figure 2.5. Diagonal cracking and shear sliding are failure modes caused by the shear behaviour of a wall and rocking is caused by its flexural behaviour. The occurrence of the different failure modes depends on the geometry of the pier, boundary conditions, axial load, mechanical properties of the masonry and geometrical characteristics of the masonry. Several experimental tests have been performed to find the relation between the different failure modes and the aforementioned parameters. In general, it has been concluded that rocking tends to occur in slender piers, shear sliding in squat piers and diagonal cracking tends to occur in moderately slender piers, as described by Magenes and Calvi (1992) and Mahmoud et al. (1995).

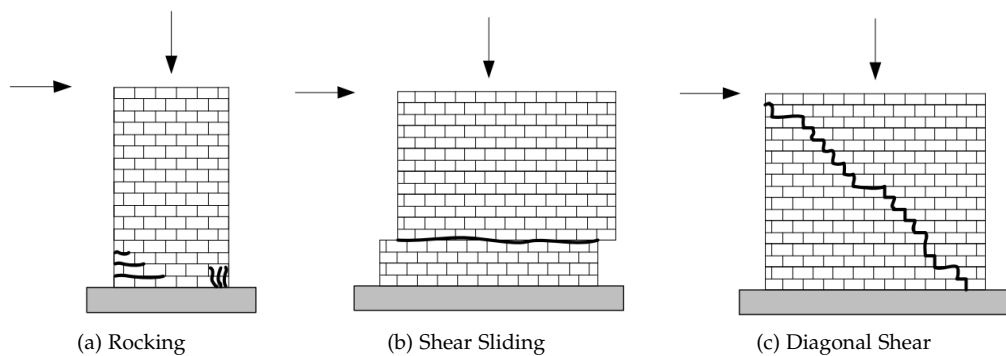


Figure 2.5: Mechanisms of Lateral Force Resistance.

Source: Source: Messali (2015)

### SHEAR CAPACITY

Two failure modes are related to the shear behaviour of a masonry wall: diagonal cracking and shear sliding. Diagonal cracking is the result of several interacting factors, where the heterogeneity of masonry plays a dominant role, according to Petrovčič and Kilar (2013). The failure occurs with a diagonal crack that typically involves both the mortar joints and the masonry bricks. The crack usually develops at the centre and propagates towards the corners. The formation of such cracks is strongly influenced by the quality of bricks and mortar. Diagonal cracking propagating through blocks tends to prevail over diagonal cracking propagating through mortar joints for increasing levels of vertical compression as stated by Mann and Muller (1980). Shear sliding occurs when cracks form continuously along a single mortar joint. This mode of failure usually presents itself in walls subjected to combined compressive and shear loads.

Several models have been developed to describe the failure associated with shear behaviour. In general, these models can be divided into two types. Those who describe masonry as a composite material where the joints and blocks are taken into account separately and models where the assumption is made that masonry behaves as an equivalent isotropic material. Most models describe the shear failure based on a Mohr-Coulomb-type criterion, which has the following shape:

$$k_{1d}\bar{\tau} \leq k_{1s}\bar{c} + \bar{\mu}\bar{\sigma} \quad (2.1)$$

where  $k_{1d}$  is a coefficient which takes into account the actual compressed part of a section, which is assumed as the ratio between its uncracked and total length. The coefficient  $k_{1s}$  depends on the slenderness of the pier and represents the ratio between the shear stress of a reference point and the average shear stress  $\bar{\tau}$ . This reference point is the location of the wall where the shear stress is determined. The masonry characteristics are taken into account by parameters  $\bar{c}$  and  $\bar{\mu}$ , which are the cohesion and friction parameters respectively. The mean vertical stress is  $\bar{\sigma}$ . The base of the pier is usually chosen as the reference point in models describing shear sliding since this section has the shortest uncracked length. The stress at the base is assumed to be equal to the mean shear stress thus  $k_{1d} = 1$ . In models describing diagonal cracked the reference stress is determined in the centre of the pier. In this case is  $k_{1s} = 1$  and  $k_{1d} > 1$ . The description of the parameters  $\bar{c}$  and  $\bar{\mu}$  is more complex because it involves the failure of both the mortar head and the bed joints. Mann and Muller (1980) developed a formulation of these parameters, taken into account two hypotheses. The first hypothesis is that bricks are much stiffer than mortar joints and the second is that no shear stresses can be transferred through the head joints. From the second hypothesis follows that the blocks are subjected to a torque, thus from vertical equilibrium follows that a non-uniform distribution of compression stresses will occur on the bed joints. These hypotheses lead to a definition of  $\bar{c}$  and  $\bar{\mu}$  which takes into account the geometrical characteristics of the masonry pattern.

$$\bar{c} = c \frac{1}{1 + \mu \left( \frac{2h}{b} \right)} \quad \text{and} \quad \bar{\mu} = \mu \frac{1}{1 + \mu \left( \frac{2h}{b} \right)} \quad (2.2)$$

where  $h$  and  $b$  are the height and width of a block respectively. Based on the same hypotheses Mann and Muller (1980) also developed a criterion for the cracking of the units. The criterion states that the reference stress in the middle of a wall has to be smaller than the tensile strength of the units  $f_{tu}$ .

$$\frac{\bar{\sigma}}{2} + \sqrt{(k_{1d}k_{2d}\bar{\tau})^2 + \left( \frac{\bar{\sigma}}{2} \right)^2} \leq f_{tu} \quad (2.3)$$

The most popular used model where the assumption is made that masonry behaves as an equivalent isotropic material is the one by Turnšek and Čačovič (1970). For the model is assumed that the reference stress in the centre of the pier has to be smaller than a tensile strength of masonry  $f_t$ .

$$\frac{\bar{\sigma}}{2} + \sqrt{(k_{1d}\bar{\tau})^2 + \left( \frac{\bar{\sigma}}{2} \right)^2} \leq f_t \quad (2.4)$$

## FLEXURAL CAPACITY

The failure mode related to the flexural capacity of a wall is rocking. A moment occurs when a horizontal load is applied on the wall at a distance from the ground. The pier begins to behave as a rigid body rotation around the corner of the pier due to this moment. This results in high compressive stresses in the corner around which the wall is rotating, while tensile stresses could occur in the other corner. Models that are used to determine the flexural capacity of a pier usually determine a reference stress at the base section of the pier. The assumption is made that the maximum normal stress occurs in the compressed toe. The compressive strength of the masonry should be higher than this reference stress in the compressed toe. It should be noted that tensile stresses are neglected in this model. This relation can be expressed in the following way according to Calderini et al. (2008):

$$\frac{\bar{\sigma}}{k_{2r}(1 - 2\kappa k_{1r})} \leq f_c \quad (2.5)$$

where  $\kappa$  is the ratio between the applied horizontal and vertical force. Coefficient  $k_{1r}$  is the shear ratio, which is the ratio between the effective height and the width. The effective height is the distance from the base to the height where the moment is equal to zero. Coefficient  $k_{2r}$  takes into account the ductility of the pier. If the assumption is made that the structure has infinite ductility, implies that  $k_{2r} = 1$ . The following expression should be applied to determine the coefficient, where  $\mu$  is the ductility of the material:

$$k_{2r} = \frac{(2\mu - 1)^2}{4(\mu^2 - \mu + 1/3)} \quad (2.6)$$

## 2.2.2 OUT-OF-PLANE FAILURE

Even though the out-of-plane action is typically not considered to be part of the building seismic load path, the walls still require sufficient capacity to avoid out-of-plane failure. Failure of load-bearing walls could lead to failure of the complete structure, due to the fact the walls will not be able any more to transfer in-plane loads. Several post-earthquake studies have been carried out where the out-of-plane failure was identified as the predominant mode of failure of a URM structure. Examples of such studies are the ones by Ingham and Griffith (2011) and Bazzurro (2009) for the earthquakes of Christchurch, New Zealand and L'Aquila, Italy respectively. Studies have shown that in various cases where the out-of-plane collapse of a wall occurred, the walls were not designed to withstand such actions. Furthermore, the failure was preventable if the walls were designed according to the relevant design likes, as elaborated by Scrivener (1993). Walls subjected to an out-of-plane load, undergo bending perpendicular to the wall. The orientation of the internal stresses due to this bending is dictated by the position of its supported edges. Walls can be classified as one-way or two-way spanning walls. One-way spanning walls undergo uniaxial bending, which can be horizontal and vertical depending on the orientation of the span. This results in cracks that run parallel to the panel's supports, as shown in Figure 2.6.

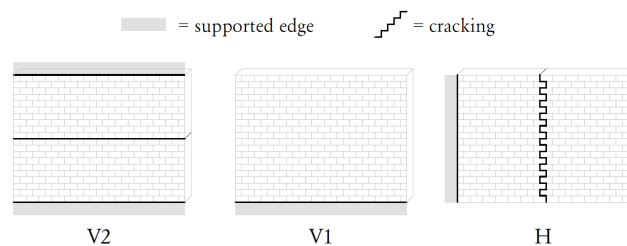


Figure 2.6: Out-of-Plane Behaviour One-way Spanning Walls.  
Source: Vaculik (2012)

Two-way spanning walls are walls which are supported by at least one vertical and one horizontal edge. Such walls undergo biaxial bending, where the internal bending stresses act in both the horizontal and vertical directions. Due to this, a crack pattern can develop which are a combination of vertical, horizontal and diagonal crack lines, as shown in Figure 2.7.

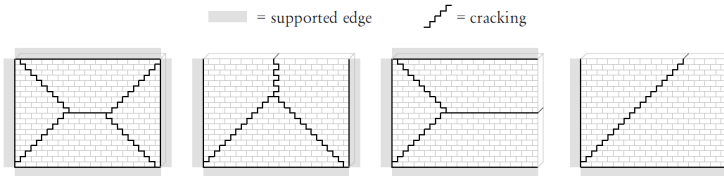


Figure 2.7: Out-of-Plane Behaviour Two-way Spanning Walls.  
Source: Vaculik (2012)

Most procedures for determining the capacity of two-way walls are based on plastic analyses. Such procedures assume simultaneous attainment of moment capacities along the various cracks. This means that at the point of ultimate strength, the wall behaves as a set of flat plates with deformations concentrated along the crack lines in the form of rotations. Several adaptations of this procedure have been developed which are applied in design codes. The most commonly employed are the virtual work method by Lawrence and Marshall (2000), fracture line method by Bazzurro (1978) and failure line method by Drysdale and Essawy (2003). The procedures differ from each other in the way the moment capacities along the cracks are determined, the inclusion of crack energies toward the internal work and the treatment of the diagonal crack slope.

2.2.3 FLOOR RELATED FAILURE

The floors of a structure should be able to transfer horizontal and vertical loads to the load-bearing walls. It is possible that during an earthquake the floors or roofs itself fails, but this type of failure is rarely observed. It is more likely that the connection between the wall and the floor fails, according to Bruneau (1994). There are different methods on how a floor can be supported by a wall. The floor could be fixed to the load-bearing walls using anchors, or the wall floor could be clamped between two walls. The connection could fail due to the capacity of the anchors is exceeded, or rupture of the wall could occur locally at the position of the anchors. A result of the failure of the connection is that gravitational forces cannot be transmitted any more from the floor to the wall, which could result in slipping of the structural elements.

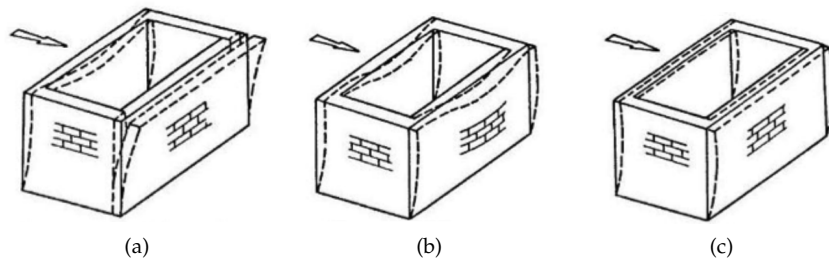


Figure 2.8: Influence of Floor Stiffness on Seismic Behaviour Walls  
Source: Javed (2009)

The structural interaction of walls between each other strongly depends on the stiffness of the connected floors. For example, flexible floors are not capable of redistributing the seismic load to the walls equally, which could significantly decrease the seismic capacity of a structure. The stiffness of the floor also influences the acceleration of the floors and the attached walls. Tena-Colunga and Abrams (1996) showed this in their study of three different buildings with different floor stiffnesses. This effect of the floor stiffness on the behaviour of a structure can be seen in Figure 2.8. Figure 2.8a shows a system with a flexible floor and walls where a proper connection with each other is lacking. Figure 2.8b shows a flexible floor, but the walls have been attached to each other. Figure 2.8c shows a rigid floor and the walls are connected to each other. Thus it can be concluded that both the stiffness of the floor and the connection between the walls have a significant influence on the behaviour of a structure.

## 2.3 NUMERICAL MODELLING STRATEGIES

The two numerical modelling strategies which are used in the case study are elaborated in this section, namely the continuum finite element method and the equivalent frame method. Different ways on how masonry can be represented computationally are briefly elucidated for each method. An elaborate description of the material models used in the case study can be found in Chapter 2.4.

### 2.3.1 CONTINUUM FINITE ELEMENT METHOD

A general description of what kind of elements can be used to model masonry using the continuum finite element method is presented hereafter. As described in Chapter 2.1, the properties of masonry are dependent on the properties of its components. These individual properties can be taken into account in various ways. The distinction can be made between micro and macro modelling. Micro modelling focusses on representing the components of masonry separately while macro modelling represents masonry as a composite material. This distinction is shown schematically in Figure 2.9.

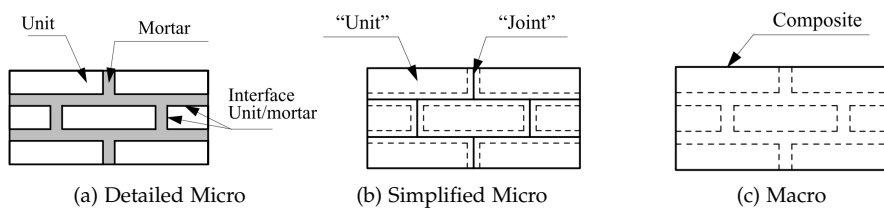


Figure 2.9: Computational Strategies for Modelling Masonry.

Source: Lourenço (2017)

#### MICRO-MODELLING

Micro-modelling is a numerical representation, where all components of the material are modelled separately. This means for masonry that the units and mortar are taken into account separately. The different components are connected using interface elements. The distinction can be made between detailed micro-modelling and simplified micro modelling, as stated by Lourenço (2017). Detailed micro-modelling represents the units and mortar using separate elements. These elements are connected by discontinuous interface elements. The properties of both the unit and mortar have to be defined separately. The units and mortar are connected by an interface element, which represents a possible crack plane

Simplified micro-modelling represents the units with separate elements, just as for the detailed method, but the mortar and the connection between the mortar and the unit is lumped into continuous interface elements. This new interface element should represent the behaviour of the mortar and the old interface as adequately as possible. The masonry is modelled as a set of blocks which are connected by a potential crack line at the new interface elements. The distinction can be made between lumped interface elements (Ngo and Scordelis 1967) which evaluate the traction and displacements at nodes and continuous interface elements (Goodman et al. 1968), which smooth the behaviour along with an interpolated field.

## MACRO-MODELLING

In practice it is not feasible to create a FEM model using micro-modelled masonry, due to the considerable computational time and due to the difficulty of defining the properties of the interface elements. Several continuum methods have been developed which do not require interface elements. The masonry is modelled as a composite material. One of these continuum models is the smeared crack model, as described by Rots and Blaauwendraad (1989). This approach is initially introduced by Rashid (1968). This approach is a simplified model which describes the composite behaviour in terms of average stresses and strains. A consequence of this assumption is that the material can be assumed to be homogeneous. Cracking is modelled as a continuous medium which is smeared over the element. It should be noted that this medium has anisotropic properties.

A popular model that is used for simulations for masonry is the Total Strain Crack model. This model describes stress as a function of the strain. Loading and unloading behaviour is modelled with secant unloading. This model has two shortcomings when the masonry is cyclically loaded, as described by Schreppers et al. (2017). The model was derived for isotropic materials, and the secant reloading curves underestimate the energy dissipation under cyclic conditions.

A type of masonry model which avoids the limitations of the Total Strain Crack model is the Engineering Masonry model. This model has been proposed by DIANA FEA and the Technical University of Delft. The Engineering Masonry model describes the unloading behaviour more realistically, compared to the Total Strain Crack model. It does so by assuming a strong stress decay with the initial linear stiffness. Anisotropy is included by considering a different stiffness in the direction of the bed and head joints. Stresses in both directions are defined by their respective strain components and the maximum value of the strain that has been reached in the lifetime of an element. The Engineering Masonry Model is described more thoroughly in Chapter 2.4.1, since this material model is used in the case study in the DIANA model.

## 2.3.2 EQUIVALENT FRAME METHOD

An alternative to using a continuum model is the equivalent frame method. An advantage of this method is that the number of degrees of freedom can be limited, which decreases the computational effort compared to the continuum FEM method. This approach subdivides a wall in a set of deformable panels, which are connected by rigid panels. The wall is modelled as an idealised frame, in which the nonlinear response of the wall is concentrated, while the rigid parts are parts which are usually not subjected to damage. The deformable parts can be divided into piers and spandrels. Piers are the main vertical resistant elements, which transfer vertical and lateral loads. Spandrels connect the piers and they couple the response of adjacent piers. Figure 2.10 shows the idealisation of the method.

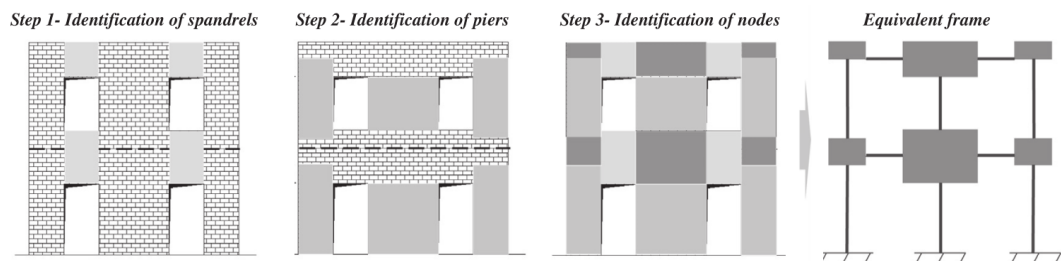


Figure 2.10: Equivalent Frame Method Idealisation.

Source: Lagomarsino et al. (2013)

The geometry of the piers and spandrels are often defined as a function of its adjacent openings. The height of a pier is equal to the height of the wall until an adjacent opening stops, plus a bit of extra effective height. A commonly accepted method is to determine this effective height, is the one proposed by Dolce (1991). He assumes a maximum 30deg angle from the corner of the opening which contributes to the effective height of the pier. Another commonly accepted method is the one proposed by Yi et al. (2006), where a maximum angle of 45 deg is suggested. This based on the fact that this is the angle over which a compression strut is most likely to develop. It should be noted that a systematic parametrical analysis has never been performed in order to define these criteria, as stated by Lagomarsino et al. (2013).

Two-dimensions models were only discussed so far, but it is also possible to model three-dimensional structure. 3MURI created a three-dimensional model based on a few hypotheses. First, the walls the load bearing elements, while the diagrams govern the sharing of horizontal actions among the walls. The effect of the flexural behaviour of the diagrams and the out-of-plane response of the walls are considered to be neglectable with respect to the global behaviour of the structure. Thus, these effects are not computed in the model. An example of a three-dimensional EFM model in 3MURI is shown in Figure 2.11.

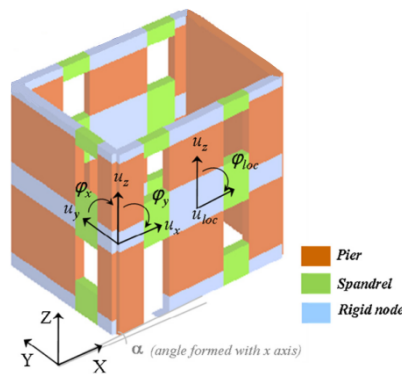


Figure 2.11: Three-Dimensional Equivalent Frame Model in 3MURI.  
Source: Lagomarsino et al. (2013)

A global coordinate system  $(X,Y,Z)$  has to be defined, in order to assemble such a three-dimensional model. The walls are described as the coordinates of one point and the angle formed with the global  $X$ -axis. By doing so is it possible to model the plane frames in the local coordinate system, while the internal nodes can still be two-dimensional nodes with three degrees of freedom. Three-dimensional nodes are used at corners where two walls intersect. These nodes are characterised by five degrees of freedom in the global coordinate system  $(u_x, u_y, u_z, \phi_x, \phi_y)$ , as shown in Figure 2.11. The rotational degree of freedom in the  $Z$ -direction is neglected in this model. These nodes are made by assembling two-dimensional nodes in each wall plane and projecting the local degrees of freedom along the global axis. The two-dimensional nodes do not have a degree of freedom orthogonal to the wall plane. The modal mass component related to the out-of-plane degree of freedom is shared with the corresponding degree of freedom of the two nearest three-dimensional nodes.

Once the masonry wall is subdivided into its components, the prediction of its overall behaviour mainly depends on the response of its individual elements. A general description of the behaviour of such elements is elaborated below, where the distinction is made the behaviour of the piers and spandrels. A more elaborate description of the material model used in the case study is presented in Chapter 2.4.2, which is the 3MURI macro-element model.

## 2.4 MATERIAL MODELS

The material models which are used in the case study are elaborated in this section. The Engineering Masonry Model is used for the Continuum FEM model the 3MURI Macro-Element model is used for the macro EFM model.

### 2.4.1 ENGINEERING MASONRY MODEL

The material model used in DIANA is the Engineering Masonry model. This model has been proposed by DIANA FEA and the Technical University of Delft. Anisotropy is taken into account by considering a different stiffness in the direction of the bed- and head-joints. The following failure mechanisms could occur when using this material model: Tensile cracking of the bed and head-joint, compressive crushing in the direction normal to the bed and head-joint, cracking in the direction normal to the diagonal staircase cracks, frictional shear sliding and out-of-plane shear failure. The behaviour of an element due to a tensile, compressive and shear force is briefly described below. It should be noted that all equations and graphs are directly taken from Schreppers et al. (2017), but the symbols have been adjusted for the sake of consistency in this report.

#### TENSILE BEHAVIOUR

The stresses in a wall are defined by the strains in the two in-plane directions and the maximum value of the strain  $\alpha_{tensile}$  that has been reached during the loading history. Secant unloading occurs based on the maximum strain that has occurred in the lifetime of an element. The corresponding stress at this maximum value of the strain that has been reached is denoted with  $\sigma_{rf}$ . Other important parameters are the tensile strength  $f_t$  and its corresponding ultimate tensile strain  $\epsilon_{ult}$ . This ultimate strain is determined using:

$$\epsilon_{ult} = \frac{2G_{ft}}{hf_t} \quad (2.7)$$

where  $G_{ft}$  is the crack energy, and  $h$  is the crack bandwidth of the element. An element is not able to transfer stresses after the ultimate tensile strain is reached. The tensile stress-strain diagram is shown in Figure 2.12. Expressions which describe the loading, unloading and reloading behaviour can be found in Schreppers et al. (2017).

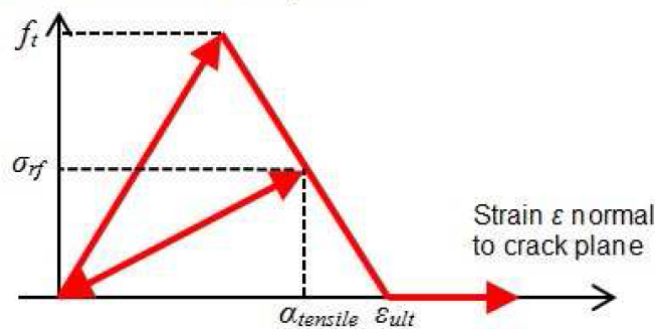


Figure 2.12: Tensile Behaviour of Engineering Masonry Model

## COMPRESSIVE BEHAVIOUR

The compressive behaviour of an element is defined by the strain component  $\epsilon$  and the minimum strain that has ever been reached  $\alpha_{comp}$  in the lifetime of an element. The occurring stress at this minimum strain is called  $\sigma_{rf}$ . Figure 2.13 illustrates the compressive behaviour of the Engineering Masonry Model, where  $\epsilon_{ult}$  is the ultimate strain,  $\epsilon_{peak}$  is the strain at the compressive strength  $f_c$  and  $\lambda$  is the unloading factor.

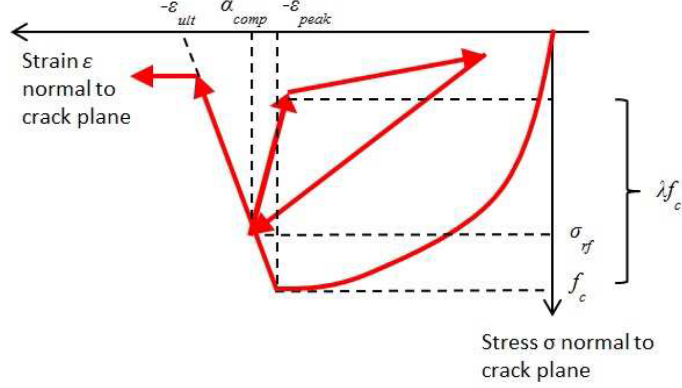


Figure 2.13: Flexural Behaviour of Engineering Masonry Model

The compressive stress-strain curve consists of a third order curve, up to the compressive strength and a linear softening curve until a residual stress of ten percent is reached. The ultimate compressive strain is equal as the strain value for which the linear softening curve would have reached a zero stress level. The following formula is applied to find this ultimate strain:

$$\epsilon_{ult} = \max \left[ \epsilon_{peak}, \frac{2G_{fc}}{hf_c} - \frac{f_c}{A^2E} - \frac{A+1}{A} \left( \epsilon_{peak} - \frac{f_c}{E} \right) + \epsilon_{peak} \right] \quad (2.8)$$

where  $G_{fc}$  is the crack energy,  $h$  is the crack bandwidth and:

$$A = \left( \frac{E\epsilon_{peak}}{f_c} \right)^{\frac{1}{3}} \quad (2.9)$$

The unloading factor is defined in such a way that  $\lambda = 0$  corresponds to unloading with the initial stiffness of the system.  $\lambda = 1$  corresponds to secant unloading to the origin with stiffness  $\sigma_{rf}/\alpha_{comp}$ . The initial stiffness is applied until the compressive stress level  $\lambda\sigma_{rf}$  is reached. Afterwards a secant stiffness  $E_{sec}$  is applied, which is defined as:

$$E_{sec} = \frac{\lambda\sigma_{rf}}{\alpha_{comp} - \lambda\frac{\sigma_{rf}}{E}} \quad (2.10)$$

The occurring stress in the material is dependent on three different conditions. First, has to be checked if a new compressive extreme is met. If a new compressive extreme is not met, the check has to be made if a strain increment  $\Delta\epsilon$  loads to a higher or lower strain than the strain at the beginning of the load increment. Compressive reloading is occurring, if the strain increases. Compressive unloading is occurring, if the strain decreases.

SHEAR BEHAVIOUR

The in-plane shear stress  $\tau$  is defined by the in-plane shear strain  $\gamma$  and the stress  $\sigma$  in the direction normal to the joint. The maximum shear stress is defined according to the Coulomb friction criterion as shown in Equation 2.11.

$$\tau_{max} = \max [0, c - \sigma \tan(\phi)] \tag{2.11}$$

where  $c$  is the cohesion and  $\phi$  the friction angle. This implies that the shear stress cannot be larger than  $\tau_{max}$  and not smaller than  $-\tau_{max}$ . The shear stress-strain diagram is shown in Figure 2.14.

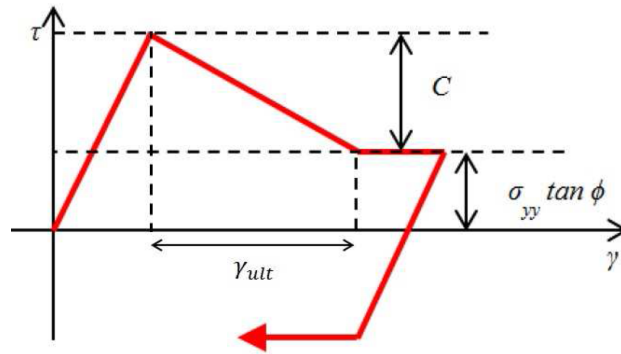


Figure 2.14: Shear Behaviour of Engineering Masonry Model

From the figure can be seen that the stress increases linearly if the shear strain increases, until it reaches  $\tau_{max}$ . The cohesion reduces after this point until its equal to zero. The strain between at  $\tau_{max}$  and  $c = 0$  is  $\gamma_{ult}$ .  $\gamma_{ult}$  is defined as:

$$\gamma_{ult} = \frac{2G_{fs}}{ch} - \frac{c}{G} \tag{2.12}$$

where  $G_{fs}$  is the shear energy and  $G$  is the shear modulus. It should also be noted that when an integration point is cracked, the cohesion is reduced to zero.

2.4.2 3MURI MACRO-ELEMENT MODEL

The components of a wall are subdivided into spandrels and piers according to the equivalent frame method as described in Chapter 2.3.2. 3MURI represents these elements using macro-elements as shown in Figure 2.15. The distinction between the joints, mortar and the joint mortar interface is not made for these elements. The assumption is made that masonry behaves as an anisotropic material, where the properties of its components are spread over the element.

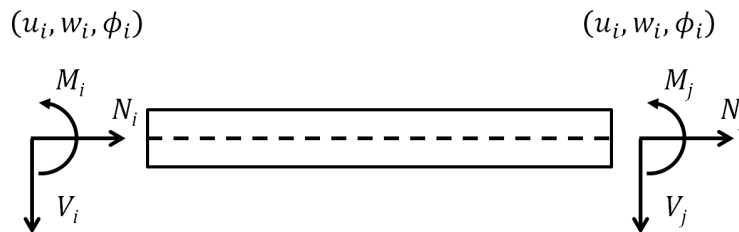


Figure 2.15: Macro-element used in 3MURI.  
Source: 3MURI (2018)



A parabolic compressive stress distribution occurs to the rotation around the toe of the wall. The surface of this stress block is approximated by a square-shaped stress block with a height ( $\kappa * f_c$ ) and length  $a$ . In 3MURI is assumed that  $\kappa$  is always equal to 0.85.  $f_c$  is the average resistance in compression of the masonry. The length  $a$  of the square-shaped stress block can be determined using the following equation.

$$a = \frac{N_{Ed}}{\kappa f_c t} \quad (2.15)$$

The moment capacity of the wall can be determined subsequently using:

$$M_{Rd} = N_{Ed}e \quad \text{and} \quad e = \frac{l - a}{2} \quad (2.16)$$

The rocking capacity of a wall can be determined by combining Equation 2.15 and 2.16.

$$M_{Rd} = \frac{Nl}{2} \left( 1 - \frac{N}{\kappa f_m l t} \right) \quad (2.17)$$

#### SHEAR SLIDING

The shear sliding capacity  $V_{Rd,s}$  is derived from the stress scheme as shown in Figure 2.17.

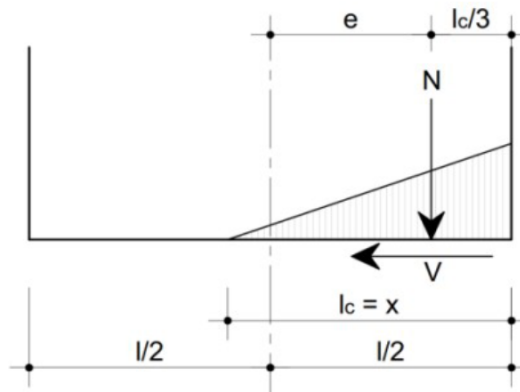


Figure 2.17: Scheme Shear Sliding.  
Source: Lanting (2016)

The shear sliding resistance of a masonry pier in 3MURI is derived based on the Mohr-Coulomb criterion, as described in Chapter 2.2.1.

$$V_{Rd,s} = c l_c t + \mu N \quad (2.18)$$

where  $l_c$  is the effective length of the wall which is under compression. This effective length is equal to the width of the wall, except for when tensional stresses occur due to the eccentricity of the axial force in the wall. These tensional stresses occur when the eccentricity of the wall is larger than the width of the wall divided by six. This results in the following equation of the effective length of the compressed part of the wall.

$$e \leq \frac{l}{6} \quad : \quad l_c = l \quad (2.19)$$

$$e > \frac{l}{6} \quad : \quad l_c = 3 \left( \frac{l}{2} - \frac{M_{Ed}}{N_{Ed}} \right) \quad (2.20)$$

If the occurring shear force  $V_{Ed}$  in the wall exceeds the shear capacity, then the occurring shear force should be reduced. The equilibrium is disturbed due to the reduction of the shear force. Thus the occurring moments  $M_i$  and  $M_j$  should be reduced as well. A consequence of the reduction is that the eccentricity reduced which also reduces the effective length the compressed part of the wall. The occurring moment is determined using the following formulas:

$$M = \alpha_v V_{Ed} h \quad \text{with} \quad \alpha_v = \frac{M_{max}}{M_{max} + M_{min}} \quad (2.21)$$

where  $\alpha_v$  is a reduction factor which depends on the boundary conditions of a wall. The reduction factor is equal to 1.0 for a cantilever and is equal to 0.5 for a wall which is clamped at both sides. If the shear resistance of the wall is exceeded, the effective wall length can be determined by substitution Equation 2.21 in Equation 2.20. This results in the following expression:

$$l_c = 3 \left( \frac{l}{2} - \frac{V_{Ed} \alpha_v h}{N_{Ed}} \right) \quad (2.22)$$

If Equation 2.22 is substituted in the Mohr-Coulomb criterion and assumption if made that  $\mu = 0.4$ , then the shear capacity can be determined for the limit state that  $V_{Ed} = V_{Rd}$ . This results in the following expressions for the shear capacity and its corresponding effective length  $l_{c,R}$ :

$$V_{Rd,s} = \frac{1}{2} N_{Ed} \left( \frac{3c l t + 0.8 N_{Ed}}{3\alpha_v c h t + N_{Ed}} \right) \quad \text{and} \quad l_{c,R} = \frac{3}{2} \left( l - \frac{3\alpha_v c l t + 0.8\alpha_v N_{Ed} h}{3\alpha_v c h t + N_{Ed}} \right) \quad (2.23)$$

The effective length  $l_{c,R}$  should comply with two limit state criteria. First, the effective length of the wall may not exceed the total width of the wall  $l$ . The second limit is based on the transition from a shear-based failure mechanism to a flexural failure mechanism. The square-shaped stress scheme as described in Equation 2.17 for flexural failure should be reached first before the effective length is reached. These limits are described in formula 2.24.

$$\frac{N_{Ed}}{\kappa c t} < l_{c,R} \leq l \quad (2.24)$$

In addition to the Mohr-Coulomb resistance, the value of the shear tension may also not exceed a limit value of  $f_{v,lim}$ . This results in the following expression of the shear capacity:

$$V_{lim} = f_{v,lim} l c t \quad (2.25)$$

The effective compressed part  $l_c$  has to be consistent with the value of  $V_{lim}$  and thus is it possible that this value is different than  $l_{c,R}$ . The following expressions can be used to find the shear resistance  $V_{lim}$  and the corresponding effective length  $l_{c,lim}$ , when the limit of the shear resistance is reached,  $V_{Ed} = V_{lim}$ .

$$V_{lim} = \frac{3}{2} N_{Ed} \left( \frac{f_{v,lim} l t}{3\alpha_v f_{v,lim} h t + N_{Ed}} \right) \quad \text{and} \quad l_{c,lim} = \frac{3}{2} \left( l - \frac{3\alpha_v f_{v,lim} l t}{3\alpha_v f_{v,lim} h t + N_{Ed}} h \right) \quad (2.26)$$

The sliding shear capacity is the minimum of  $V_{Rd}$  and  $V_{lim}$ , as shown in Equation 2.27.

$$V_{Rd} = \min(V_{Rd}, V_{lim}) \quad (2.27)$$

DIAGONAL SHEAR BEHAVIOUR

Diagonal shear failure in 3MURI is computed using the Turnsek-Cacovic criterion, as described in Chapter 2.2.1. The limit state criteria for the diagonal shear resistance can be obtained by rewriting Equation 2.4. This results in the following equation:

$$V_{Rd,s} = lt \frac{1.5\tau_0}{b} \sqrt{1 + \frac{N_{Ed}}{1.5\tau_0 lt}} \tag{2.28}$$

where  $b$  is a shape factor which depends on the geometry of the pier with a limit of  $1 \leq b \leq 1.5$ .

FAILURE MODE INTERACTION

Depending on a pier's slenderness, boundary conditions, vertical loading and geometrical characteristics of the masonry components, one of three types of in-plane failure mechanisms could occur. Other coefficients which have to be defined are the masonry friction coefficient  $\mu$ , pier shear ratio  $\alpha_v$  and shear stress distribution coefficient  $b$ . The pier shear ratio and shear stress distribution coefficient are both solely depended on the slenderness of the pier. Expressions for these parameters are elaborated by Petrovčič and Kilar (2013). From Equation 2.17, 2.27 and 2.28 can be concluded that the maximum lateral force is only depended on the mean axial stress  $N_{Ed}$  the pier slenderness  $\lambda$  and the strength of the masonry. It is thus possible to represent the lateral strength as a failure mode interaction surface. The ultimate lateral strength in this surface is equal to the minimum failure mode for a specific pair of the axial load and slenderness. An example of such a graph is shown in Figure 2.18. Such a graph can be made for each set of material parameters.

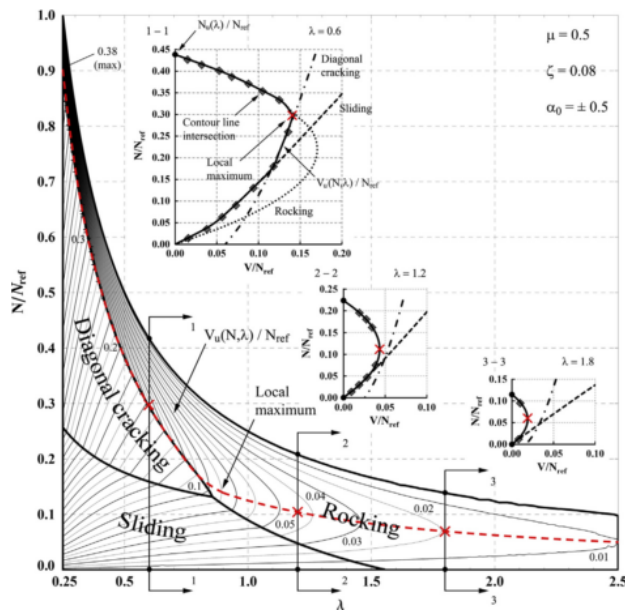


Figure 2.18: Failure Mode Interaction Surface Contour Graph. Source: Petrovčič and Kilar (2013)

The normalised ultimate lateral strength is represented by the contour lines. Each contour in Figure 2.18, corresponds with an increase of the ultimate lateral strength of 0.01. Both the axial compressive force and maximum lateral force have been normalised by a reference axial force. This has been done to scale the values on the vertical axis in such a way the values range from 0 to 1. In this case, has been chosen that the reference axial force is equal to the compressive strength at  $\lambda = 0.25$ . The red line represents the maximum local maxima for each slenderness. From the failure mode interaction surface can be seen which failure mode is relevant for a specific slenderness. For example, it can be seen that if  $\lambda > 1.5$  then only rocking failure would occur. It should be noted that it is not always easy to find the type of failure, because the surface intersections of the failure modes overlap closely in some cases.

#### SPANDREL BEHAVIOUR

Spandrels are the elements which connect the piers in a URM structure. Such elements are similar to the pier elements, but a different bed-joint orientation has to be taken into account. In general only shear cracking failure and rocking failure are taken into account. For shear cracking failure the assumption is made that the vertical stress acting in the spandrels is equal to zero. This is due to the fact that above and underneath the spandrels no material is present, thus the vertical load will be significantly small. This results in that the shear strength is only provided by the cohesion in the masonry. The shear capacity can therefore be expressed as:

$$V_{Rd,s} = \tau_0 h_{sp} t_{sp} \quad (2.29)$$

where  $h_{sp}$  and  $t_{sp}$  are the height and thickness of the spandrel respectively. The rocking capacity is based on the assumption that a tension member is included at the bottom of the spandrel. Also, the assumption is made that the bending moments are equal on each side of the spandrel. By doing so, the rocking capacity can be expressed as:

$$M_{Rd} = \frac{F_p h_{sp}}{2} \left( 1 - \frac{F_p}{\kappa f_c h_{sp} t_{sp} h t} \right) \quad (2.30)$$

which is similar to the expression for the pier as shown in Equation 2.17.  $F_p$  is equal to the minimum of tension resistance in the assumed tension member and  $0.4 f_c h_{sp} t_s$ . From Equation 2.29 and Equation 2.30 can be seen that the failure modes only depend on the slenderness of the spandrel. This is different compared with the piers because also the axial force acting on the element was of importance.



## SEISMIC ANALYSIS METHODS

---

This chapter provides an overview of the existing knowledge of the studied seismic analysis methods. The studied methods are the modal response spectrum (MRS), nonlinear pushover (NLPO) and nonlinear time history (NLTH) method. The theoretical background of all the methods is presented first, where the equation of motion is used as a starting point. Subsequently, all the relevant characteristics of the methods are described, where the focus lies with parameters and methods which need to be defined in the modelling phase. Concerning the NLPO method, three different calculation methods for determining the target displacement are presented, namely the regular N2-method, included in the Eurocode 8, and an adaptation of the N2 which is developed specifically for URM structures by Guerrini et al. (2017).

### 3.1 MODAL RESPONSE SPECTRUM

The modal response spectrum (MRS) analysis is used to obtain the likely maximum response of a structure due to a seismic load. The ground motion in this model is introduced using response spectra. A structure is idealised as multiple single degree of freedom (SDoF) systems, which represent the different modes of a structure. The response of all these systems is combined afterwards. Nonlinear material behaviour is taken into account by using a behaviour factor, which reduces the seismic load applied to the structure.

#### 3.1.1 THEORY

A good starting point for explaining the theoretical background of the MRS method is the equation of motion (EoM) of a linear SDoF system. The derivation of this equation is shown in Appendix A.1. It is common practice to divide the EoM, as shown in Equation A.4, by the mass of the system  $m$  and to rewrite the formula using the natural frequency  $\omega_n$  and the damping ratio  $\zeta$ , which results in Equation 3.1.

$$\ddot{x}(t) + 2\zeta\omega_n\dot{x}(t) + \omega_n^2x(t) = \ddot{u}_g(t) \quad (3.1)$$

where:

$$\omega_n = \sqrt{\frac{k}{m}} \quad \text{and} \quad \zeta = \frac{c}{2\omega_n m} \quad (3.2)$$

It is clear from the Equation 3.1 that the response of a linear SDoF system only depends on its natural frequency and damping ratio. Thus two systems which have the same values of  $\omega_n$  and  $\zeta$  have the same response. Thus it is possible to characterise the response of all possible linear SDoF systems to a specific ground motion. This is done with a response spectrum, which is a graph of the peak value of a response quantity as a function of the natural period and the damping ratio. It is common use to make different plots for a fixed damping ratio and where the response quantity is shown versus the natural period. For example, the deformation response spectrum is a plot of the peak displacement  $x_p$  against the natural period  $T_n$  for a fixed damping ratio. Thus the following expression can be used to determine the response spectra of the deformation:

$$x_p(T_n, \zeta) = \max |x(t, T_n, \zeta)| \quad (3.3)$$

An example of how an elastic response spectrum can be created is given by Tsouvalas (2017b). He shows the acceleration of three SDOF systems with a different natural period due to the same seismic input. If the peak values of the accelerations of the various systems are combined in one graph, it is possible to create the response spectrum for that ground motion. This method is shown in Figure 3.1.

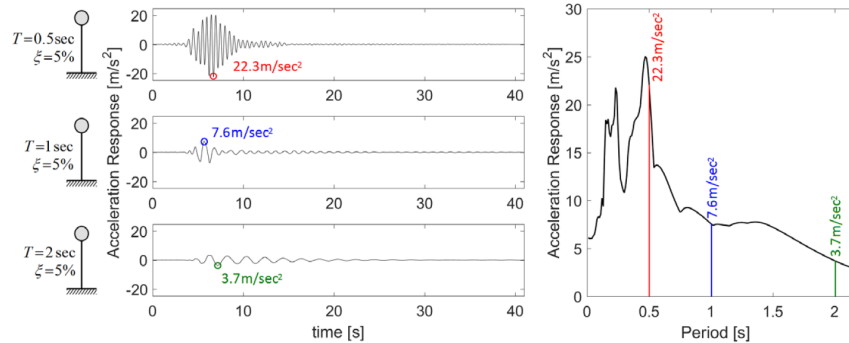


Figure 3.1: Elastic Acceleration Response Spectrum for 1995 Earthquake in Kobe, Japan.  
Source: Tsouvalas (2017b)

An advantage of this method is that if the response spectrum for a given ground motion is known, the peak value of the displacement for any linear single degree of freedom system can be found. Thus using the response spectrum method is it possible to transform a dynamic problem into a static problem, by captioning the ground motion in an elastic response spectrum. As elaborated above, the method can only be applied if response spectra for a given ground motion are known. Research has been performed to develop elastic design response spectra which display the maxima of several single degree of freedom systems, subject to the same ground motion. Since it is not practical to develop a spectrum for every possible earthquake that could happen, simplified design response spectra have been proposed by the building codes. These curves are based on the seismic hazard and the soil properties of a region. The design spectra are not indented to match the response spectrum for any particular ground motion but are constructed to represent the average characteristics of many possible ground motions. An example of how a design spectrum can be constructed is shown in Figure 3.2. It should be noted that different ground motion signals could lead to the same elastic response spectrum. This is due to the fact that the spectrum only represents the maximum response values and neglects any other information of the response.

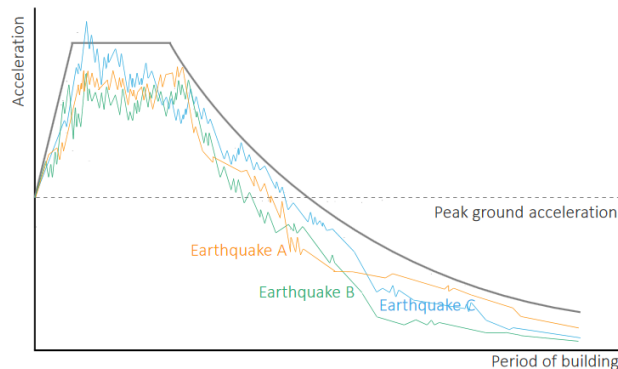


Figure 3.2: Example of Design Spectrum Based on Earthquake Spectrum A,B and C.  
Source: Timur (2017)

Two types of elastic design response spectra are proposed in the Eurocode 8. This distinction is made based on the surface wave magnitude that is approximated by a probabilistic seismic analysis. Furthermore, five ground types are considered. The effect of the stiffness of the soil on its corresponding spectrum is shown in Figure 3.3. For the Groningen case, a special elastic ground acceleration spectrum has been prescribed in NPR 9998. The ground peak acceleration including soil factor should be used as input for the construction of the spectra. These typical ground peak accelerations of the affected area in Groningen have been studied and can be found using an online tool. Another difference with the Eurocode 8 is that the relationship between the peak ground acceleration and the plateau value of the spectrum is always 2.5 in the Eurocode and this a variable in NPR 9998.

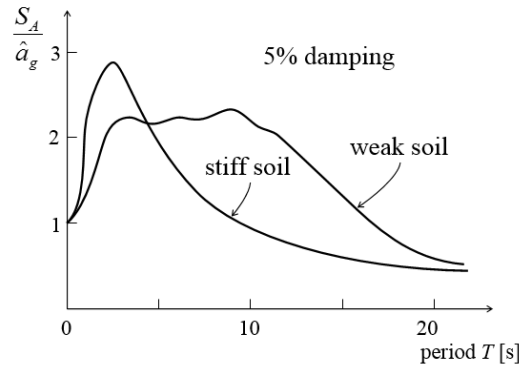


Figure 3.3: Influence Soil Conditions on Spectrum.  
Source: Vrouwenvelder (2016)

### 3.1.2 BEHAVIOUR FACTOR

The modal response spectrum method as described previously does not take into account nonlinear material behaviour. This type of behaviour is included by introducing a behaviour factor  $q$ . This purpose of this behaviour factor is to reduce applied load, anticipating the fact that the response will undertake as nonlinear deformation. This behaviour factor can be determined using a ductility factor  $\mu$ , which is defined as the ratio between the maximum displacement  $u_m$  and the yield displacement  $u_y$  of an elasto-plastic model. Design inelastic spectra haven been proposed, based on the belief that there is a relationship between the natural period  $T_n$ , the ductility factor and the behaviour factor. It has been observed that for short period structures the behaviour factor is close to one and for long periods the reduction factor is close to the ductility factor. Several mathematical relationships have been proposed based on these observations, and one that is commonly used is one proposed by Newmark and Hall (1973) as shown in Equation 3.4

$$q = \begin{cases} 1 & T_n < T_a \\ \sqrt{2\mu - 1} & T_b < T_n < T_c \\ \mu & T_n > T_c \end{cases} \quad (3.4)$$

Behaviour factors can be obtained from NPR 9998 based on the characteristics of a structural system. It should be noted that viscous damping is already taken into account in these factors. Using the behaviour factor and the values of  $T_B$ ,  $T_C$ ,  $T_D$  and  $p$ , which are location depended parameters, it is possible to formulate the inelastic design spectrum using the following formulas:

$$0 \leq T \leq T_B \quad : \quad S_d(T) = a_g S \left[ 1 + \frac{T}{T_B} \left( \frac{p}{q} \right) - \frac{2}{3} \right] \quad (3.5)$$

$$T_B \leq T \leq T_C \quad : \quad S_d(T) = a_g S \frac{p}{q} \quad (3.6)$$

$$T_C \leq T \leq T_D \quad : \quad S_d(T) = a_g S \frac{p}{q} \left[ \frac{T_C}{T} \right] \quad (3.7)$$

$$T_D \leq 4 \quad : \quad S_d(T) = a_g S \frac{p}{q} \left[ \frac{T_C T_D}{T^2} \right] \quad (3.8)$$

### 3.1.3 PEAK RESPONSE FOR MDF SYSTEMS

In Chapter 3.1.1 is presented how the peak values of forces and deformations can be found using MRS for SDoF systems. This method can also be applied for a multi-degree of freedom (MDoF) system, by transforming the MDF system into several SDF systems. This can be done by looking into all relevant modes of an MDoF system separately. The responses of the SDoF systems can then afterwards be combined to estimate the behaviour of the MDoF system. NPR 9998 specifies two requirements for which modes should be taken into consideration in this method. First, the sum of the effective modal masses of the modes taken into account amounts to at least 90 per cent of the total mass of the structure. Second, all modes with an effective model mass greater than 5 per cent of the total mass should be taken into account. These conditions should be verified for each relevant direction. Some approximation must be introduced in combining the peak model responses  $r_p$  because their information on when the peak responses occur is not included in this method. It could be assumed that all modal peaks occur at the same time. This provides an upper bound of the peak value of the total response.

$$r_p = \sum_{n=1}^N |r_{np}| \quad (3.9)$$

This upper bound value is usually too conservative. A method which provides a better estimate of the total peak response is a method developed by Rosenblueth (1951). This method is called the square-root-of-sum-of-squares (SRSS) method.

$$r_p = \left( \sum_{n=1}^N r_{np}^2 \right)^{1/2} \quad (3.10)$$

The peak response of each mode is squared, afterwards summed and the square root of this summation provides the peak response of the MDF system. This method provides accurate results, as long as the natural frequencies are well separated. According to NPR 9998, the response of two modes  $i$  and  $j$  can be considered independent of each other, if their natural periods  $T_i$  and  $T_j$  satisfy the following condition:

$$T_i \leq 0.9T_j \quad (3.11)$$

A method which overcomes the limitations of the SRSS rule is the complete quadratic combination (CQC) rule:

$$r_p = \left( \sum_{i=1}^N \sum_{n=1}^N \rho_{ip} r_{ip} r_{np} \right)^{1/2} \quad (3.12)$$

The peak responses of the  $i$ th and  $n$ th mode and the correlation coefficient  $\rho_{in}$  are multiplied for all relevant modes.  $\rho_{in}$  varies from 0 to 1 and is equal to 1 for  $i = n$ . Several formulations for the correlation coefficient were published over the years, where the one published by Rosenblueth and Elorduy (1969) was the earliest. The formulation of the correlation coefficient that is now widely used is the one by Kiureghian (1981). In this equation the correlation coefficient is solely dependent on the viscous damping  $\zeta$  and the ratio  $\beta_{in}$ , which is defined as  $\beta_{in} = \omega_i / \omega_n$ . If the assumption is made that the damping for all frequencies is equal, the equations is as follows:

$$\rho_{in} = \frac{8\zeta^2(1 + \beta_{in})\beta_{in}^{3/2}}{(1 - \beta_{in})^2 + 4\zeta^2\beta_{in}(1 + \beta_{in})^2} \quad (3.13)$$

### 3.2 NONLINEAR PUSHOVER

The nonlinear pushover (NLPO) analysis is a nonlinear static method used for the seismic analysis of structures. A pushover analysis is a procedure in which the magnitude of the lateral load excited in a structure is increased monotonically until failure. The lateral load is applied in a predefined load pattern. The relation between the control displacement and base shear is plotted subsequently in a so-called capacity curve. This capacity curve is used to determine the seismic capacity of a structure. In this chapter the theoretical background of the pushover method is elaborated, where the equation of motion is used as a starting point. Secondly, two commonly pushover methods are described, namely the capacity spectrum method and the N2-method.

#### 3.2.1 THEORY

The description of the theoretical background NLPO analysis is based on the work of Tsouvalas (2017a). The equation of motion as derived in appendix A.2, is used as the basis for the elaboration of the background, just as was done for the description of the theory behind MRS analyses. The equation of motion is shown in Equation 3.14.

$$M\ddot{x} + C\dot{x} + f_s(x, \dot{x}, t) = -Mr\ddot{u}_g(t) \quad (3.14)$$

When trying to solve this differential equation, it is logical to look for a response which has the following shape:

$$x_i = \sum_{n=1}^N \hat{\Phi}_r q_r \quad (3.15)$$

where  $x_i$  is the response of mode  $i$  and  $\hat{\Phi}_r$  is the eigenmode of node  $r$ . This means that all the modes are coupled, thus the response of mode  $i$  is influenced by the sum of all modes  $r$ . This coupling has to be taken into account, due to the nonlinear stiffness of the system. An assumption has to be made, to make the problem solvable with the NLPO method. This assumption reads:

$$x_i = \sum_{n=1}^N \hat{\Phi}_r q_r \approx \hat{\Phi}_i q_i = \Phi q \quad (3.16)$$

In Equation 3.16 is assumed that  $q_r$  is zero for all modes in which  $r \neq i$ . This means that the individual modes are not influencing each other. This approximation is theoretically only valid for linear systems, but the assumption can also be made for nonlinear systems if the response of the structure is such that the total response of the system can be found by searching for each mode individually. This assumption is valid for structures which have a high mass participation in certain modes. This is only the case for structures which are not severely irregular. Consequences of this assumption are elaborated in a further stage of this report. Substitution of the assumed displacements as shown in Equation 3.16 in the equation of motion 3.14 results in:

$$M\Phi\ddot{q} + C\Phi\dot{q} + f_s(\Phi q, \Phi\dot{q}, t) = -Mr\ddot{u}_g(t) \quad (3.17)$$

Pre multiplying this equation with  $\Phi^T$  results in:

$$\Phi^T M \Phi \ddot{q} + \Phi^T C \Phi \dot{q} + \Phi^T f_s(\Phi q, \Phi \dot{q}, t) = -\Phi^T M r \ddot{u}_g(t) \quad (3.18)$$

Several notations are introduced to shorten the equation which shorten Equation 3.18 to:

$$\mathbf{M}^* \ddot{\mathbf{q}} + \mathbf{C}^* \dot{\mathbf{q}} + \mathbf{f}_s^* \mathbf{q} = -\Phi^T \mathbf{M} \mathbf{r} \ddot{u}_g(t) \quad (3.19)$$

where:

$$\Phi^T \mathbf{M} \Phi = \mathbf{M}^*, \quad \Phi^T \mathbf{C} \Phi = \mathbf{C}^* \quad \text{and} \quad \Phi^T \mathbf{f}_s(\Phi \mathbf{q}, \Phi \dot{\mathbf{q}}, t) = \mathbf{f}_s^* \quad (3.20)$$

The model mass matrix  $\mathbf{M}^*$  and the model stiffness matrix  $\mathbf{f}_s^*$  are diagonal, which follows from the orthogonally principle. The modal damping matrix  $\mathbf{C}^*$  is fully populated, but by introducing Rayleigh damping is it possible to force the matrix diagonal. A description of Rayleigh damping is presented in Chapter 3.4.2. Due to the fact that all matrices in 3.19 are diagonal, is the EoM a set of uncoupled equations. Thus it is possible to rewrite the equation in scalar form:

$$m_{ii}^* \ddot{q}_i + c_{ii}^* \dot{q}_i + f_{si} = -L_i \ddot{u}_g \quad (3.21)$$

where:

$$L_i = \Phi_i^T \mathbf{M} \mathbf{r} \quad (3.22)$$

Equation 3.21 can be simplified by dividing the equation by  $m_{ii}^*$  which results in:

$$\ddot{q}_i + 2\zeta_i \omega_i \dot{q}_i + \frac{f_{si}}{m_{ii}^*} = -\Gamma_i \ddot{u}_g \quad (3.23)$$

in which:

$$\omega_i^2 = \frac{k_{ii}^*}{m_{ii}^*}, \quad \zeta_i = \frac{c_{ii}^*}{2m_{ii}^* \omega_i} \quad \text{and} \quad \Gamma_i = \frac{L_i}{m_{ii}^*} \quad (3.24)$$

Another transformation of coordinates is introduced and substituted in Equation 3.23 to make sure that only the ground acceleration appears on the right-hand side of the equation.

$$q_i = \Gamma_i D_i \quad (3.25)$$

$$\ddot{D}_i(t) + 2\zeta_i \omega_i \dot{D}_i(t) + \frac{f_{si}(D, \dot{D}, t)}{L_i} = -\ddot{u}_g(t) \quad (3.26)$$

The only unknowns in the equation above is the displacement  $D_i$ , and the nonlinear force-displacement relation  $f_{si}$  and the ground acceleration. Thus if the ground motion and nonlinear force-displacement relation are introduced in some way, the equation can be solved to find the displacements. This force-displacement relationship can be derived from the capacity curve, and the ground motion is introduced using response spectra. The total response of the structure can be found subsequently by substituting  $D_i$  in Equation 3.16. This results in:

$$\mathbf{x}_i(t) = \hat{\Phi}_i \Gamma_i D_i(t) \quad (3.27)$$

It should be noted that it is not allowed to sum the responses to the different modes, because superposition only holds for linear systems.

## 3.2.2 CAPACITY CURVE

The most important aspect of the NLPO method is the determination of the capacity curve. The capacity curve is the relationship between the base shear and the displacement of a control node. Three methods are generally accepted to determine the capacity curve:

- Mechanistic hierarchy of strength analysis.
- Pseudo nonlinear analysis using sequential elastic analysis
- Nonlinear finite element analysis.

Since only the nonlinear finite element method is applied in this study are the other analysis types not further elaborated. An important aspect is the assumed load distribution applied to the structure. These loads are representing the inertia forces which would be experienced by a structure due to a seismic event. In a conventional pushover analysis, only the magnitude of the load is increasing while the distribution of the load remains constant. The inertia forces could be approximated more accurate if the load pattern would vary during the pushover analysis. Research on such adaptive pushover methods has been performed by Shakeri et al. 2008 and Gupta and Kunnath 2000.

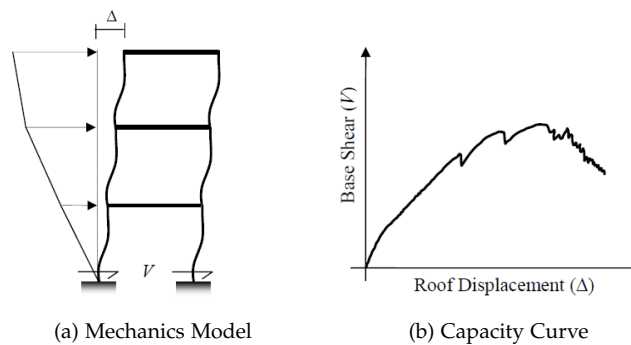


Figure 3.4: Schematic Representation of Pushover Analysis Procedure

Eurocode 8 and NPR 9998 prescribe constant load patterns that should be applied for the pushover analysis. Since constant distribution methods are incapable of capturing the variations of the structural behaviour of a structure during an earthquake, at least two different load patterns are required. The intention behind the multiple load patterns is to bind the loads that could occur during the actual dynamic response. The following two load distributions are prescribed:

- A uniform distribution based that is proportional to the mass. A uniform acceleration is applied to the structure.
- A modal pattern based on the lateral force distribution determined with an elastic analysis. This generally corresponds to a triangular load pattern based on the first dominant mode.

The pushover analysis can be performed after the load distribution is defined. The result of such an analysis is a capacity curve, which is the relation between base shear force  $V_b$  and the control node displacement  $u_n$ . This control displacement may be taken at the centre of the mass of the roof of the building.

### 3.3 TARGET DISPLACEMENT METHODS

Several different target displacement calculations methods have been developed and implemented in guidelines. The first commonly applied methods were the capacity spectrum method and the displacement coefficient method. These were described in ATC-40 and FEMA-273 respectively, with are both building codes from the United States. The most commonly applied method in Europe is the N2-Method. An adaptation of the capacity spectrum method is prescribed in NPR 9998. It should be noted that even though NPR 9998 describes the capacity spectrum method, it is mentioned in the code that other methodologies may also be applied. Three methodologies are studied in this report, namely: Capacity Spectrum Method (NPR 9998) and the N2-Method (Eurocode 8) and an adapted version of the N2-Method which has been developed for low period URM structures. This method has been developed by Guerrini et al. (2017).

#### 3.3.1 N2-METHOD (EUROCODE 8)

The method prescribed in Eurocode 8 is an adoption of the N2-method as proposed by Fajfar (1999). A characteristic of this method which differs from the other methods is that the determination of the target displacement depends on whether the equivalent idealised SDoF system is in the short, medium or long-period range. This check is performed by comparing the natural period of the equivalent idealised SDoF system with the corner period of the demand. Non-linear material is only taken into account if the structure is in the short period range, and if the factor  $q_u$  is larger than 1. This factor is explained more thoroughly later in this chapter.

The first step of the N2-method is to determine the horizontal elastic response spectrum based on the viscous damping, soil conditions and location of a structure. Such a spectrum is typically shown as a graph for a constant viscous damping and with the spectral acceleration and natural period on its axis. It is necessary to transform this graph into an acceleration - displacement format, as shown in Figure 3.5.

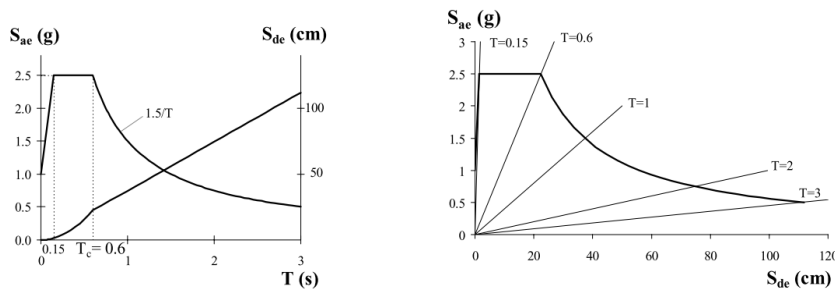


Figure 3.5: Transformation Spectrum from Traditional to Acceleration-Displacement Format  
Source: Fajfar (1999)

The following relation applies to transform an elastic spectrum to the elastic its acceleration - displacement format:

$$S_{ead} = \left( \frac{T}{2\pi} \right)^2 S_e \tag{3.28}$$

The second step is to transform the MDoF system into an equivalent SDoF system. This is done by transforming the capacity curve from its force-displacement format  $F_b - d_n$  to a force-modal displacement graph  $F^* - d^*$ . This transformation can be done by applying Equation 3.29 where the original capacity curve is written in a  $F_b - d_n$  format and the capacity curve of the SDoF system is written in  $F^* - d^*$  format. The asterisk next to a symbol indicates that it is related to a property of the SDoF system.

$$F^* = \frac{F_b}{\Gamma}, \quad d^* = \frac{d_n}{\Gamma} \quad \text{and} \quad \Gamma = \frac{\sum F_i}{\sum \left( \frac{F_i^2}{m_i} \right)} \quad (3.29)$$

Using this idealised system it is possible to find the yield force  $F_y^*$ , which is equal to the force at the formation of the plastic mechanism. An idealised force-displacement diagram has to be constructed based on the aforementioned  $F^* - d^*$  relation. This idealised force-displacement relationship is idealised with an equivalent relationship, where a constant stiffness assumed until the yield point  $F_y^*$  of this system. The post-yield stiffness is assumed to be equal to zero. The initial stiffness is determined in such a way that the area under the actual and idealised force-deformation curves are equal. This method is shown graphically in Figure 3.6. This area is the deformation energy up to the formation of the plastic mechanism. The yield displacement  $d_y^*$  can be found based on this assumption using:

$$d_y^* = 2 \left( d_m^* - \frac{E_m^*}{F_y^*} \right) \quad (3.30)$$

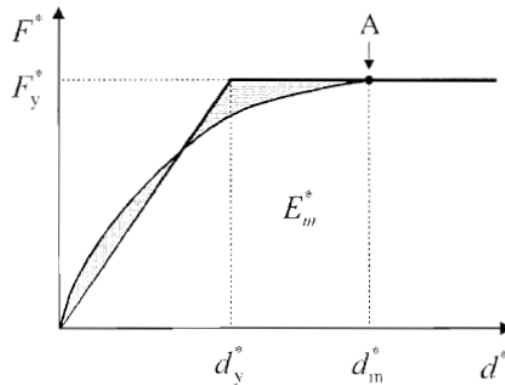


Figure 3.6: Stiffness Relation of Equivalent SDF System.  
Source: Eurocode 8

The elastic period  $T^*$  of this equivalent SDOF system can be determined, using the effective mass  $m_{eff}$ , the yield strength  $F_y^*$  and yield displacement  $d_y^*$ .

$$T^* = 2\pi \sqrt{\frac{m_{eff} d_y^*}{F_y^*}} \quad \text{and} \quad m_{eff} = \sum m_i \phi_i \quad (3.31)$$

The target displacement of the equivalent SDF system assuming unlimited elastic behaviour is given by:

$$d_{et}^* = S_{ead}(T^*) \quad (3.32)$$

Nonlinear material behaviour has to be taken into account if the response of the SDF system is nonlinear. The response is considered to be nonlinear if the acceleration at the yield point of the idealised SDF  $F_y^*/m_{eff}$  is smaller than the spectral acceleration  $S_{ead}$  at period  $T^*$ . For medium and long-range periods is assumed that the response is always elastic. A structure is considered short range if  $T^* < T_C$ . This is shown graphically in Figure 3.7. The following formulas are applied to determine the target displacement  $d_t^*$ .

$$F_y^*/m_{eff} > S_{ead}(T^*) \text{ and } T^* < T_C \quad : \quad d_t^* = d_{el}^* \tag{3.33}$$

$$F_y^*/m_{eff} < S_{ead}(T^*) \text{ and } T^* < T_C \quad : \quad d_t^* = \frac{d_{el}^*}{q_u} \left( 1 + (q_u - 1) \frac{T_C}{T^*} \right) > d_{el}^* \tag{3.34}$$

$$T^* > T_C \quad : \quad d_t^* = d_{el}^* \tag{3.35}$$

The factor  $q_u$  is the ratio between the acceleration with unlimited elastic behaviour and in a structure with limited strength.

$$q_u = \frac{S_{ead}(T^*)m_{eff}}{F_y^*} \tag{3.36}$$

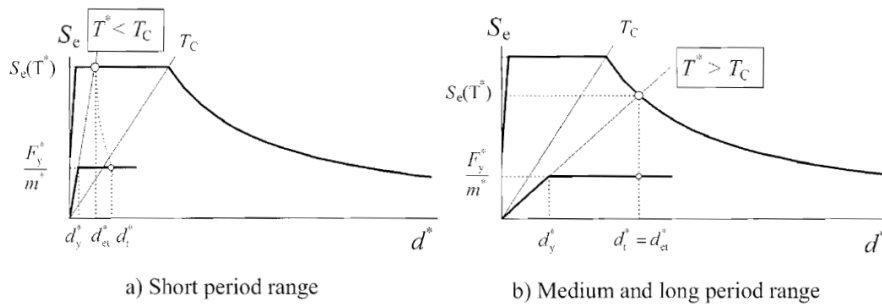


Figure 3.7: Graphical Representation of Target Displacement.  
Source: Eurocode 8

The last step is to transform this target displacement  $D_t^*$  of the SDF system to the target displacement  $d_t$  of the MDF system. This transformation is executed by applying the same transformation factor as was used to transform the MDF to the SDF system:

$$d_t = \Gamma d_t^* \tag{3.37}$$

## 3.3.2 GUERRINI

A method has been developed by Guerrini et al. (2017) for the evaluation of inelastic demands for short-period masonry structure. Short period structures are structures with a fundamental period between 0.1 and 0.5 s. This method has been developed because a significant underestimation of the ductility demand and inelastic displacement ratio was observed when using the N2-method and other similar methods for short-period structures. It was found that the amount of energy dissipated by material hysteresis has a significant influence on the displacement demand, even though it is not accounted for in the N2 method. An adapted formulation is proposed for Equation 3.34 is proposed which is used to relate the inelastic and elastic displacement demands. The following equation is proposed:

$$d_t^* = \frac{d_{el}^*}{q_u} \left( \frac{(q_u - 1)^c}{\left(\frac{T}{T_{hyst}} + \alpha_{hyst}\right) \left(\frac{T}{T_c}\right)^b} + q_u \right) \quad (3.38)$$

Parameters  $\alpha_{hyst}$ ,  $b$ ,  $c$  and  $T_{hyst}$  are calibrated with the results of multiple NLTH analyses performed on a set of oscillators. Sets of parameters were obtained for three ranges of hysteric dissipation, specifically for mainly flexure dominated (FD) systems ( $13\% \leq \xi_{hyst} < 15\%$ ), intermediate systems ( $15\% \leq \xi_{hyst} < 18\%$ ) and mainly shear dominated (SD) systems ( $18\% \leq \xi_{hyst} < 20\%$ ). The values are shown in Table 3.1

Table 3.1: Calibrated Parameters for Proposed Equation.  
Source: Guerrini et al. (2017)

Case	$\alpha_{hyst}$ (-)	$b$ (-)	$c$ (-)	$T_{hyst}$ (s)
Mainly FD $13\% \leq \xi_{hyst} < 15\%$	0.7	2.3	2.1	0.055
Intermediate $15\% \leq \xi_{hyst} < 18\%$	0.2	2.3	2.1	0.030
Mainly SD $18\% \leq \xi_{hyst} < 20\%$	0	2.3	2.1	0.022

## 3.3.3 CAPACITY SPECTRUM METHOD (NPR 9998)

The capacity spectrum method was initially proposed by Freeman and Tyrell (1975). The main difference of this method in comparison with the N2-method is that inelastic behaviour is taken into account by reducing the demand based on a level of equivalent damping. This equivalent viscous damping depends on the inherent damping of the structural system, the hysteric damping and the soil conditions. A brief explanation of all relevant steps is presented below. The first step of the capacity spectrum method is to transform the elastic acceleration response spectrum into an elastic displacement response spectrum. This transformation is done in the same way as for the N2-Method. The following relation has to be applied for the transformation:

$$S_{ead} = \frac{T^2}{4\pi^2} S_e \quad (3.39)$$

This next step is to reduce  $S_{ead}$  to take into account nonlinear behaviour. This can be done by multiplying the elastic ADRS spectrum with the spectral reduction factor  $\eta_{\xi}$ .

$$S_{nlad} = \eta_{\xi} S_{ead} \quad (3.40)$$

where:

$$\eta_{\xi} = \left( \frac{7}{2 + \xi_{sys}} \right)^{0.5} > 0.55 \quad (3.41)$$

where  $\xi_{sys}$  is the effective equivalent viscous damping. The effective equivalent viscous damping is a combination of the inherent damping  $\xi_0$ , the hysteric damping  $\xi_{hys}$  and the soil damping  $\eta_{soil}$ . The inherent damping is taken as 5% as is specified in NPR 9998. The hysteric damping is derived based on the global ductility of a system. Equation 3.42 is given to determine the hysteric damping if a ductile failure mechanism occurs.

$$\xi_{hys} = 0.42 \left( 1 - \frac{0.9}{\sqrt{\mu_{sys}}} - 0.1\sqrt{\mu_{sys}} \right) \leq 0.15 \quad (3.42)$$

where  $\mu_{sys}$  is the ductility of the structure. The soil damping can be determined by taking into account the soil properties. An extensive procedure on how the soil damping could be included is shown in NPR 9998. The next step of the capacity spectrum method is to convert the capacity curve into an equivalent single degree of freedom system. This is done in exactly the same matter as is prescribed in EN-1998, as described in Equation 3.29. The pushover curve of the equivalent system has to be divided by the effective mass of the system subsequently using the following equation:

$$S_a = \frac{F^*}{m_{eff}} \quad (3.43)$$

where  $S_a$  is the generalised capacity curve. This generalised capacity curve has to be bi-linearised subsequently. This is done by first determining the initial lateral stiffness of the equivalent SDoF system, by taken the secant stiffness at a base shear equal to sixty percent of the maximum base shear. Second, the maximum spectral displacement  $u_{cap;sys}$  is taken as the lateral near collapse displacement capacity of the equivalent SDoF system. Third, the spectral acceleration of the SDoF system  $S_{a,y}$  is computed assuming an elastoplastic force-displacement relationship and equal energy criterion, which can be determined as follows:

$$S_{a,y} = \frac{u_{cap;sys} K_{init} - \sqrt{(u_{cap;sys} K_{init})^2 - 2E_m K_{init}}}{m^*} \quad (3.44)$$

An example of a bi-linearised pushover curve is shown in Figure 3.8.

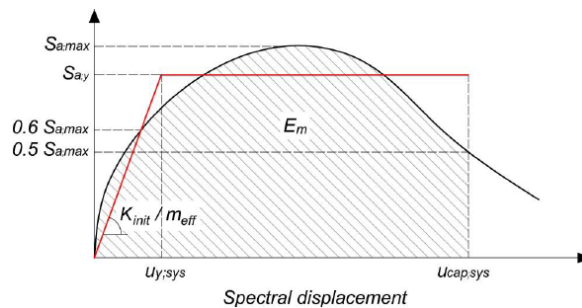


Figure 3.8: Example of a Bi-Linearised Capacity Curve  
Source: NPR 9998:2018

Both the capacity  $S_a$  and demand  $S_{nlad}$  are expressed in the same units, namely: acceleration on the vertical axis and displacement on the horizontal axis. If both spectra are now drawn in the same graph, it is possible to find the target displacement  $d_t^*$ . This point can also be calculated by using the following expressions:

$$k^* = \frac{V_{cap}}{u_{cap}}, \quad T^* = 2\pi\sqrt{\frac{m^*}{k^*}} \quad \text{and} \quad x_t = S_{nlad}(T^*) \quad (3.45)$$

where  $k^*$  and  $T_{eff}$  are the effective stiffness and natural period of the equivalent SDoF system respectively. These values are derived from the displacement capacity  $u_{cap}$  and base shear capacity  $V_{cap}$  of the equivalent SDoF system. It should be noted that  $T_{eff}$  according to NPR 9998 represents a different value than  $T^*$  which had to be determined to calculate the target displacement according to Eurocode 8.  $T_{eff}$  is the effective period of the SDoF system, which depends on the ultimate capacity in terms of displacement and base shear and  $T^*$  is the fundamental period of the SDoF system and depends on the yield displacement and base shear capacity.

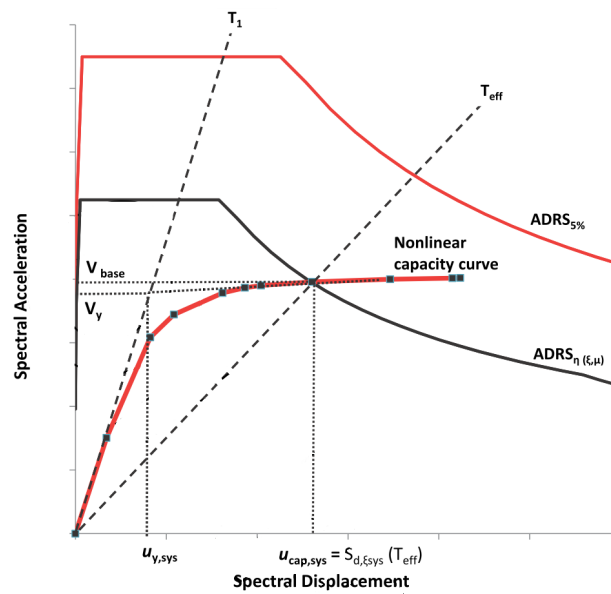


Figure 3.9: Capacity Curve Assessment  
Source: NPR 9998:2017

### 3.4 NONLINEAR TIME HISTORY

The NLTH analysis is a nonlinear dynamic method used for the seismic analysis of structures. The seismic load is taken into account by applying a ground motion signal to the soil or directly to a structure. Several earthquake signals have to be applied, to take into account the considerable spread an earthquake scatter could have at a single location. Nonlinearity is taken into account by applying nonlinear material properties in the model and by including geometrical and transient nonlinearity in the analysis. The nonlinear analysis is executed by determining the response of the structure per timestep by using a numerical iteration method.

#### 3.4.1 THEORY

The theoretical background of the NLTH analysis presented in this chapter is based on the work of Gavin (2016). Symbols have been changed with respect to his work, due to consistency reasons. A good basis to describe the background of the NLTH method is the equation of motion (EoM) of a multiple degree of freedom (MDoF) system. The derivation of this EoM can be found in Appendix A.2. It should be noted that bolted capital symbol represent matrices, bolted lowercase symbols represent vectors and regular lowercase symbols represent scalars. The EoM of an MDoF system is shown in Equation 3.46.

$$\mathbf{M}\ddot{\mathbf{x}}(t) + \mathbf{C}\dot{\mathbf{x}}(t) + \mathbf{f}_s(\mathbf{x}, \dot{\mathbf{x}}, t) = -\mathbf{M}\mathbf{r}\ddot{u}_g(t) \quad (3.46)$$

The difficulty in solving this differential equation is the nonlinear stiffness term. The NLTH method overcomes this problem by solving the equation numerically. It does so by discretizing the time scale in timesteps  $t = t_{i+1}$ . These timesteps are subsequently substituted in the EoM, which results in Equation 3.47.

$$\mathbf{M}\ddot{\mathbf{x}}(t_{i+1}) = \mathbf{C}\dot{\mathbf{x}}(t_{i+1}) + \mathbf{f}_s(\mathbf{x}(t_{i+1}), \dot{\mathbf{x}}(t_{i+1}), t_{i+1}) + \mathbf{M}\mathbf{r}\ddot{u}_g(t_{i+1}) \quad (3.47)$$

A numerical procedure is required to find the acceleration, velocity and displacement at  $t = t + 1$ . Most numerical procedures use methods which extrapolate  $\dot{\mathbf{x}}(t_{1+i})$  and  $\mathbf{x}(t_{1+i})$  from already known data. If  $\mathbf{x}(t_{1+i})$  and  $\dot{\mathbf{x}}(t_{1+i})$  are known is it possible to determine  $\ddot{\mathbf{x}}(t_{1+i})$  by applying Equation 3.47. Thus by using a numerical method it is possible to find all kinematic quantities, by extrapolating two of the three forward in time and solving the third one analytically. Several numerical integration algorithms are developed to extrapolate the kinematic parameters. The most commonly used integration scheme for solving NLTH problems is the Newmark method. This method approximates the displacements and velocities at timestep  $i + 1$  with:

$$\mathbf{x}_{i+1} \approx h\dot{\mathbf{x}}_i + h^2 \left[ \left( \frac{1}{2} - \beta \right) \ddot{\mathbf{x}}_i + \beta\ddot{\mathbf{x}}_{i+1} \right] \quad (3.48)$$

$$\dot{\mathbf{x}}_{i+1} = \dot{\mathbf{x}}_i + h \left[ (1 - \gamma) \ddot{\mathbf{x}}_i + \gamma\ddot{\mathbf{x}}_{i+1} \right] \quad (3.49)$$

The parameters  $\beta$  and  $\gamma$  determine certain characteristics of the method like the stability, the order of accuracy and if the method is implicit or explicit. Commonly used values for these parameters are given by Gavin (2016). If  $\beta = 1/4$  and  $\gamma = 1/2$  the Newmark method is unconditionally stable. The method is equal to the linear acceleration method if  $\beta = 1/6$  and  $\gamma = 1/2$  and the method is identical to the central difference method if  $\beta = 1/4$  and  $\gamma = 1/2$ . Several relationships are introduced of the increments of the kinematic variables, the nonlinear stiffness relation and the ground acceleration, solely to keep further equations as brief and clear as possible.

$$\delta x_i = x_{i+1} - x_i, \quad \delta \dot{x}_i = \dot{x}_{i+1} - \dot{x}_i \quad \text{and} \quad \delta \ddot{x}_i = \ddot{x}_{i+1} - \ddot{x}_i \quad (3.50)$$

$$\delta f_s = f_s(x(t_{i+1}), \dot{x}(t_{i+1})) - f_s(x(t_i), \dot{x}(t_i)) \quad \text{and} \quad \delta \ddot{u}_{gi} = \ddot{u}_{g(i+1)} - \ddot{u}_{gi} \quad (3.51)$$

Equation 3.48 can be rewritten now by expressing the acceleration by the other parameters. This leads to the following expression:

$$\delta \ddot{x}_i = \frac{1}{\beta h^2} \delta x_i - \frac{1}{\beta h} \dot{x}_i - \frac{1}{2\beta} \ddot{x}_i \quad (3.52)$$

Futhermore, if Equation 3.52 is substituted in Equation 3.49, it is possible to find an expression for the finite difference relationship of the velocity:

$$\delta \dot{x}_i = \frac{\gamma}{\beta h} \delta x_i - \frac{\gamma}{\beta} \dot{x}_i + h \left( 1 - \frac{\gamma}{2\beta} \right) \ddot{x}_i \quad (3.53)$$

The aforementioned increments should now be substituted in the EOM as shown in Equation 3.46. This results in the incremental equilibrium over timestep  $h$ .

$$M \delta \ddot{x}_i + C \delta \dot{x}_i + \delta f_s = M r \delta \ddot{x}_{gi} \quad (3.54)$$

By substituting the expressions for  $\delta \ddot{x}_i$  and  $\delta \dot{x}_i$  in Equation 3.54 and by re-grouping the equation in such a way that the change in displacement is expressed terms of velocity and acceleration, can the expression be written in the following matter:

$$\left[ \frac{1}{\beta h^2} M + \frac{\gamma}{\beta h} C \right] \delta x_i = \left[ \frac{1}{\beta h} M + \frac{\gamma}{\beta} C \right] \dot{x}_i + \left[ \frac{1}{2\beta} M - h \left( 1 - \frac{\gamma}{2\beta} \right) C \right] \ddot{x}_i - \delta f_r + M r \ddot{x}_{gi} \quad (3.55)$$

This nonlinear system of equations can be solved using several numerical methods, which are further elaborated in Chapter B.1. The goal of solving the equations is to find the increment of the displacement  $\delta x_i$ . This displacement increment should added afterwards to the initial displacement using:

$$x_{x+1} = x_i + \delta x_i \quad (3.56)$$

The velocities  $\dot{x}_{x+1}$  can also be found by applying the just found displacement increment in Equation 3.49.

$$\dot{x}_{i+1} = 2\dot{x}_i - \frac{h}{2}\ddot{x}_i + \frac{3}{h}\delta x_i \quad (3.57)$$

The displacement  $x_{x+1}$  and the velocity  $\dot{x}_{x+1}$  were the only unknowns in Equation 3.47, thus it is possible to solve the EOM to find the acceleration  $\ddot{x}_{x+1}$ .

$$\ddot{x}(t_{i+1}) = M^{-1} [C\dot{x}(t_{i+1}) + f_s(x(t_{i+1}), \dot{x}(t_{i+1}), t_{i+1}) + M r \ddot{u}_g(t_{i+1})] \quad (3.58)$$

3.4.2 DAMPING

An important aspect of an NLTH analysis is defining the damping matrix. It is not practical to determine the global damping matrix using the damping properties of its elements. This is due to the fact that the damping properties of materials are not as well defined as for the stiffness properties. Another reason is that it is impossible to take into account additional energy dissipation mechanisms, like friction in connections. In practice, the assumption is made that similar damping mechanisms occur throughout the structure. The most commonly used idealisation of the damping matrix is called Rayleigh Damping. The basis of the method is the assumption that the damping is proportional to the mass and stiffness of the structure:

$$C = a_0M + a_1K \tag{3.59}$$

The constants  $a_0$  and  $a_1$  can be determined by looking into the modal damping, which is defined as:

$$C^* = \Phi^T C \Phi = \Phi^T a_0 M \Phi + \Phi^T a_1 K \Phi = a_0 M^* + a_1 K^* \tag{3.60}$$

The derived damping matrix is diagonal due to the fact that the mass and stiffness matrix are also diagonal and due to the orthogonality principal. The matrix can now be decoupled and the damping coefficient  $\lambda_i$  can be expressed as:

$$\zeta_i = \frac{c_{ii}^*}{2m_{ii}^*} = \frac{a_0 m_{ii}^* + a_1 k_{ii}^*}{2m_{ii}^* \omega_i} = \frac{a_0}{\omega_i} + \frac{a_1 \omega_i}{2} \tag{3.61}$$

From Equation 3.61 can be seen that in the stiffness term the damping is inversely proportional to the frequency and that the mass term is directly proportional to the frequency. This is graphically shown in Figure 3.10.

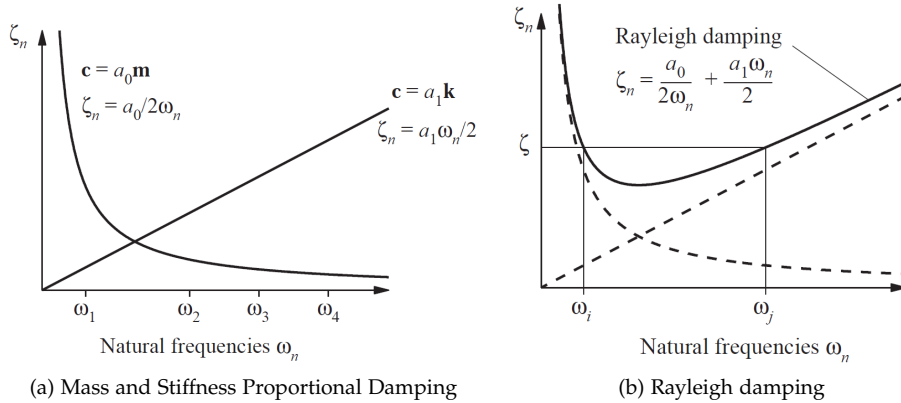


Figure 3.10: Variation of Modal Damping Ratios with Natural Frequency. Source: Chopra (2013)

The coefficients  $a_0$  and  $a_1$  can be solved by by estimating the modal damping ratios  $\zeta_{a_i}$  and  $\zeta_{a_j}$  for specified modes  $i$  and  $j$ . If both modes have the same damping ratio  $\zeta$ , can the coefficients be expressed as:

$$a_0 = \zeta \frac{\omega_i \omega_j}{\omega_i + \omega_j} \quad \text{and} \quad a_1 = \zeta \frac{2}{\omega_i + \omega_j} \tag{3.62}$$

## 3.4.3 GROUND MOTION INPUT

NPR 9998 prescribes two methods on how the seismic load can be modelled for an NLTH analysis. These methods are the direct and indirect method. The direct method models the soil with 3D elements, on which the ground motion signals are applied at a depth of 30 meters. The indirect method represents the soil by means of springs and dampers at the base of the structure, on which the ground motion signals are directly applied. Both methods are elaborated more in-depth underneath.

## DIRECT METHOD

The direct method models the soil and structure with nonlinear properties. The seismic load is applied as a force at a depth of 30 meters. This force is the product of a damping coefficient and a velocity. Dampers in  $x, y$  and  $z$  different directions are used to transfer the forces to the soil column. The viscous damping coefficients have to be determined using Equation 3.63.

$$C_h = \rho AV_s \quad \text{and} \quad C_v = \rho AV_v \quad (3.63)$$

where  $C_h$  should be applied for horizontal dampers and  $C_v$  for vertical dampers.  $\rho$  is the density of the elastic medium, and  $A$  is the plan area tributary to each damper. The shear wave velocity  $V_s$  and pressure wave velocity  $V_p$  depend on the soil properties. A schematical overview of the direct method is shown in Figure 3.11a.

## INDIRECT METHOD

The indirect method divides the analysis into two parts, with the goal to reduce the total computational time. First, the same steps as for the direct method are executed, but the difference is that the structure is modelled with linear properties, while the material properties of the soil block are still nonlinear. The output of this step are the forces and velocities at the bottom of the foundation of the structure. The second part of the indirect method is to model the structure with nonlinear properties and to model the soil as springs and dampers underneath the degrees of freedom of the foundation. The output of step 1 is subsequently used to determine the load that should be applied to the free ends underneath the springs and dampers.

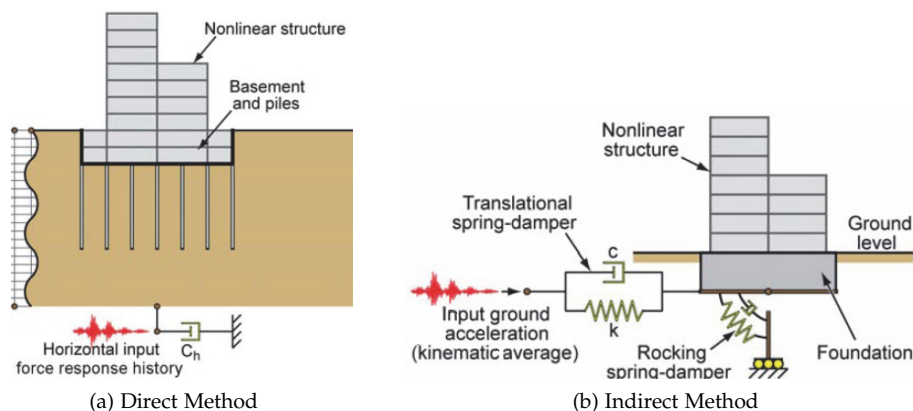


Figure 3.11: Soil Structure Interaction Representation Methods

Source: NPR 9998:2017

Part II

CASE STUDY



## STRATEGY

This chapter provides an overview of the overall strategy, which is employed to acquire results, which are used to achieve the main objectives of this study. First, the building stock in Groningen is studied, and these buildings are subdivided based on their typology. A structure is chosen afterwards, which suits the characteristics of the low-rise URM apartment building typology and fulfils the pre-requisites for performing an NLPO Analysis. Second, comparison methods are prescribed on how the conclusions can be drawn based on the output of the studied analyses.

### 4.1 BUILDING STOCK AND TYPOLOGIES GRONINGEN

Building typology is the study of and documentation of a set of buildings which have similarities in their type or form. The geometry and material properties of the studied structure in the case study should be complying with a commonly occurring typology in Groningen. This is important, because if the case study is representative of a certain typology, then the conclusions of this study could be used for the analysis of other structures from the same typology. The grouping of the buildings can be performed based on a combination of similar features like building use, adjacency, material and structural system. A database is currently under development to subdivide all structures based on their features, which are affected by earthquakes in Groningen ARUP and NAM (2018). All relevant features which are taken into account in defining the typology in this study are shown in Figure 4.1.

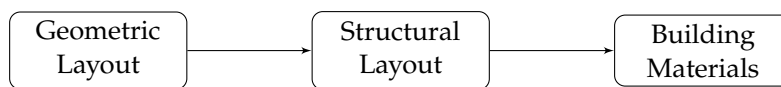


Figure 4.1: Building Classification Steps

The first subdivision that is made in this database is based on the geometry of the buildings. Four relevant categories are defined by ARUP and NAM (2018), which are shown in Figure 4.2. A fifth defined category are tower structures, but since the amount of these structures on relatively low, they are not indicated in the pie chart.

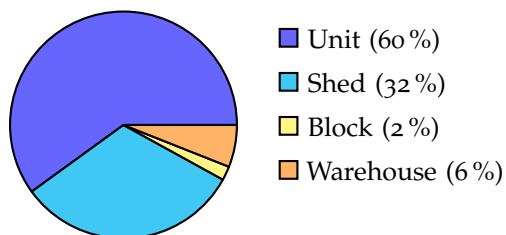


Figure 4.2: Geometric Layout Classification

- Shed: Small sized buildings
- Unit: Medium sized buildings
- Block: Buildings that contain horizontal and vertical repetition of unit structures
- Barn/Warehouse: Large span buildings

The most commonly occurring typology are unit structures. Purely based on this fact would it make sense to also select a unit structure for the case study, but the applicability of the NLPO method on this type of structure has already extensively been studied by Dijkema (2018), Michalaki (2015) and Kumar (2016). Thus the decision has been made to study a block type structure, since this type of structure has been studied less. The structures which belong in the block category can in their part be sub-divided based on their structural layout. The following unit buildings layout are described by ARUP and NAM (2018):

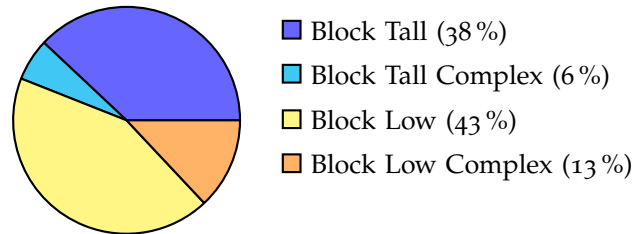


Figure 4.3: Structural Layout Classification

where the "Tall" means that a structure is larger than 10m and "Complex" means that the building is formed by multiple structures with a different structural layout. The last step of the classification process is to combine the structural layout category with its building year and available inspection data. By doing so is it possible to determine the expected properties of the walls and floor types. ARUP and NAM (2018) provide an overview of the expected properties of block structures, as shown in Figure 4.4. The walls are subdivided into calcium silicate (CS), clay brick (CB) and concrete (CO) walls. With the second index is indicated if cavity walls are present (CW) or not (NCW). The last index indicates the floor type, which could be concrete (CF) or timber (TF) floors.

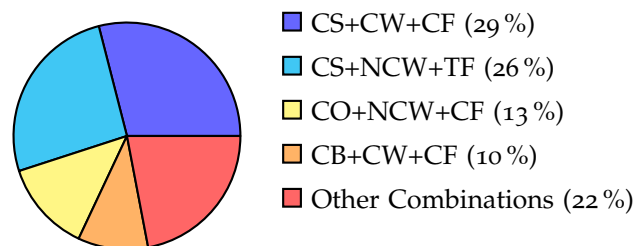


Figure 4.4: Material Walls and Floors Classification

Bases on the pie charts shown in Figure 4.3 and 4.4, it would make sense to choose a structure for the base study which does not have a complex structural layout, has calcium silicate cavity walls and concrete floors. The structure which is selected for the case study complies with all these criteria.

## 4.2 CHARACTERISTICS OF THE STUDIED BUILDING

A building which has already been studied by VIIA has been chosen for the case study. It concerns a low-rise URM apartment building. A front view of the building is shown in Figure 4.5. The building could be described by the 'block tall' structural layout classification, as described in Chapter 4.1. These are buildings which are expected to contain horizontal and vertical repetitions of unit structures without large spans, where the gutter height is larger than 10 meter. The building was constructed in 1968. The building is located in the province of Groningen, but the exact location of the building is not shown in this report, due to privacy reasons. The structure can be divided into three parts from which the wall configuration is almost the same. Thus, the decision has been made to only model part of the structure, to reduce the computational demand. Furthermore, a staircase can be found next to the structure, which can be considered as structurally detached. Thus, this staircase is not taken into account in this study.



Figure 4.5: Front View of Building

It is of interested to analyse the NLPO method for this structure for several reasons. First, because the structure is of a considerable size, which makes an NLTH analysis time-consuming. Furthermore, the NLPO method is considered to be more conservative than the MRS method. Thus, especially for structures of a considerable size, it is possible to reduce the amount of required retrofitting significantly when applying the NLPO method, compared to the MRS method. Moreover, the wall configuration is regular. Thus the NLPO method is applicable to the structure. Furthermore, the stiffness of the structure is of a different magnitude in the longitudinal and transverse direction. Therefore a study of this structure is deemed useful, to see in what extent the NLPO method is applicable in a relatively weak and relatively strong direction of the building.

## 4.2.1 STRUCTURAL LAYOUT AND MATERIALS

The top view of the structure which is analysed is shown in Figure 4.6. The masonry which is part of the façade is now shown in this top view. The same wall configuration can be found on all floors of the structure. More detailed drawings of the front, top and side view can be found in appendix C. The numbering system that is applied to indicate the floor levels is also presented in this appendix. A coordinate system has also been defined in Figure 4.6, which is used throughout the report.

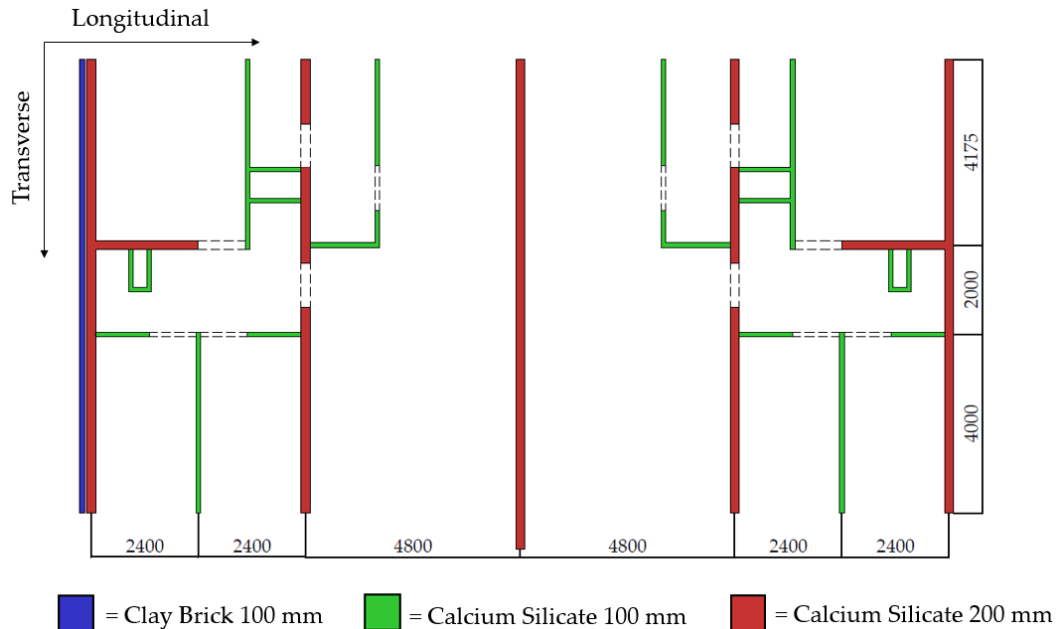


Figure 4.6: Top View First Floor

The structure contains 100 and 200 millimetre thick walls. The 100-millimetre walls separate the rooms within the structure, and these walls are non-load bearing. The 200-millimetre walls are apartment-separating walls, and they are load bearing. These apartment-separating walls provide stability during a seismic event. The seismic capacity in the longitudinal direction of the structure is considerably less, due to the lack of load-bearing walls in that direction. The reason for this significant difference in seismic strength in both directions is that initially, the only horizontal load acting on the structure is a wind load. Furthermore, the surface area on the front of the structure is considerably higher than on the sides of the structure. Therefore the wind load that was taken into account when designing the structure was significantly higher in the transverse direction, in comparison with the transverse direction. Furthermore, the distinction has to be made between primary and secondary seismic elements. Primary seismic elements are elements which are part of the structure which should withstand the seismic load. Secondary seismic elements are elements which are not meant to transfer a seismic load and failure of these elements does not lead to global failure of the structure. Even though, some limit state criteria apply to the secondary seismic elements. All of the 200-millimetre thick walls are primary seismic elements, and the 100 millimetre thick walls are secondary elements.

An overview of all the materials which can be found in the structure is presented in Table 4.1. The structure is founded by concrete prefab piles, which are attached to concrete foundation beams. The bottom floor is a ribbed floor while all other floors are in situ constructed concrete floors. The roof of the building is also made out of in situ concrete. All walls are made out of calcium silicate, except for the capacity wall, which is made out of clay brick. The inner and outer leaves are connected by anchors. The balconies and galleries are supported by concrete beams, which are supported by the walls. Timber lintels can be found underneath all the spandrels.

Table 4.1: Overview Materials Building

	<b>Material</b>	<b>Thickness (mm)</b>
Supporting Beams	Concrete	430x230
Foundation piles	Concrete	320x320
Foundation strips	Concrete	550
Floors and Roof	Concrete	150
Load Bearing Walls	Calcium Silicate	200
Non Load Bearing Walls	Calcium Silicate	100
Outer leaf cavity walls	Clay Brick	100
Inner leaf cavity walls	Calcium Silicate	100
Lintels	Timber	50x50

#### 4.2.2 SOIL PROPERTIES

The properties of the soil underneath the building are of importance for the seismic analysis. Several ground penetration tests have been performed close to the building. A representative soil composition has been formulated based on the penetration tests. It should be noted that this step has been executed by a geotechnical engineer from VIIA and not by the author of this study. The output of this study is presented in Table 4.2.

Table 4.2: Representative Soil Composition

<b>Top Layer</b>	<b>Bottom Layer</b>	<b>Description</b>
0.0	0.5	Sand
-0.5	-1.5	Clay
-1.5	-2.5	Peat
-2.5	-4.0	Clay
-4.0	-5.5	Peat
-5.5	-7.0	Sand
-7	-30	Pot Clay

## 4.2.3 ADDITIONAL LOADS

The dead weight of the structure and the variable loads acting on the structure influence the seismic capacity of a structure significantly. The permanent and variable load should be taken into account in determining the seismic load. The dead weight of the structural elements is automatically taken into account by DIANA and 3MURI, but the dead load of non-structural elements and the variable load has to be manually given as input. The inertia effects of the variable load may be reduced, due that it is not likely that the maximum variable load and a seismic event occur at the same time. The following formula is given in Eurocode 8 and NPR 9998 for determining the additional load  $E_d$  that should be taken into account for determining the seismic load.

$$E_d = \Sigma G_{k,j} + \varphi \psi_{2i} Q_{k,i} \quad (4.1)$$

where  $G_{k,j}$  are the masses of structural and non-structural elements and  $Q_{k,i}$  the variable loads. The coefficients  $\varphi \psi_{2i}$  take into the likelihood of the variable loads during a seismic event and also the reduced participation of the masses in the motion of the structure due to the non-rigid connection between them. The permanent load acting on the roof is compromised of a 0.40 kN/m<sup>2</sup> load that is specified for a roof without gravel and a 0.20 kN/m<sup>2</sup> load for the lowered ceiling. A variable load acting on the roof does not have to be taken into account, because it has to been taken into account because of  $\psi_{2i} = 0$  for the roof while performing a seismic analysis. The permanent load acting on the floors and galleries of 1.00 kN/m<sup>2</sup> is due to the floor covering. The variable load acting on these elements is 1.75 kN/m<sup>2</sup> or 2.00 kN/m<sup>2</sup> for the floors and galleries respectively, which are the values specified by NEN-EN 1991-1-1 for Class A structures. These loads have to be reduced with coefficients  $\varphi = 0.3$  and  $\psi_{2i} = 0.6$ , which results in a variable load of 0.32 kN/m<sup>2</sup> and 0.36 kN/m<sup>2</sup> for the floors and galleries respectively. An overview or the additional loads including coefficients is presented in Table 4.3.

Table 4.3: Overview Additional Permanent and Variable Loads

	<b>Permanent Load</b>	<b>Variable Load</b>	<b>Total Load</b>
	<b>kN/m<sup>2</sup></b>	<b>kN/m<sup>2</sup></b>	<b>kN/m<sup>2</sup></b>
Roof	0.60	-	0.60
Floors	1.00	0.32	1.32
Gallery	1.00	0.36	1.36

### 4.3 COMPARISON STRATEGIES

The comparison strategies which have been applied to fulfil the two main objectives are defined in this chapter. The comparison strategies are based on the limit state criteria as defined in NPR 9998. Thus, a description of these criteria is presented first. Afterwards, the comparison strategy for each of the objectives is presented separately. Ultimately, the limitations of the case study are shown.

#### 4.3.1 NEAR COLLAPSE LIMIT STATE CRITERIA

Three different limit states are defined in NPR 9998, namely: Near Collapse (NC), Significant Damage and Damage Limitation. The extent of this research is limited to the NC limit state, which states that the stability of a building is heavily damaged with a low residual strength and stiffness in the horizontal direction. However, vertical elements should still be able to transfer vertical loads. The capacity of the structure is such that the building will not collapse within a short time limit after the earthquake, but it is likely that the building will collapse due to another seismic event. This level is achieved corresponding to a seismic action with a probability of exceedance of 2 % in 50 years. Which translates to a return period of 2475 years. The verification of a building is done using the following expression:

$$E_d \leq R_d \quad \text{where} \quad R_d = \frac{R \left( \frac{f_k}{\gamma_m} \right)}{\gamma_M} \quad (4.2)$$

where  $E_d$  is the design value of the seismic load and  $R_d$  is the design value of the resistance. The characteristic values of the material properties  $f_k$  have to be divided by the partial material factor  $\gamma_M$  and by the partial factor for the material properties  $\gamma_m$ . The partial material factor takes into account modelling uncertainties and dimensional deviations, which is prescribed by NPR 9998 to be 1.0. The partial factor for the material properties depends on the type of material and the used material model. If degradation effects are taken into account,  $\gamma_m$  can be taken as 1.0, which is the case for the nonlinear methods. For linear analyses, like MRS, it is prescribed by NPR 9998 to apply a partial factor for the material properties of 1.5.

The design value of the seismic load is defined as the seismic load which has applied in a model, when performing a check for a particular characteristic load. This load will be described in terms of peak ground acceleration (PGA) at ground level. The relation between the design and characteristic load varies per analysis method. The maximum admissible seismic load acting on the structures according to each of the studied methods is expressed in terms of the characteristic seismic load.

The structural behaviour is investigated at the NC limit state for each method, however each method requires a different way to achieve this scope. An overview of the limit state criteria per analysis type is presented in Table 4.4. The out-of-plane check can only be performed using the NLTH method. Thus, global failure due to the out-of-plane failure of an element would lead to an unfair comparison with the other methods, because out-of-plane failure cannot occur due to the nature of MRS and NLPO. Special measures will be taken to prevent out-of-plane failure, if it is the governing failure mechanism according to NLTH method. However, it should be noted that in practice, a Nonlinear Kinematic Analysis (NLKA) has to be executed next to the MRS and NLPO method to overcome the lack of these methods to check the out-of-plane capacity of walls. This NLKA is not performed, because it would not contribute to the objectives of this study.

Table 4.4: Limit State Criteria per Analysis Type

	MRS	NLTH	NLPO
In-Plane Wall Capacity	✓	✓	✓
Out-of-Plane Wall Capacity	X	✓	X
Inter-story Drift	X	✓	✓

It is usually also required to perform checks on the floors and foundation. However, in Chapter 2.2.3 was shown that the failure of floors due to a seismic event is not likely. Thus, this type of failure is not taken into account. Furthermore, failure of the foundation is not taken into account, because the decision was made to scale the seismic signal at ground level. The near collapse limit state criteria which have to be applied according to each analysis method are presented hereafter.

#### MODAL RESPONSE SPECTRUM

The NC limit state criteria which have to be met according to the modal response spectrum method are based on the in-plane capacity of the piers and spandrels. The lateral force in each primary seismic element may not exceed the shear and flexural capacity of that element. Redistribution of forces is not allowed due to the fact that MRS is a linear method.

The capacity checks which have been performed on the piers are prescribed in NPR 9998. The following expression is given to determine capacity  $V_{Rd,s}$  of a pier based on the shear sliding failure mechanism:

$$V_{Rd,s} = f_{vd}D't \quad \text{where} \quad f_{vd} = \frac{f_{vm0}}{\gamma_m} + 0.4 \frac{N}{D't} < 0.065f_m \quad (4.3)$$

where  $D'$  is the width of the compressed area and  $f_{vd}$  is the masonry shear strength taken into account the presence of the vertical load  $N$ . The mean shear strength in the absence of the vertical load is  $f_{vm0}$  and the mean compressive strength is  $f_m$ . The assumption is made for the determination of the shear capacity of a wall that only the compressive zone is able to transfer shear forces.

The flexural capacity is based on the toe-crushing mechanism. The assumption is made that flexural failure of a pier always occurs due to compression in one of its corner and not due to tension in the other corner. Equation 4.4 is given to determine the flexural capacity of a wall. Where  $H_0$  is the distance between the section where the flexural capacity is attained and the contraflexure point, which is equal to the height of each wall if the wall is clamped on both sides.

$$V_{Rd,f} = \frac{DN}{2H_0}(1 - 1.15v_d) \quad \text{where} \quad v_d = \frac{N}{Dtf_m} \quad (4.4)$$

The maximum admissible seismic load acting on the structure according to the MRS method is prescribed in terms of the maximum PGA at ground level of the characteristic seismic load  $E_k$ . The design load  $E_d$  which has to be applied in the model to check if the structure is complying to the characteristic load is determined using Equation 4.5, where  $q$  is the behaviour factor.

$$E_d = \frac{E_k}{q} \quad (4.5)$$

#### NONLINEAR PUSHOVER

Three limit state criteria are prescribed by NPR 9998 for NLPO analyses, which have to be applied when determining the capacity curves. These capacity curves are determined by incrementally increasing the lateral load acting on the structure according to a predefined vertical distribution of the lateral load, until one of the NC limit state criteria are met. NPR 9998 prescribes that at least one uniform and one modal lateral load pattern has to be applied. The uniform distribution is proportional to the mass of the structure, which could be modelled as a uniform acceleration acting on the structure. The modal pattern is based on the lateral force distribution determined with an elastic analysis. This generally is similar to a triangular load pattern based on the governing eigenmode.

The first criterion is the dynamic instability of the structure, which can occur due to the absence of static convergence of an analysis or due to the lack of vertical load bearing capacity of a structure. The second criterion is a strength degradation of 80% with respect to the base shear capacity. The last criterion is an inter-story drift limit. The inter-story drift limit for brittle inelastic mechanisms is equal to 0.6 % and is to 1.5 % for ductile inelastic mechanisms. The inter-story drift has to be determined by dividing the displacement of the top of an pier with respect to the bottom by the height of that pier.

The allowable seismic load according to the NLPO method is determined by evaluating the demand and capacity of a structure. The demand of the structure is defined according to three different methods, namely the Capacity Spectrum method according to NPR 9998, the N2-method according to Eurocode 8 and an adopted N2-method which has been developed for short-period URM structures, according to Guerrini. A description of all these methods can be found in Chapter 3.3.

#### NONLINEAR TIME HISTORY

The limit state criteria for NLTH can be divided into two categories: explicit and indirect checks. Explicit checks are checks which are directly related to the stability of the model, and indirect checks are related to inter-story drift limits. Concerning the explicit checks, the limit state criteria shall not be exceeded in each of the simulations. The capacity of the structural elements is directly taken into account in the material model of the masonry. Exceedance of the capacity of these elements results in the failure of that element. If the failure of this element results in the collapse of the structure, then the global NC limit state is reached. This is the point where the results of the NLTH analysis are diverging. If the assumption is made that all elements are modelled correctly and the analysis properties are correct, then divergence can only occur due to global failure of the structure.

The second type of criteria are the drift limits. The mean of the response of all simulations may not exceed the inter-story drift limits. Drift limits have to be applied during an NLTH analysis because it is deemed difficult to capture post-peak behaviour using the available masonry material models. The drift limits have been introduced to provide an additional upper limit. For example, it could be numerically correct for a wall to reach a high drift limit without collapsing, but the results should not be trusted. NPR 9998 specifies that the same drift limits as for the NLPO method have to be applied.

The maximum admissible seismic load according to the NLTH method is prescribed in terms of the maximum PGA at ground level of the characteristic seismic load  $E_k$  at the moment of failure. The design load  $E_d$  which has to be applied in the model to check if the structure is complying for the characteristic load is determined using:

$$E_d = E_k \times \gamma_n \quad (4.6)$$

where  $\gamma_n$  is a factor relating to the number of ground motion sets used and to the type of limit state criteria applied. The values of  $\gamma_n$  which are specified in the NPR 9998 are presented in Table 4.5. It is important to note that the limit state may not be exceeded in each of the simulations for the explicit checks, while the mean of the response of all simulations may not exceed the inter-story drift limits.

Table 4.5: Values of  $\gamma_n$  according to NPR 9998:2018

	<b>7 Signals</b>	<b>11 Signals</b>
Explicit Checks	1.40	1.25
Indirect Checks	1.10	1.00

#### 4.3.2 COMPARISON STRATEGY: CONTINUUM FEM AND MACRO EFM

The comparison strategy of the studied computational discretisation methods for the NLPO method can be found hereafter. A study of a single case study is performed using a continuum FEM and Macro EFM model. The results of the case study are subsequently evaluated and compared with each other. Based on the comparison is it possible to draw conclusions which in their part can be extrapolated to conclusions for the entire typology of the structure.

The first point of interest is the behaviour of the structure under static conditions, which gives an indication of the stiffness distribution of the structure, and it shows how the gravity and the live loads are transferred to the foundation. The mass of the structure according to both programs can also be determined by this analysis, which gives an indication the loads were introduced correctly. The mass can be determined by summing up the vertical reaction forces.

The second point of interest is the results of the modal eigenvalue analyses. The output of these analyses are the modal shapes, natural periods and modal mass participation of the eigenmodes. These properties indicate the overall behaviour of a structure. Especially the modal shapes are of importance because one of the lateral load patterns applied to the structure according to the NLPO method is based on the model shape of the governing eigenmode.

The next step is to compare the capacity curves according to the two discretisation methods. Characteristics which are of interest are the base shear capacity and the displacement capacity in terms of displacements of the control node. Furthermore, it is also of interest to study the initial slope of the capacity curve, during its elastic branch because it indicates the initial stiffness of the structure.

Moreover, the position and type of inelastic mechanisms are studied. In DIANA this is done by looking into the crack widths, principal stresses and masonry state parameter. Damage in 3MURI is presented by indicating if an element has already surpassed its force or displacement capacity. The displacement profile also provides information about where in the structure the most damage can be expected.

The last step of the comparison strategy is to analyse the maximum allowed seismic load in terms of maximum PGA at ground level. The maximum allowed seismic load is determined according to the NC limit state criteria as prescribed in NPR 9998. However, three different methods are used to determine the maximum seismic load, namely: NPR 9998, Eurocode 8 and Guerrini. The maximum seismic load is determined by incrementally scaling the demand until one of the demand is exceeding the capacity. The demand of the structure is represented by the response spectra which are determined by the NLTH analysis of the soil-block.

#### 4.3.3 COMPARISON STRATEGY: MRS, NLPO AND NLTH

The seismic response of the case study structure is determined, using three different methods, namely MRS, NLPO and NLTH. The comparison of the results of these methods quite a challenge, due to the differences in the methods and due to the fact that different limit state criteria have to be applied for each method. An overview of the differences in methods is presented in table 4.6. The procedure of how the methods are executed and how these differences are taken into account is presented hereafter for each method separately.

Table 4.6: Differences in Seismic Analysis Methods

	<b>Material Properties</b>	<b>Description of Seismic Load</b>
MRS	Linear	Response Spectra
NLPO	Nonlinear	Response Spectra
NLTH	Nonlinear	Time-Dependent Load

The MRS analysis is performed by using a fixed base model. A difference with the NLPO and NLTH analyses is that linear material properties have to be applied. These linear material properties are based on the cracked stiffness properties, as prescribed by NPR 9998. The seismic load is represented by response spectra, which are determined by an NLTH analysis of a representative soil-block. The method of how the response spectra are determined is described in Chapter 4.3.4. The MRS analysis is executed in the longitudinal and transverse direction separately. The response spectra are linearly scaled until one of the limit state criteria is exceeded.

The NLPO analysis is executed by using a fixed base model with nonlinear material properties. The demand and the capacity of a structure are defined separately. The capacity of the structure is defined in terms of capacity curves. These capacity curves are determined by incrementally loading the structure until one of the limit state criteria is met. The structure is loaded by applying a predefined vertical distribution of the lateral load. Two different lateral load patterns are taken into account, which are a uniform distribution and a distribution based on the shape of the governing eigenmode. The demand is defined in terms of response spectra, which are determined by an NLTH analysis of a representative soil-block. The method of how the response spectra are determined is described in Chapter 4.3.4. Subsequently, the target displacement is determined using three different methods, namely: the Capacity Spectrum method according to NPR 9998, the N2-method according to Eurocode 8 and an adopted N2-method which has been developed for short-period URM structures, according to Guerrini. The demand is linearly scaled until the target displacement and the displacement capacity are equal.

The NLTH analysis is performed by using a model with nonlinear material properties, where the seismic load is introduced as a time-dependent load at a depth of 30 meters. The seismic is applied in the longitudinal, transverse and vertical direction simultaneously. An incremental dynamic approach is applied, in which the multiple NLTH analyses are performed, each scaled to several levels of seismic intensity. The seismic signals are scaled at ground level.

Based on the aforementioned differences in methods, the following comparison strategy has been defined. The first point of interest is the maximum admissible seismic load according to the methods. The maximum admissible seismic load is defined as the load at which the near collapse (NC) one of the limit state criteria is exceeded, according to NPR 9998. However, it should be mentioned that each method requires a different way to achieve this scope. The maximum admissible seismic load is found by incrementally scaling the seismic load until one of the limit state criteria is exceeded. The maximum admissible seismic load is expressed in terms of PGA at ground level.

Furthermore, the force-displacement behaviour according to the various analyses is also of interest. The force-displacement behaviour is represented by plotting the base shear versus the displacement of the roof of the structure. This results in a straight line for the MRS analyses because it is a linear analysis. The force-displacement behaviour according to the NLPO method is represented by the capacity curves. The force-displacement behaviour according to the NLTH analyses is captured by performing multiple NLTH analyses for several magnitudes of the seismic load. The maximum predicted displacement and corresponding base shear of each of these analyses is subsequently determined. By plotting these points in a graph, it is possible to formulate a capacity curve for each studied signal.

The last step is to look into the inelastic mechanisms which occur and the failure mechanisms. This is done by looking into the displacement pattern over the height of the structure at the moment of failure and by looking into damage parameters like occurring crack widths and the masonry status parameters from the engineering masonry model. It should be noted that the failure mechanism can be determined for each analysis method, but the inelastic mechanisms can only be determined for the nonlinear methods since the evolution of damage does not occur when linear material properties are applied.

#### 4.3.4 REPRESENTATION OF THE SEISMIC LOAD

The seismic load for the NLTH method is introduced as a time-dependent load at a depth of 30 meters, while for the MRS and NLPO methods the seismic load is introduced using response spectra at ground level. Thus, it is necessary to make these two ways of representing a seismic load as equivalent as possible. It should be noted that it is not possible to make these two methods completely equivalent, because some properties of an NLTH load are lost when creating a spectrum. For example, the hysteretic aspect of a real seismic load is lost in a spectrum, because only the maximum response of an SDF system is represented with response spectra. It is possible though, to formulate a ground motion spectrum at ground level, based on the results of a seismic load which is applied at a depth of 30 meters.

Seven representative ground motion signals for Groningen, based on NPR 9998:2015 spectra, have been developed by ARUP (2016). These ground motions are intended to be applied at a depth of 30 meters. The ground motion signals are based on seven real earthquake signals, which have been selected taking into account the project area specific attributes. These signals are matched and processed so that they are suitable for analysis, by matching the signals in such a way, that the response spectra at ground level due to these signals match the response spectra as defined in NPR 9998:2015.

These horizontal signals are introduced at the bottom of the soil column in the transverse, longitudinal and vertical direction. The accelerations at ground level caused by these signals are measured. It is possible to determine the response spectra based on the measured accelerations at ground level, by applying the measured acceleration signals to several SDoF systems, from which the natural period of the SDoF systems is incrementally increased. It should be noted that the viscous damping of these SDoF systems is kept constant at 5%. By doing so, it is possible to determine the maximum response of the SDoF systems, due to the accelerations of the soil at ground level. The outer envelope of the response spectra of the seven signals is used as input for the MRS and NLPO analyses. The results of this methodology are presented in appendix F.1.

### 4.4 LIMITATIONS OF CASE STUDY

Several limitations of the aforementioned comparison strategy have to be taken into account. It is important to note that the possible influence of these assumptions, may partially limit the extent of the conclusions. Some limitations are inherent to the methods and some are related to the modelling assumptions which were made.

#### 4.4.1 LIMITATIONS INHERENT TO SEISMIC ANALYSIS METHODS

The horizontal seismic load applied in the NLTH analysis is of a bilateral nature, while MRS and NLPO study each direction separately. As a consequence, it is possible that damage which occurs due to the seismic load in one direction, might influence the behaviour of the structure in the other direction, which is not accounted for in MRS and NLPO. Furthermore, the vertical component of the seismic load is not taken into account in the MRS and NLPO method. This vertical component of the seismic load could have a weakening effect, especially on structures in which the connections are friction based. Moreover, the axial load in a pier has a significant influence on the capacity of that pier, which varies during an NLTH analysis, but is constant in MRS and NLPO analyses.

Furthermore, hysteretic effects taken into account in an NLTH analysis, which are cannot be captured with MRS and NLPO. Hysteretic effects which influence the behaviour of a structure significantly are viscous damping and energy dissipation.

Moreover, the uncracked stiffness properties of masonry have to be applied in the nonlinear analyses, while the cracked stiffness properties are applied for the MRS analysis. As a consequence, the initial stiffness and natural periods according to the methods will be different.

#### 4.4.2 LIMITATIONS MODELLING ASSUMPTIONS

Next to the limitations which are inherent to the methods, also several modelling assumptions could have a significant effect on the results. First, the seismic signals which are applied for the NLTH analysis are based on seven real earthquake signals, which have been matched and processed in a way that the response spectra at ground level due to these signals match the response spectra as defined in NPR 9998:2015. However, the choice and duration of these signals are not prescribed by the NPR 9998, and a different set of signals could lead to different results. Second, the seismic signals have been scaled at ground level and SSI effects are not taken into account in the NLTH analysis as a consequence. These SSI effects could have a positive effect on the seismic resistance of a structure according to the NLTH method.

Concerning the 3MURI model, several assumptions which were made in the approach might have influenced the results. Several structural elements which were modelled in DIANA were not modelled in 3MURI due to limitations of the program, which could result in a different behaviour of the structure. Second, the assumption is made that the modelling approach provides accurate results for both the NLPO analysis in DIANA and 3MURI. Extensive research has been performed by VIIA on the effects of the modelling assumptions in the DIANA model, while such research has not been performed concerning 3MURI. Thus, no guarantee can be given that the assumptions in 3MURI are able to describe the behaviour of the structure accurately.

Furthermore, the engineering masonry model is applied in DIANA and the 3MURI macro-element model is used in 3MURI. However, the choice of these material models for masonry are not prescribed by the NPR 9998 and the choice of a different material model, could significantly influence the results.

Ultimately, the decision has been made to only study a single structure and the assumption is made that the results of the case study can be generally applied to the entire typology. However, it must be noted that significant alterations in geometry and building materials might influence the results. For example, higher mode effects could become relevant if the wall configuration is more irregular compared to the case study, which are difficult to capture with an NLPO analysis. Furthermore, the results of the NLPO method generally less reliable for structures with flexible diaphragms, and only rigid diaphragms were considered in the case study.

## MODEL AND SETUP

---

The characteristics of the DIANA and 3MURI models are described in this chapter. The description of the DIANA model is subdivided into four parts. First, the characteristics of the DIANA model which are relevant for all analyses are elaborated. The changes that have been to this general model to make the model suitable to perform an MRS, NLPO or NLTH analysis with respectively are presented afterwards. A description of how the analyses are performed can also be found. The characteristics of the 3MURI model can be found in the last section of the chapter. All properties of the models are briefly explained in this chapter, to keep this chapter as organised as possible. A more elaborate description and tables with all relevant material properties can be found in Appendix D. Ultimately, validation checks of the DIANA and 3MURI modal are presented.

### 5.1 DIANA CONTINUUM FEM MODEL

A DIANA model is used to perform the NLTH, NLPO and MRS analyses. It should be noted that an NLTH analysis has already been performed of the studied structure by an engineer within Royal HaskoningDHV. The model used for this analysis is used as a basis for all performed analyses in DIANA. It is mentioned in the report which parts of the case study are not the work of the author of this document. This chapter is subdivided into four parts. First, the characteristics of the DIANA model which are relevant for all analyses are elaborated. The changes that have been made to this general model to make the model applicable to the studied analyses are presented afterwards.

#### 5.1.1 GENERAL MODEL

The characteristics of the model described in this chapter are used for the MRS, NLTH and NLTH analyses. It should be noted that the entire general model has not been created by the author of this study. All material properties have been taken from NPR 9998 or derived from studies done by VIIA.

## WALLS

The wall configuration in DIANA of the second floor is presented in Figure 5.1. The same wall configuration can also be found on all other floors. All walls have been modelled using two-dimensional shell elements (T15SH/Q20SH). These are curved shell element which follows the Mindlin-Reissner theory. The elements are based on linear interpolation and Gauss integration over the element area. It should be noted that the inner and outer leaf of the cavity walls are modelled separately. The material model which is used is the engineering masonry model, as described in Chapter 2.4.1. The applied material properties for calcium silicate and clay brick respectively, can be found in the appendices in Table D.1, which are prescribed in NPR 9998.

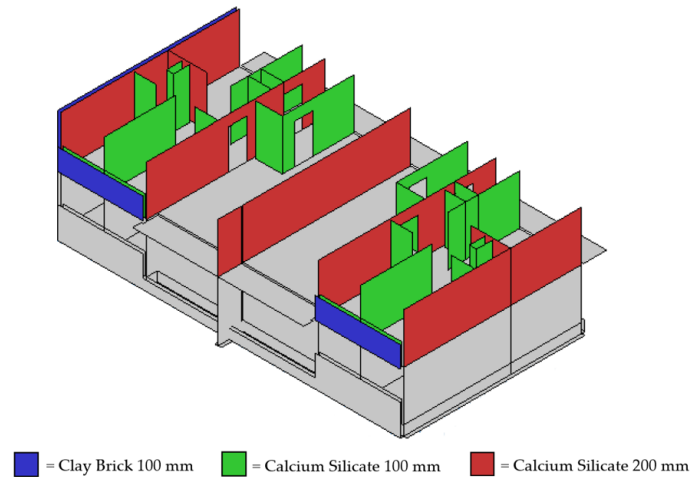


Figure 5.1: Walls Configuration in DIANA

Two types of connections between walls can be found in the structure. Those where the connection is continuously bonded and those where a small gap can be found between the walls which is filled by mortar. The type of connection has a considerable influence on the behaviour of a wall. The connection between the two walls is modelled as a closed connection without a special interface element if the walls are continuously bonded. Special interface elements are used to model the connection if the connection is not continuously bonded. These interface elements are only able to transfer compressional forces in the normal direction. Shear and tension forces cannot be transferred through these elements. The position of these nonlinear elements is presented in Figure 5.2. It should be noted that these elements can be found on all floors.

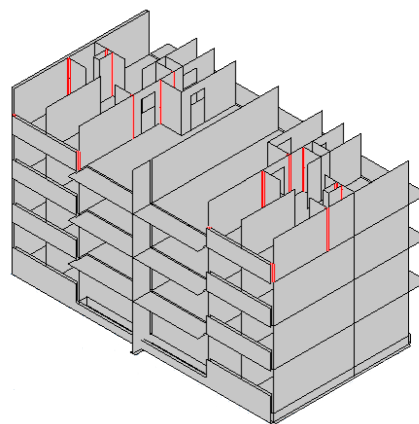


Figure 5.2: Nonlinear Line Interfaces on the Fourth Floor

It is not required to apply interface in the connection between the floors and walls, due to the fact that the assumption is made that the strength of the connection has the same capacity as the bed joints of the wall. Thus it is not deemed necessary to model the connection using non-linear interface elements.

#### ANCHORS

The inner and outer leaf of the cavity walls are connected by anchors. These anchors are modelled using 2-node spring elements (SP2TR) which can only transfer forces in the normal direction. The capacity of these anchors depends on the distance between the two leaves. An elasto-plastic behaviour is assumed where the springs deform linearly until it reaches its capacity. The stiffness in the plastic range is assumed to be zero. The anchors are not able to transfer shear forces. The mechanical behaviour of these anchors is presented in Figure 5.3.

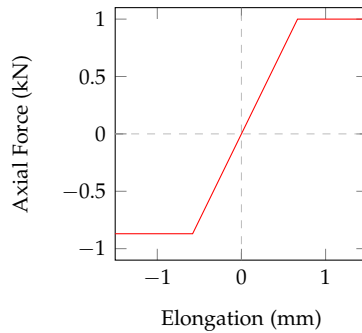


Figure 5.3: Force-Elongation Behaviour of Anchors

#### FLOORS

The floors are modelled with the same shells elements as the walls. The first floor is a ribbed floor. This floor is modelled with linear orthotropic material properties. The floor has to be modelled with these orthotropic properties because the joints are hardly able to transfer shear stresses and the Young's modulus differs per direction. An example of a ribbed floor and the chosen coordinate system is shown in Figure 5.4. The connection between the walls and floor is a continuous one. Thus the floor is able to transfer moments to the wall. All other floors and the roof are massive concrete walls with a thickness of 150 millimetres. They are modelled using linear concrete properties. The material properties of the ribbed floor and the linear concrete can be found in the appendices in Table D.2 and Table D.3 respectively.

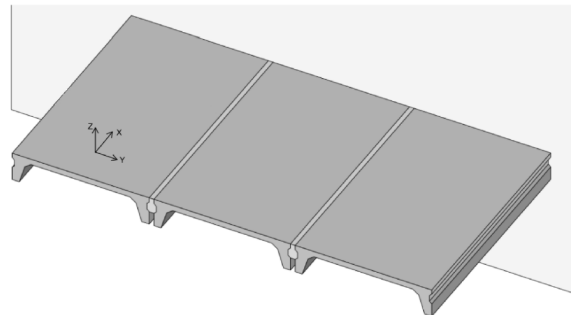


Figure 5.4: Coordinate System Ribbed Floor  
Source: VIIA (2017b)

## GALLERIES AND BALCONIES

Galleries and balconies can be found on the front and back of the structure. They are supported by concrete beams, which in their part are supported by the walls. The galleries are modelled with the same shell elements as were used for the floors. The concrete beams are modelled with two-node, three-dimensional beam elements (L12BEA). These are fully numerical integrated Mindlin beam elements which follow a 1-point Gauss integration scheme along the bar axis. Linear concrete is used for both elements, for which the material properties can be found in the appendices in Table D.2. The position of these beams is shown in Figure 5.5.

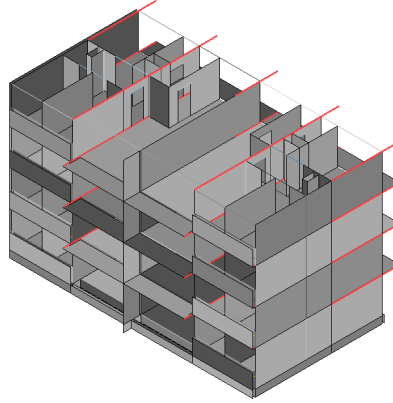


Figure 5.5: Concrete Beams in DIANA model

## LOADS

Surface loads acting on the floors are taken into account by increasing the density of the floors on which the load is acting. The applied densities in DIANA are shown in Table D.6. The weight of the windows, the facade and internal walls which are not modelled are taken into account by applying line loads. The magnitude of these line-loads is described by VIIA (2017b). Two different magnitudes of line-loads are applied in the model, those of  $0.55 \text{ kN/m}$ , which represent the doors and  $0.7 \text{ kN/m}$  which represent the glass in the facade. The position where those line-masses are applied is shown in Figure 5.6.

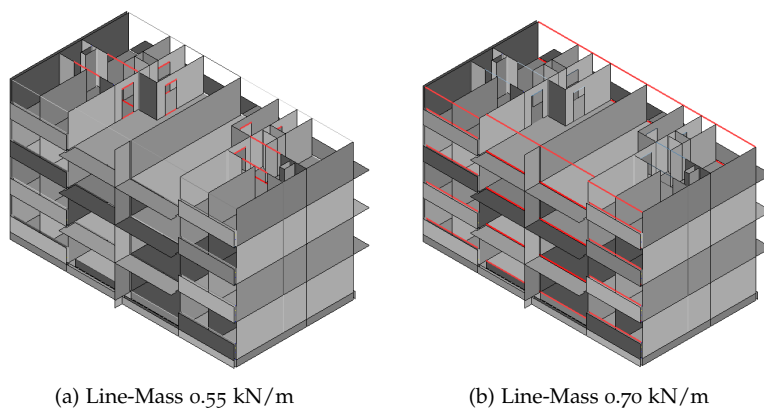


Figure 5.6: Applied Line-Masses in DIANA

### 5.1.2 MODAL RESPONSE SPECTRUM ANALYSIS

Two measures need to be taken, to transform the general DIANA model to a model which is suitable for an MRS analysis. First, all non-linear material properties need to be made linear. Second, the seismic load according to MRS standards need to be applied.

#### LINEAR MATERIAL PROPERTIES

The only nonlinear elements in the structure are the masonry walls and nonlinear interface elements which connect the walls to each other. NPR 9998 specifies that the cracked properties of masonry should be applied for an MRS analysis. It is also specified that the stiffness properties of cracked masonry, may be taken as half of the uncracked masonry properties. The properties of the cracked masonry are presented in appendices in Table D.7. The properties of the nonlinear interface elements have been adjusted in such a way, that they are not able to transfer any forces any more. This has been done by changing the stiffness of the elements to a neglectable small value.

#### SEISMIC LOAD

The seismic load for an MRS analysis is applied as a base excitation. This base excitation will be amplified per eigenmode based on a modal response spectrum. A design modal response spectrum has to be used. This spectrum can be determined by dividing the elastic spectrum by the behaviour factor  $q$ . This behaviour factor is specified in NPR 9998 to be equal to 1.5 for unreinforced masonry. It is also specified that it is allowed to multiply this factor by 1.33 for horizontal excitations when checking the structure according to the NC limit state criteria. This results in a behaviour factor of 2.

#### ANALYSIS PARAMETERS

A model response analysis is a built-in option in DIANA. Parameters which have to be defined for this analysis is the response spectrum, the number of eigenmodes that have to be considered, the modal superposition method and the modal damping coefficient. The number of eigenmodes that have to be taken into account is based on regulations as specified in the NPR 9998. It is specified that the sum of the modal mass participation of the eigenmodes, should be at least 90 %. In Chapter G.2 is shown that this is the case if 450 eigenmodes are taken into account. Furthermore, the CQC method is chosen as the modal superposition method, because in Chapter 3.1.3 was shown that this method also provides reliable results if the modes are not well separated from each other. The modal damping coefficient that is taken into account is 5%, which is the value as is prescribed in the NPR 9998. An overview of all relevant analysis parameters is presented in Figure 5.1. A reference is added to a chapter or an appendix where extra information can be found, with respect to each analyses parameter.

Table 5.1: MRS Analysis Parameters

Analysis Settings	Applied in Model	Reference
No of Eigenmodes	450	Chapter 5.3.1
Behaviour Factor	2.00	Chapter 3.1.2
Modal Superposition	CQC	Chapter 3.1.3
Modal Damping Coefficient	5%	-

### 5.1.3 NONLINEAR PUSHOVER ANALYSIS

The only measure that is required to make the general model applicable for an NLPO analysis is to apply the lateral loads. Two different lateral load patterns are required namely a uniform and a model load pattern. Capacity curves need to be determined in both the longitudinal and transverse direction and the positive and negative direction. Thus in total, there are eight different load cases.

#### LATERAL LOAD PATTERNS

The lateral load patterns are applied by adding a load in terms of accelerations to the structure. Two different load patterns of the applied accelerations are applied. The first load pattern is a uniform load, which is applied by applying an acceleration which is constant over the height of the structure. The second load is a load pattern which is based on the governing eigenmode of the structure. This load is applied by using the built-in modal pushover analysis function in DIANA. The shape of the governing eigenmodes is determined by performing a modal eigenvalue analysis, from which the results are presented in Chapter 5.3.1. The shape of the governing eigenmode in the longitudinal and transverse direction is presented in Figure 5.7.

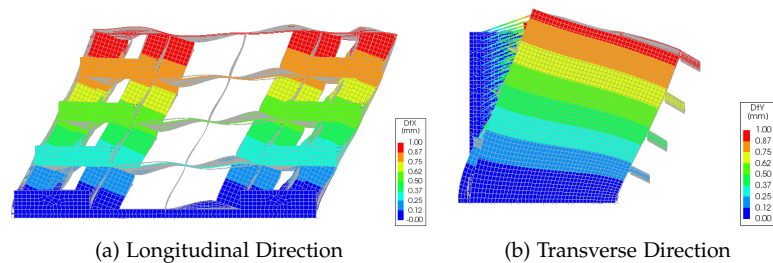


Figure 5.7: Governing Eigenmodes according to DIANA

#### ANALYSIS PARAMETERS

Parameters which have to be defined for an NLPO analysis in DIANA are the iterative method, the type and magnitude of the convergence norm, the arc length control method, the type of nonlinearities which are taken into account, the maximum number of iterations and the load step size. The secant method is chosen as the iterative method, for which a description can be found in Appendix B.1. The advantage of the secant method compared to the regular Newton-Raphson method is that the stiffness matrix does not have to be updated every iteration, which saves time. However, it should be mentioned that more iterations are required due to the lower convergence rate. Furthermore, the advantage over the linear stiffness method is that fewer iterations are required. The convergence norm was chosen to be energy because both the out of balance force and relative displacements are taken into account. A convergence norm of  $10^{-4}$  was chosen based on common practice. A force-controlled pushover analysis is executed, and in general, it is difficult for DIANA to find convergence during a force controlled pushover analysis because the load-displacement curve could become horizontal and could even decline.

Arc length control is applied during the analysis to overcome this difficulty, where the type of arc length control method is the spherical path method. However, it should be mentioned that the updated normal plane method has also been experimented with, and it did not influence the results. More information about the arc length control method can be found in Appendix B.3. The nonlinearities which are taken into account are physical and geometrical nonlinearities. The size of the load step has been chosen together with the maximum number of iterations. Both parameters have been iteratively varied until the convergence norm was met for almost all iterations. An overview of all analysis parameters for the performed NLPO analyses is presented in Table 5.2. A reference is added to a chapter or an appendix where extra information can be found, with respect to each analyses parameter.

Table 5.2: NLPO Analysis Parameters

Analysis Settings	Applied in Model	Reference
Iterative Method	Secant	Appendix B.1
Convergence Norm	Energy	Appendix B.2
Arc Length Control	Spherical Path	Appendix B.3
Nonlinear effects	Phys, Geo	-
Maximum no. of iterations	20	-
Convergence Tolerance	$10^{-4}$	-
Abort criterion	10000	-
Load step size	0.1 m/s <sup>2</sup>	-

#### 5.1.4 NONLINEAR TIME HISTORY ANALYSIS

Several measures are required to make the general model suitable for an NLTH analysis. Elements which have to be added are foundation strips, foundation piles and the soil-block. The seismic load is applied to the bottom of this soil-block using dampers and springs.

##### FOUNDATION

The foundation of the building consists of concrete prefab piles which are attached to the concrete foundation strips. The foundation strips are modelled with a linear concrete model for which the material can be found in the appendices in Table D.2. The foundation piles are modelled as embedded beam elements in the soil-block, for which the properties can be found in the appendices in Table D.4. Both the properties of the pile and the interface between the pile and the soil-block are defined by these properties.

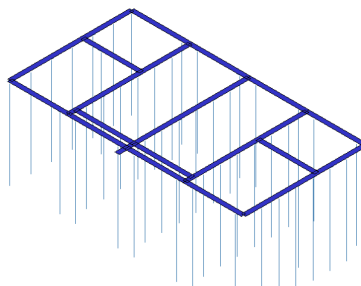


Figure 5.8: Foundation Strips and Piles in DIANA

The connection of the pile and the foundation strips is modelled by a set of springs, an additional 1D beam element and a tying. An overview of all the elements is presented in Figure 5.9. The tying, as indicated with, has the sole purpose of increasing the numerical stability of the model. While the springs, as indicated with E, and the additional 1D element, as indicated with B, are used to model the failure mechanisms of the structure. The spring elements deform linearly elastically until they reach a specific critical value of the internal load, after which the stiffness of the elements becomes zero. The additional 1D element is modelled using a nonlinear concrete model. Failure of the foundation is not considered in this report. Thus the properties of the springs have been adjusted in such a way, that failure of the foundation cannot occur. This is done by assigning a capacity of the piles which can never be reached. It should be noted that the properties of the piles and the connection of the piles and the foundation have a significant influence on the behaviour of a structure due to a seismic event and a proper selection of these properties quite a challenge. However, due to the fact that failure of the foundation and soil structure interaction is considered outside of the scope of this report, these properties are not studied more in detail. The used properties are based on extensive research that has been performed by VIIA, and the assumption is made that using these properties results in a realistic behaviour of the foundation.

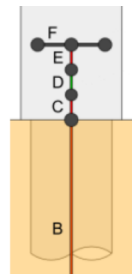


Figure 5.9: Connection Pile and Foundation Strip

Source: VIIA (2017b)

#### SOIL

The soil-block is modelled until a depth of 30 meters because reference accelerations are given at this depth. Due to the relatively high amount of elements required to model this soil-block was chosen to replace part of the soil-block by a smaller small soil-column. This can be done because the sole purpose of the soil at a depth of approximately 5 to 30 meter is to determine the influence of the soil, on possible amplification or damping of certain frequencies of the ground motion signal. It should be noted though that the properties of this soil-column should be equivalent of the part of the ground block that it replaces. How this is done is outside the scope of this study, but an elaboration of this method can be found in VIIA (2017a). In Figure 5.10 is shown how the soil-block and column are modelled.

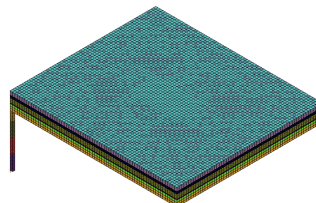


Figure 5.10: Soil-Block and Soil-Column in DIANA

## SEISMIC LOAD

There are two different methods prescribed in the NPR 9998 for executing an NLTH analysis, namely the direct and indirect method. The differences between these types of analysis are elaborated in Chapter 3.4.3. The decision has been made to perform the analysis using the indirect method. This is mostly due to the fact that the computational time can significantly be decreased using this method. The following steps have been taken to execute these analyses. The first step is to change the nonlinear DIANA model in such a way that the material properties of the structure become linear. The material properties of the soil are still nonlinear. Seven NLTH analyses are subsequently executed, one for each seismic signals. The results of these analyses are the forces and velocities at the top of the foundation piles. The position on where this data is extracted is at the bottom node of the springs as indicated with an E in Figure 5.10. The next step is to create a new model based on the original nonlinear model. However, all elements underneath the nodes in which the results were extracted are removed from this model. Thus, the soil-block, soil-column and foundation piles are not included any more. Furthermore, springs and dampers are added to the model, which represent the behaviour of the upper layer of the soil. The last step is to apply loads to all these springs and dampers, which represent the forces and velocities which were measures during the previous steps. Thus by doing so, it is possible to represent a seismic signal at a depth of 30 meters, by several loads underneath the top node of the foundation piles. These loads applied to the foundation are subsequently linearly scaled, to determine the response of the structure, for different magnitudes of the load. It should be noted that when the seismic signal at ground level scaled is scaled by a certain scaling factor, then the PGA at ground level that corresponds to that seismic load is equal to the PGA of the original seismic load times the scaling factor.

## ANALYSIS PARAMETERS

Most of the analysis parameters which are used for the NLTH analysis are the same as for the NLPO analysis and also the same reasoning could be applied. For example, the iterative method, the type of convergence norm and the convergence tolerance are the same. The Newmark method is used as the time integration method, and Rayleigh damping is applied. An elaboration of these methods can be found in Appendix 3.4.1 and Chapter 3.4.2 respectively. The use of these parameters is based on common practice. The same nonlinear effects are taken into account as for the NLPO method. However, transient effects are also taken into account. The step size is based on the fact that the minimum frequency of the seismic load is smaller than 15 Hz a minimum of six time steps is required to capture a time step with linear steps. The minimum step size can subsequently be determined, by dividing the frequency by the minimum amount of steps that are required.

Table 5.3: NLTH Analysis Parameters

Analysis Settings	Applied in Model	Reference
Damping	Rayleigh	Chapter 3.4.2
Time Intergration Method	Newmark	Chapter 3.4.1
Iterative Method	Secant	Appendix B.1
Convergence Norm	Energy	Appendix B.2
Nonlinear effects	Phys, Geo, Trans	-
Maximum no. of iterations	10	-
Convergence Tolerance	$10^{-4}$	-
Abort criterion	10000	-
Step size	0.01 s	-
No. of steps	1050	-

## 5.2 3MURI MACRO EFM MODEL

A 3MURI model is used to perform an NLPO analysis using the equivalent frame method. It should be noted that the modelling possibilities are way more limited compared to DIANA. Thus several modelling solutions have to be performed, to create an as equivalent model as possible compared to DIANA. These modelling solutions are related to the walls of the structure and to additional loads that have been added, to replace elements which could not be modelled.

### WALLS

It is not possible to model cavity walls in 3MURI. This the decision has been made to leave out the outer leaf of the cavity wall, which can be found at the side of the structure. No measures were taken to find an equivalent way to include this outer leaf. It is also not possible to model the walls in the façade of the structure, due to the fact that 3MURI is not able to find convergence if the gap between a wall and the floor above is too large. A similar kind of problem occurred for openings between internal walls, where the walls are not connected to each other by spandrels. Dummy walls have been added in these openings and at the front and back of the façade to solve the convergence problems. The properties have been chosen in such a way that they do not affect the global behaviour of the structure. Material properties of the dummy wall can be found in appendices in Table D.10. The configuration of all modelled walls on the first floor 3MURI model is shown in Figure 5.11. The same wall configuration is repeated for all other floors.

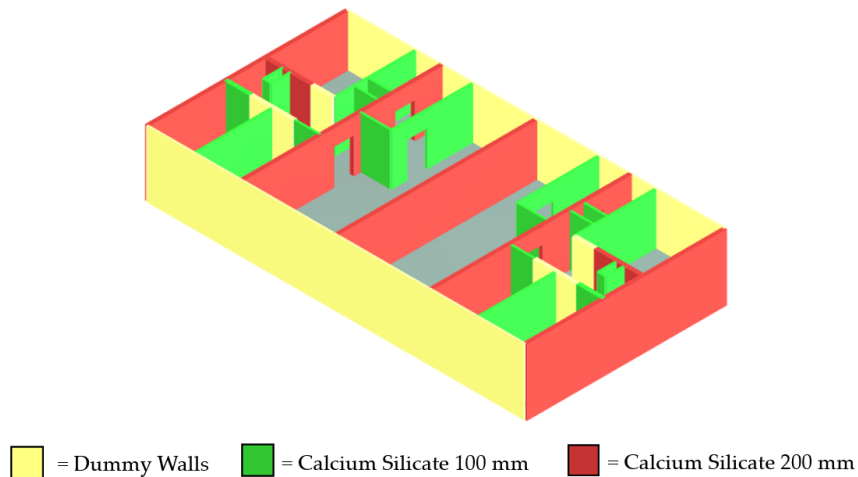


Figure 5.11: Walls Configuration in 3MURI

It should also be noted that the masonry of the walls can be modelled using two different kinds of shear failure criterion. Mohr-Coulomb could be used, which represents shear sliding and Turnsec-Cacovic, which represents diagonal shear failure. The capacity curves using both criteria will be analysed, from which the one with the lowest capacity will be studied more in detail.

## EQUIVALENT STATIC LOADS

It is not possible to model several elements in 3MURI, which were modelled in DIANA, due to the limitations of the program. The elements which could not be taken into account are the outer leaves of the cavity wall in the façade, the galleries, the extension of the roof above the galleries, the balconies and the concrete beams. All of these elements do not contribute to the global seismic capacity of the structure, but the mass of these elements has to be taken into account for determining the seismic response of the structure. The mass these elements is calculated first and subsequently applied to the structure in 3MURI. The mass of the concrete beams is added as a line load, acting on the walls. All other loads are applied as point loads acting on the edge of the walls. Some of these loads would have normally be applied to the floor, but it only possible in 3MURI to apply point loads directly to the walls. The positions of were the additional loads have been applied have been assigned with an identification number, as shown in Figure 5.12.

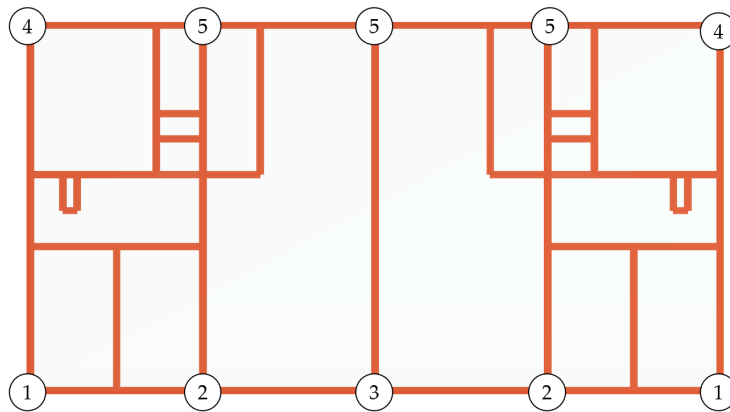


Figure 5.12: Equivalent loads in 3MURI

The magnitude of the point load differs per position and floor level. The numbering convention which is used for the floor levels can be found in Appendix C. The loads acting on floor 1, 2 and 3 are the same for each floor. The point loads are determined by multiplying the line loads with the length over which the load is acting, and subsequently dividing this load over the walls which are the closest to this line load. Different loads are determined for five positions. A summary of all the equivalent point loads which are applied to the model are shown in Table 5.4. An elaboration of how the load on each position is determined can be found in Appendix D.3.2.

Table 5.4: Equivalent Loads in 3MURI

	Ground Floor	Floor 2,3,4	Roof	Unit
Position 1	7.30	7.30	1.15	kN
Position 2	8.95	25.8	3.30	kN
Position 3	3.30	36.4	3.30	kN
Position 4	1.65	18.5	16.1	kN
Position 5	3.30	37.0	32.2	kN

Furthermore, it is not possible in 3MURI to assign a density to the floors in 3MURI. Thus equivalent surface loads have been determined to model the own weight of the floors. These densities have been determined by dividing the densities of the floors which are applied in DIANA, by the thickness of each floor. The results of this calculation are presented in Table 5.5.

Table 5.5: Surface Loads in 3MURI

Element	Value	Unit
Roof	4.27	kN/m <sup>2</sup>
Floor 1,2,3	4.97	kN/m <sup>2</sup>
Ground Floor	3.97	kN/m <sup>2</sup>

### 5.3 MODEL CHECKS

The DIANA and 3MURI model are validated in this chapter. This is done by first looking into the results of a modal eigenvalue analysis. Subsequently, an analysis under static conditions is performed to check if the deformations and the internal forces throughout the structure are as they should be. The modal mass participation provides a method for judging the significance of each eigenmode.

#### 5.3.1 MODAL EIGENVALUE ANALYSIS

A modal eigenvalue analysis is performed to find the eigenmodes of the structure. Important properties of the eigenmodes are the natural period, shape and the modal mass participation. The modal eigenvalue analysis would give a good indication if any modelling mistakes were made in the geometry of the structure. Furthermore, a modal eigenvalue analysis also provides a good indication if any mistakes were made in the geometry and connections in the structure.

#### GOVERNING EIGENMODES

The governing eigenmodes of the structure according to DIANA are presented in Figure 5.13. The natural period and modal mass participation are shown in the caption of the figure. It is clear that both the eigenmodes are typical sway modes. Furthermore, the fact that DIANA is able to execute the modal eigenvalue analysis is an indication that all elements are properly connected to each other.

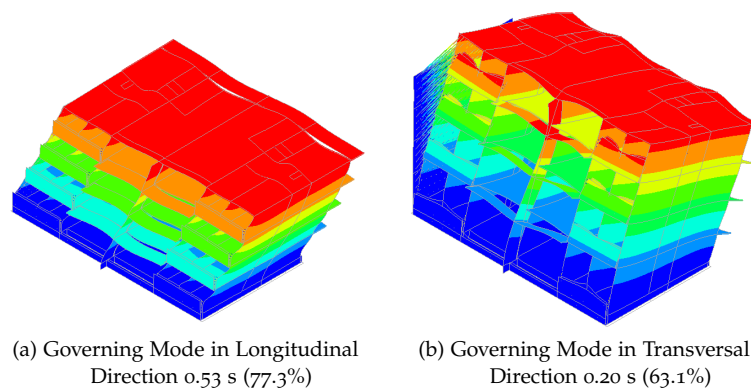


Figure 5.13: Governing Eigenmodes according to DIANA

The governing eigenmodes according to the 3MURI model are shown in Figure 5.14. Due to the fact that it is not possible to obtain three-dimensional images of the eigenmodes in 3MURI, it is chosen to show the top view of the model. The black lines indicate the original position of the walls at the top of the structure. The purple lines indicate the deformation of the top walls of the structure, which correspond to the eigenmode. It can clearly be seen that two typical sway modes are occurring, similar to the ones in DIANA. The natural period and the modal mass participation is comparable to that of the results of the DIANA model.

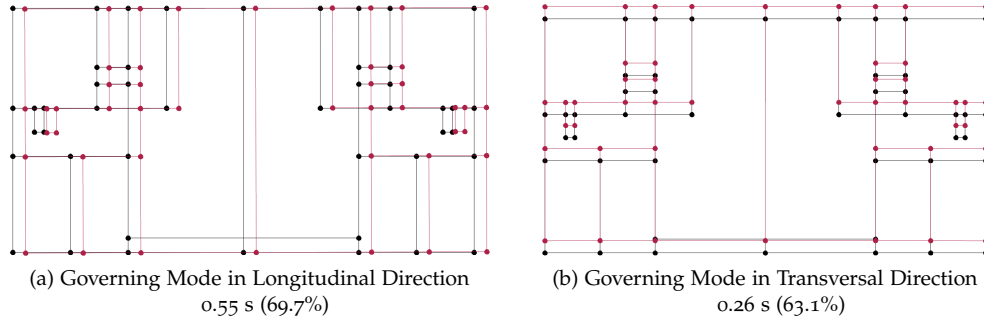


Figure 5.14: Governing Eigenmodes according to 3MURI

Not only the natural period of the structure and modal mass participation of the structure is of importance, but also the modal shapes. The modal shape indicates in which way a structure is most likely going to deform due to a dynamic load. The modal shapes are also used directly as input in the MRS and NLPO method because the load is applied in these shapes. The modal shape of the governing eigenmode in each direction are shown in Figure 5.15. These modes are presented by showing the normalised displacement of each floor, where the normalised displacement is determined by dividing the displacement of each floor by the displacement of the top roof. It can be seen that the modal shapes in the transverse direction are almost the same in 3MURI and DIANA. The modal shapes in the longitudinal direction are slightly different in both programs. The displacement is more localised on the first floor in 3MURI in comparison with DIANA. Thus a weak floor mechanism of the first floor is more likely to occur in 3MURI.

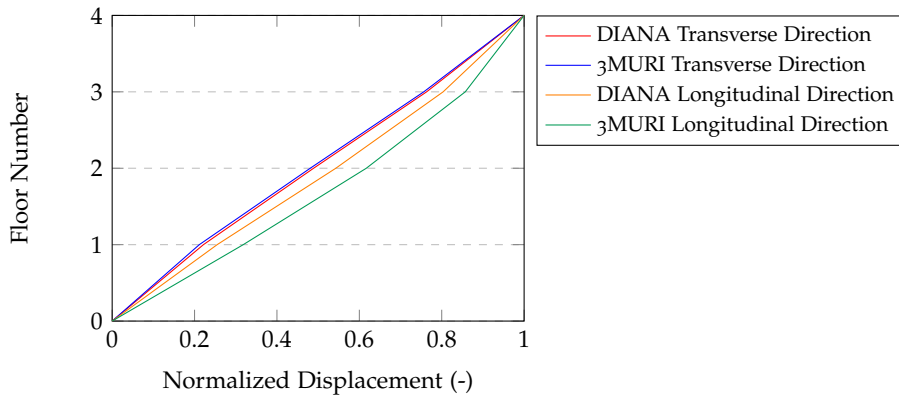


Figure 5.15: Shape Governing Eigenmode per Load Case

## 5.3.2 ANALYSIS UNDER STATIC CONDITIONS

Analyses under static conditions are performed in DIANA and 3MURI to validate both models and to compare the results with each other. Aspects which can be studied after a static analysis are the deformations, internal forces and reaction forces. The analyses are performed by applying the dead weight and live loads to the structure. The output of the static analysis in DIANA are deformations, internal forces and reaction forces. The only available output of a static analysis in 3MURI are internal forces and reaction forces. It is not possible to extract the deformations from the static analysis.

## DEFORMATIONS

The deformations in the longitudinal, transverse and vertical direction, due to the gravity loads, are presented in Figure 5.16. All occurring deformations follow a displacement pattern which can be explained. The deformations in the horizontal directions and are all relatively small. This is due to the fact that only loads are applied to the structure in the vertical direction. The centre of mass in the longitudinal direction is exactly in the middle, due to the fact that the structure is symmetric in that direction. Thus the resultant the dead weight does not have an arm with respect to the centre of the structure. Thus the deformations in the longitudinal direction are the same everywhere in the structure. This is not the case for the deformations in the transverse direction. The centre of mass in the transverse direction is slightly positioned to the side with the gallery. A moment occurs due to the eccentricity of the dead load with respect to the centre of the structure. Thus deformations occur in the transverse direction, to the side with the galleries. When looking at the deformations in the vertical direction, can clearly be seen that the highest deformations occur in the galleries. This is due to the fact that the galleries are cantilevers. Another important aspect for the deformations in all directions is that the deformations are equal to zero at the location of the supports. Based on the deformations can be concluded that all elements are properly connected and that the dead loads are applied in the correct direction. It is not possible in 3MURI to view the deformations on a static analysis.

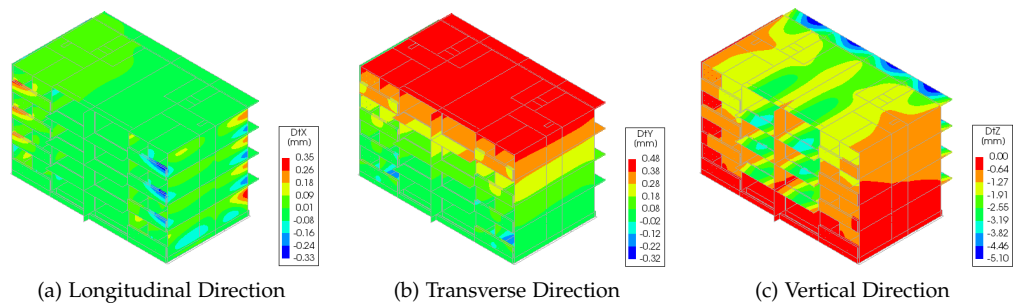


Figure 5.16: Deformations according to DIANA

## INTERNAL FORCES

The internal forces of the static analysis can be extracted from DIANA and 3MURI. It makes sense to check the reaction forces first, before comparing the internal forces, to check if the magnitude of the total load is the same in both models. The mass of the structure including live loads according to both programs is shown in Table 5.6. The mass of the structure in DIANA is determined by adding up all the vertical reaction forces, and the mass in 3MURI is determined by adding up all the internal forces at the bottom of all walls.

Table 5.6: Mass of Structure according to DIANA and 3MURI

	DIANA	3MURI	Unit
Mass Structure	9834	9786	kN

The next step is to compare the internal forces from both models. The internal forces are presented in DIANA by showing the distributed forces over the width of the wall. The distributed internal vertical force is shown in Figure 5.17. From the image can be seen that the compressive forces increase from the top to the bottom of the structure, which is an indication that the dead weight and live loads are applied correctly.

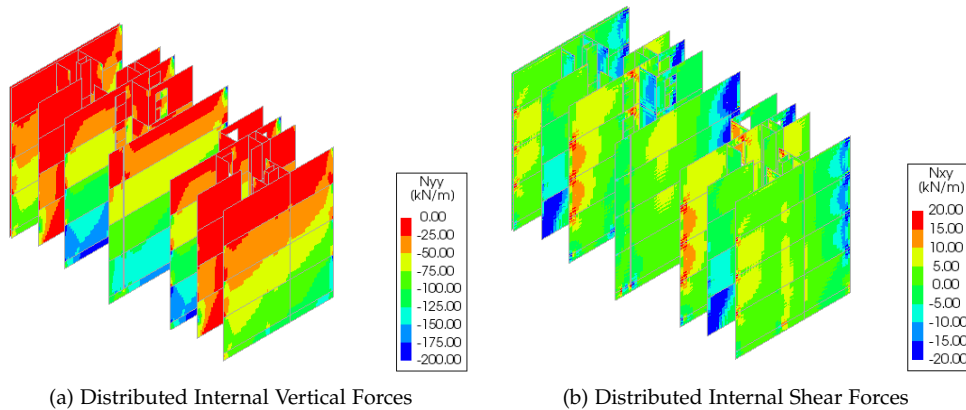


Figure 5.17: Internal Distributed Forces according to DIANA

It is not possible to obtain images of the internal forces in 3MURI like was done in DIANA. The only available output in 3MURI is resultant force per wall. To check if the transfer of the dead load is similar in DIANA and 3MURI it is necessary to calculate the resultant forces per wall in DIANA. This is done by taking the average distributed vertical force per wall and by multiplying this value with the width of that wall. The results of this calculation and the output of 3MURI is shown in Table 5.7. The Numbering system of the walls is shown in Figure 5.18.

The magnitude of the vertical loads in the walls is comparable in both directions. This indicates that the distribution of stiffness is comparable in both models. It should be noted though that the vertical force in walls in the transverse direction is slightly higher in 3MURI, while the vertical force of walls spanning in the longitudinal direction is higher in DIANA. However, it is not expected that the results are influenced significantly by this difference.

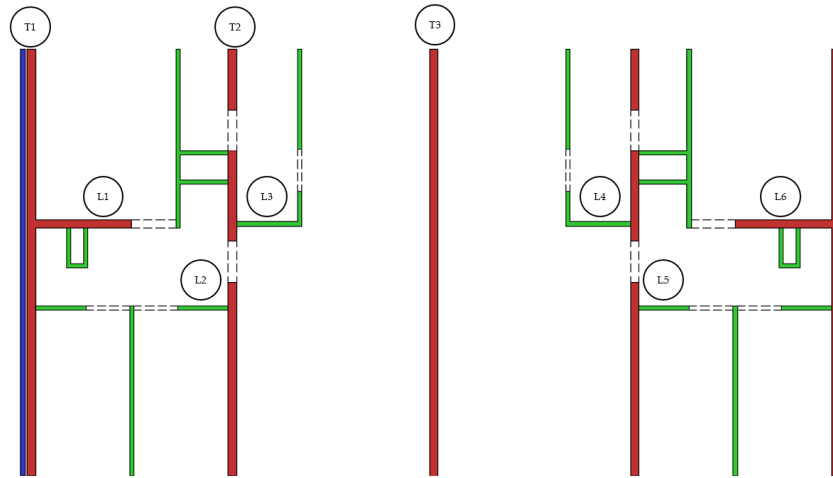


Figure 5.18: Wall Numbering System

Table 5.7: Internal Load Distribution

Wall no.	3MURI	DIANA	Unit
T1	1497	1454	kN
T2	1290	1231	kN
T3	1556	1486	kN
L1	195	225	kN
L2	90	108	kN
L3	77	92	kN

Part III

RESULTS



## COMPARISON OF PROCEDURES

---

This chapter is comprised of a comparison of the results which have been acquired by the case study. The comparison is divided into two parts, based on the two objectives of this thesis. It should be noted a more elaborate description of the results of each method can be found in Appendix G, H, and I for the MRS, NLPO and NLTH results respectively. Only a brief representation of the results which are directly related to the objectives of this study are presented in this chapter.

### 6.1 COMPARISON RESULTS OF CONTINUUM FEM AND MACRO EFM ANALYSES

A comparison of the studied computational discretisation methods for the NLPO method can be found hereafter. The studied methods are continuum FEM and macro EFM. DIANA is applied to model the structure according to continuum FEM, and 3MURI is used to create the macro EFM model. The methods are first compared with each other by looking into the results an analysis under static conditions and a modal eigenvalue analysis. Furthermore, the capacity curves according to the studied methods are compared. Moreover, the failure mechanisms are compared with each other and maximum admissible seismic load according to the NC limit state criteria is presented.

#### 6.1.1 COMPARISON ANALYSES UNDER STATIC CONDITIONS

The analyses under static conditions are performed by only taking into account the self-weight and live loads acting on the structure. The seismic load is not taken into account. This comparison is of interest because several elements have been modelled in the DIANA model, which were not modelled in 3MURI, due to the limitations of the latter. For example, the balconies and galleries have not been modelled in 3MURI. However, the mass of these elements has been taken into account by applying equivalent loads. It should be noted that the elements which have not been modelled, do not contribute to the overall capacity of the structure. However, it of importance that the total mass of both models is the same because it influences the results of the NLPO analyses. The mass of the structure according to both models is presented in Table 6.1, from which can be concluded that the mass is similar.

Table 6.1: Mass of Structure according to DIANA and 3MURI

	DIANA	3MURI
Mass Structure	9834 kN	9786 kN

The internal force distribution due to the self-weight of the structure is also of importance since it gives an indication of the distribution of stiffness throughout the structure. The vertical force distribution of several walls is presented in Chapter 5.3.2. It can be seen that the magnitude of the vertical force in each wall is comparable in both models.

## 6.1.2 COMPARISON MODAL EIGENVALUE ANALYSES

The results of the modal eigenvalue analyses are of importance for the NLPO analyses for several reasons. First, the modal mass participation of the governing eigenmodes should be larger than 60 %. Otherwise, the structure is not recommended by NPR 9998 to perform an NLPO analysis of the structure. Second, one of the vertical distributions of the lateral load has to be based on the shape of the governing eigenmode. In Chapter 5.3.1 is shown that the modal mass participation of the governing eigenmode in the transverse and longitudinal direction according to DIANA and 3MURI is higher than 60 %, as also presented in Table 6.2. It should be noted that even though the governing eigenmode in the longitudinal direction has a slightly higher modal mass participation in DIANA compared to 3MURI, it does not influence the results of the NLPO analysis. Because only the shape of the eigenmode is used as input, the modal mass participation only provides an indication if the NLPO method is applicable.

Table 6.2: Participating Modal Mass of the Governing Eigenmodes

	DIANA	3MURI
Longitudinal	77.3 %	69.7 %
Transverse	63.1 %	63.1 %

Another difference in the results of the modal eigenvalue analyses are the magnitudes of the natural periods of the governing eigenmodes, as presented in Table 6.3. These natural periods in 3MURI are higher compared to DIANA, from which can be concluded that the structure behaves stiffer according to DIANA. A reason for this difference is that walls in 3MURI do not provide any stiffness in the out-of-plane direction. Thus, the structure in 3MURI behaves more flexible, which results in a higher natural period. However, it should be noted though that the difference in natural period does not influence the results of the NLPO analysis, because it is not used as input in the method.

Table 6.3: Natural Period of the Governing Eigenmodes

	DIANA	3MURI
Longitudinal	0.53 s	0.55 s
Transverse	0.20 s	0.26 s

The modal shapes of the governing eigenmodes are presented in figure 6.1. It can be seen that the shape of the eigenmodes in 3MURI and DIANA are the same in the transverse direction. However, a difference can be seen in the longitudinal direction, where a relatively higher displacement of the first floor occurs in 3MURI in comparison to DIANA. As a result, it is more likely for damage to occur on the first floor while a modal load distribution is applied in 3MURI compared to DIANA.

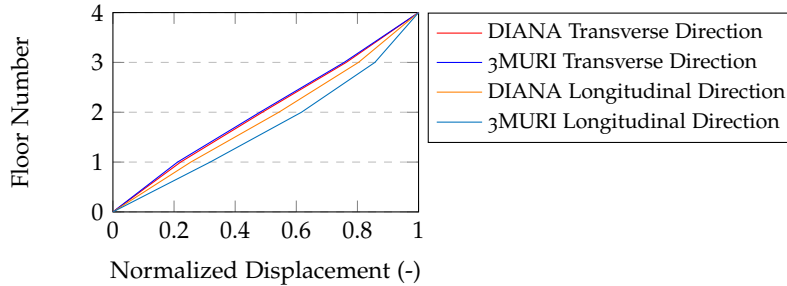


Figure 6.1: Shape Governing Eigenmode per Load Case

### 6.1.3 COMPARISON CAPACITY CURVES

The capacity curves are determined by applying a lateral load to the structure using a particular vertical distribution of the load. It is specified in NPR 9998 that at least two vertical distributions of the lateral load have to be applied. Furthermore, a capacity curve has to be determined in each of the four directions. These directions are the positive longitudinal direction, negative longitudinal direction, positive transverse direction and negative transverse direction. Thus in total, eight capacity curves have to be determined for a single NLPO analysis. However, only the governing case of the positive and negative direction has to be studied. Thus, only the governing load case of these two is presented. These capacity curves are presented in Figure 6.2. The limit state criterion which was met is presented next to the curves. The first limit state criterion which was met in 3MURI for all load cases is dynamic instability (DI) of the structure. Dynamic instability could occur due to two reasons. First, due to the absence of static convergence of an analysis. Second, due to the lack of vertical load bearing capacity of a structure. In DIANA a different criterion was met in the transverse and longitudinal direction. In the transverse direction, a base shear strength degradation (SD) of 80 % occurred before any other criteria were met. In the longitudinal direction, the 1.5 % inter-story drift limit (DL) was exceeded first.

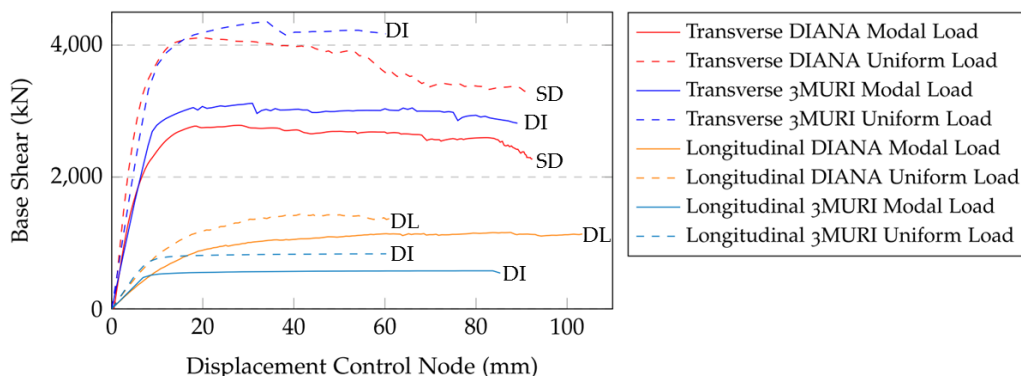


Figure 6.2: Pushover Curves

An overview of the characteristics of the capacity curves is presented in Table 6.4. The base shear capacity and displacement capacity are denoted with  $V_b$  and  $u_{cap}$  respectively. The initial stiffness  $k_{init}$  is determined by dividing the base shear at a displacement of the roof of a few millimetres.

Table 6.4: Overview Characteristics Capacity Curves

Direction	Load Pattern	Program	$k_{init}$ (kN/mm)	$V_b$ (kN)	$u_{cap}$ (mm)	Violated Criterion
Transverse	Modal	DIANA	309	2785	99.7	Strength Degredation
Transverse	Modal	3MURI	281	2994	89.1	Dynamic Instability
Transverse	Uniform	DIANA	489	4109	91.6	Strength Degredation
Transverse	Uniform	3MURI	435	4353	60.2	Dynamic Instability
Longitudinal	Modal	DIANA	66	1159	103.4	Drift Limits
Longitudinal	Modal	3MURI	69	576	85.3	Dynamic Instability
Longitudinal	Uniform	DIANA	95	1443	62.5	Drift Limits
Longitudinal	Uniform	3MURI	99	835	60.3	Dynamic Instability

The first point of interest when comparing the capacity curves according to DIANA and 3MURI is that the initial stiffness in both models for all load cases is similar. This indicates that the structure according to both models acts similarly in its elastic range. This was as expected because in Chapter 6.1.1 and Chapter 6.1.2 was already shown that the behaviour of the structure according to the analysis under static conditions and modal eigenvalue analysis according to both programs was similar.

The second point of interest is the base shear capacity according to the studied programs. The base shear capacity in the longitudinal direction is considerably larger according to DIANA in comparison with 3MURI. This is probably due to the fact that the out-of-plane behaviour of walls is not taken into account in 3MURI. The stiffness of the walls in the longitudinal direction is considerably lower than the strength of the walls in the transverse direction. An effect of this is that the out-of-plane behaviour of the walls spanning in the transverse direction has a considerable influence on the strength in the longitudinal direction. This out-of-plane behaviour is taken into account in the DIANA model, but it is neglected in the 3MURI model.

Furthermore, the lack of out-of-plane stiffness in 3MURI can be seen by looking at the position in the capacity curves of where the capacity curve becomes horizontal. This is the point where the structure does not have any more force capacity, but only displacement capacity. The deformation at which this point occurs is significantly smaller in 3MURI in comparison with DIANA when looking at the results in the longitudinal direction. This is due to the fact that after the force capacity of all piers has been reached, they only have deformation capacity. However, from the DIANA results can be seen that hardening behaviour occurs, after the capacity curve according to 3MURI already becomes horizontal. This is mostly to the fact that the forces in the walls spanning in the longitudinal direction are redistributed to the walls spanning in the transverse direction. Subsequently, the out-of-plane capacity of the transverse walls starts contributing to the global capacity. The effect of the redistribution of forces to walls spanning in the perpendicular loading direction cannot be seen by looking at the capacity curves which were determined by loading the structure in the transverse direction. This is as expected, because the capacity of the walls spanning in the transverse direction, is significantly higher as the wall spanning in the longitudinal direction.

The base shear capacity in the transverse direction according to both models is similar, where the base shear capacity according to 3MURI is even slightly higher in comparison with DIANA. One of the reasons for the slightly higher base shear capacity could be related to the differences in material models. Marco-elements are used in 3MURI, from which the force-capacity is based on design equations for the piers and spandrels as given in NPR 9998:2017. However, DIANA defines the strength of the piers and spandrels with a continuous material model, based on the strains which occur in the pier.

The last point of interest is the deformation capacity that was found for the various load cases. In all cases can be seen that the deformation capacity according to DIANA is similar to that of 3MURI, except for the load case in the transverse direction using a modal load pattern. 3MURI was not able to find convergence any more after a deformation of the control node of 62 millimetres, while a drop of the capacity also occurs in DIANA at this deformation. It is likely that also this drop in capacity occurred in 3MURI, but the program was not able to find convergence any more. This can be explained due to the differences in material models, which are presented in figure 6.3. The engineering masonry model is used in DIANA, which described the behaviour on a continuous scale. Thus even if the force capacity of a particular part of a pier is exceeded, the material model is able to redistribute the forces to other parts of that pier. Another aspect is that softening behaviour occurs after the force capacity of an element has been exceeded, which provides a more smooth transition of the force capacity is exceeded. The material model in 3MURI is based on a macro level. If the capacity of a pier is exceeded the stiffness of the entire element becomes zero. An effect of this is that it is more difficult to redistribute forces throughout the model. Thus, is it also more difficult to find convergence if the displacement capacity of an element is exceeded.

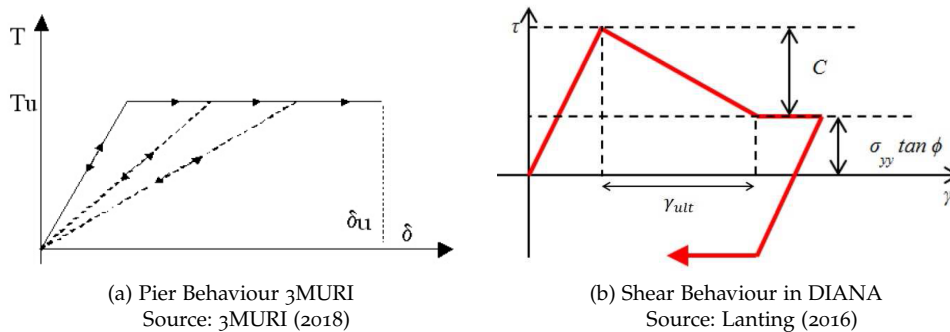


Figure 6.3: Comparison Material Model DIANA and 3MURI

## 6.1.4 DAMAGE AT FAILURE

The damage at failure indicates what kind of inelastic mechanisms are occurring in the structure according to the studied load cases. Another reason why the damage at failure is of interest is because the type of inelastic mechanism which occurs in the structure determines which inter-story drift limit has to be applied. The inter-story drift limits are 1.5 % for a ductile response and 0.6 % for a brittle response. The type of inelastic mechanism is determined by looking into the deformation profile at the moment of failure, the damage parameters and by studying the shape of the capacity curves. The displacement profile at the moment of failure is presented in Figure 6.4.

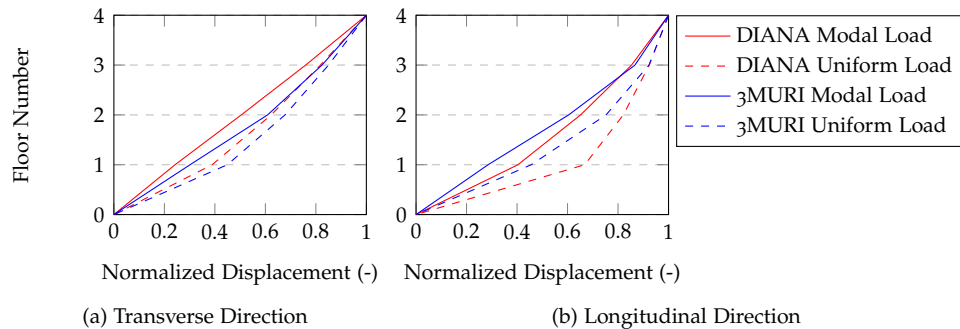


Figure 6.4: Displacement Profile

The normalised displacement is determined by dividing the displacement of each floor by the displacement of the roof. It can clearly be seen that the displacement profile for all load cases in both programs is similar. This is an indication that also damage also occurs in both programs occur on the same floors. This is supported by the figures which are shown in Chapter H.4. In this chapter is shown that the position of the damage is the same according to both programs. The wall numbering convention can be found in Figure H.10.

In the longitudinal could clearly be seen that shear related mechanisms occur wall L1, L2, L3, L4, L5 and L6. In DIANA, these inelastic mechanisms are indicated by the diagonal crack patterns. Furthermore, the bed joint status, head joint status and shear status parameters all show diagonal failure patterns. Moreover, the compressive strains in the structure do not surpass the critical compressive strain. In 3MURI, it is not possible to extract such detailed output, due to the fact that the behaviour of the structure is defined on a macro level. However, shear inelastic mechanisms could be found in the same walls as in DIANA. A distinction between the two programs is that in DIANA could clearly be seen that considerably damage occurs on the first floor compared to the other floors for the uniform load pattern, while 3MURI showed a similar damage on all floors. This difference occurs mostly due to the fact that 3MURI does not quantify the amount of damage that occurs, it only specifies in which elements the force capacity is exceeded. However, from the displacement profile according to 3MURI can be concluded that the inter-story drifts of the first floor a considerably higher than the other floors. Thus the conclusion can also be made from the results of 3MURI, that more damage occurs on the first floor, compared to the other floors. Furthermore, the problem that the magnitude of the damage of a pier is not visible is not a problem inherent to a macro EFM model, but it is a problem of the program 3MURI. This problem could be fixed by indicating the amount of displacement capacity which each pier still have during each stage of the capacity curve.

In the transverse direction, a combination of flexural and shear-like inelastic mechanisms are visible. Most damage occurs in wall T2 according to both 3MURI and DIANA. However, some elements failed according to 3MURI while in DIANA only a considerable amount of damage could be found. On the other hand, the elements which fail first according to 3MURI, are the elements in which the most damage occurs according to DIANA.

It is of importance to determine if the inelastic mechanisms which occurred are brittle or ductile because the magnitude the inter-story drift limit depends on it. In 3MURI was shown that the capacity curves using the Mohr-Coulomb material model were more conservative than using the Turnsec-Cacovic material model. The Mohr-Coulomb model is based on a shear sliding mechanism, which is a ductile mechanism. However, the damage parameters from DIANA diagonal patterns in the piers. This could be a diagonal shear failure mechanism, which is brittle, or a stairs-like pattern due to a bed joint sliding mechanism, which is ductile. However, the capacity curves show that a significant amount of plastic deformations occurs after the yield point. Thus it can be concluded that the type of shear failure mechanism is a bed joint sliding failure mechanism. Thus the behaviour of the structure can be considered as ductile.

#### 6.1.5 PGA AT NC

In the previous chapter was shown that ductile inelastic mechanisms are predicted according to all load cases. Thus, it can be concluded that the 1.5 % drift limit has to be applied. The maximum admissible seismic loads in terms of PGA at ground level according to the NC limit state criteria, are presented in Table H.6. It can be seen that the governing load case is the load case in the longitudinal direction when applying the uniform load distribution. The maximum admissible seismic load which correspond to this load case are presented in Table 6.5. This maximum PGA at ground level has been determined according to three different methods, namely: the regular N2-method, included in the Eurocode 8, and an adaptation of the N2 which is developed specifically for URM structures by Guerrini et al. (2017).

Table 6.5: Maximum Admissible Seismic Load according to the NLPO Method

	<b>Max PGA NPR 9998</b>	<b>Max PGA Eurocode 8</b>	<b>Max PGA Guerrini</b>
DIANA	0.27 g	0.18 g	0.17 g
3MURI	0.30 g	0.17 g	0.14 g

It can be concluded that for the case study the maximum admissible seismic load is similar according to DIANA and 3MURI. This is mostly due to the fact that for all capacity curves the displacement capacity is governing and the displacement capacity according to both programs is similar. It should also be noted that even though the displacement capacity according to DIANA is higher than the displacement capacity according to 3MURI, the maximum PGA according to NPR 9998 is lower. This is due to the shape of the used response spectrum, which is irregular, in comparison with a design spectrum as would normally be applied. The displacement capacity of a design spectrum as defined in NPR 9998 is constant for natural periods higher than the corner period  $T_c$ . Thus, the maximum admissible seismic loads for cases in which the displacement capacity is governing is the same for structures which a different base shear capacity. However, due to the fact that the response spectrum used in the case study is irregular, it is possible that different base shear capacities can lead to different results, even if the displacement capacity is governing.

However, when looking at the maximum admissible seismic load according to the other load cases, as presented in Chapter [H.2.4](#), a significant difference can be found when looking at the load case in the transverse direction, when applying the uniform load distribution. The maximum admissible seismic load according to 3MURI is significantly smaller, due to the fact that the displacement capacity is considerably smaller. The reason why the displacement capacity is due to the fact that 3MURI is less capable in redistributing forces compared to DIANA, as described in Chapter [6.1.3](#).

Furthermore, the maximum admissible seismic load according to NPR 9998 and Eurocode 8 is considerably different. The reason for this difference is explained thoroughly in Chapter [H.2](#). The reason for this difference is not discussed in this chapter, because it is not related to the properties of a continuum FEM and macro EFM model, but to the properties of the methods that are used to determine the target displacement.

The last aspect which should be noted is that even though the maximum admissible seismic load according to DIANA and 3MURI is similar, it should be noted that if the capacity of a structure is not sufficient, a significantly larger amount of retrofitting could be required according to 3MURI in comparison with DIANA. This difference in the required amount of retrofitting is due to the fact that in most cases, it is only possible to increase the base shear capacity of a structure. Thus even in a case in which the displacement capacity is governing and the displacement capacity according to 3MURI and DIANA is similar, the base shear capacity greatly influences the required amount of retrofitting. For example, this would be the case in the longitudinal direction, since the base shear capacity is almost two times smaller in 3MURI in comparison with DIANA.

## 6.2 COMPARISON RESULTS OF MRS, NLPO AND NLTH ANALYSES

A comparison between the results of the MRS, NLPO and NLTH analyses can be found hereafter. These methods are first compared with each other by looking into the force-displacement behaviour according to the studied methods. Moreover, the failure mechanisms and damage at failure are shown. Ultimately, the maximum admissible seismic load according to the NC limit state criteria is presented.

### 6.2.1 FORCE-DISPLACEMENT BEHAVIOUR

The force-displacement behaviour according to the studied analysis methods is visualised by showing the displacement of the control node versus the corresponding base shear at that displacement. The force-displacement behaviour is presented up until one of the NC limit state criteria are met. The force-displacement behaviour in the longitudinal direction according to all analysis methods is presented in Figure 6.5. The force-displacement plots for the MRS analysis are straight lines, due to the fact that MRS is a linear analysis. The plots for the NLPO analysis are the capacity curves. The force-displacement behaviour according to the NLTH method is presented by first creating hysteresis plots of each of the scaled signals. Subsequently, the maximum displacement and corresponding base shear are determined for each of the hysteresis plots and these points are plotted.

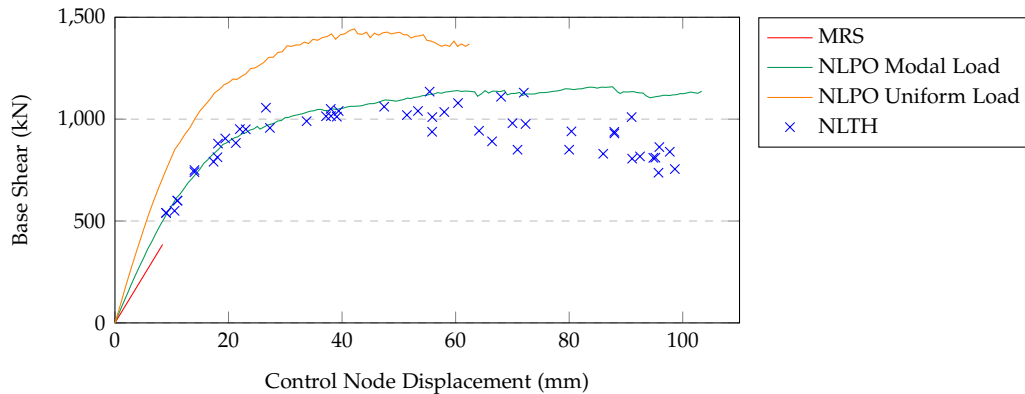


Figure 6.5: Comparison Force-Displacement Behaviour - Longitudinal Direction

The first point of interest is the initial slope of all the curves because it represents the stiffness in the elastic stage. The initial stiffness of the MRS curve is the lowest, which is a result of the properties of the masonry in the MRS model. The cracked stiffness of the masonry is applied, which means that the Young's modulus is half of the Young's modulus used in the nonlinear models. Furthermore, the results of the NLTH analyses seem to be in line with the results of the NLPO analysis using the modal load distribution pattern. A reason for this is that the modal mass participation of the governing eigenmode in the longitudinal direction is 77.3 %, which is relatively high. Thus, it can be expected that the results of the NLTH analysis are in line with the NLPO analysis, which uses a load pattern shape which is based on this eigenmode.

Furthermore, the displacement capacity of the different methods is of interest. The displacement capacity of the NLTH and NLPO using the modal load distribution are similar, while the displacement capacity according to the MRS is approximately ten times smaller. A reason for this difference is that the capacity of a structure according to the MRS method, solely depends on the force capacity of its elements. If the capacity of a single primary seismic element is exceeded, does that result in the failure of the structure. When looking at the capacity curve using the modal load distribution, it can be seen that the slope of the curve starts to change, at the displacement capacity according to the MRS method. Thus at this point, the force capacity of an element has been reached, which results in that the forces are redistributed throughout the structure, which a linear method like MRS cannot do. This also results in a lower base shear capacity for MRS than the other studied methods.

It is also of interest that the base shear capacities according to the nonlinear methods seem to be in line with each other, which can also be explained by the high modal participation of the governing eigenmode in the longitudinal direction. However, a difference between the results of the NLPO and NLTH results is the amount of degradation that occurs. The capacity curve according to the NLPO method seems to be horizontal, while the NLTH results show a decreasing base shear for an increase of the control node displacement. This can be explained by the fact that hysteretic behaviour is taken into account in the NLTH analysis, and it cannot be taken into account due to the nature of the NLPO method.

The force-displacement behaviour in the transverse direction is presented in Figure 6.6. The conclusions which were drawn related to the force-displacement behaviour according to the MRS method in the longitudinal direction are in line with the results in the transverse direction, except for the base shear capacity. The ratio between the base shear capacity according to the MRS and NLPO method in the longitudinal direction is 1:3 and the ratio in the transverse direction is 2:3. Thus, the MRS method is able to achieve a relatively higher capacity in the transverse direction, in comparison with the longitudinal direction. This difference can be explained by the fact that the out-of-plane strength is not taken into account in the MRS method, while it is taken into account in the NLPO method. As already explained when comparing 3MURI with DIANA in Chapter 6.1.3, the out-of-plane capacity of the walls spanning in the transverse direction has a significant influence on the capacity in the longitudinal direction. This out-of-plane capacity is not taken into account in the MRS method because the out-of-plane capacity is activated after the walls spanning in the longitudinal direction start to deform plastically, which is not possible to capture with a linear method.

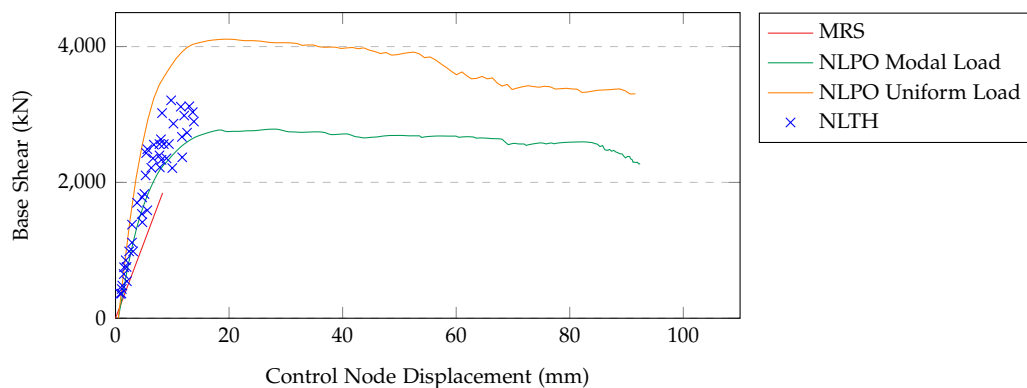


Figure 6.6: Comparison Force-Displacement Behaviour - Transverse Direction

Another difference can be found when looking at the force-displacement behaviour of the NLTH method in comparison with the NLPO method. In the longitudinal direction, the results of the NLTH analyses seem to be in line with the results of the NLPO analysis using a modal load distribution. However, the force-displacement behaviour in the transverse direction according to the NLTH method seems to fall in between the capacity curves according to the uniform and modal load distribution patterns. This difference in results can be explained by looking at the modal mass participation in both directions. The modal mass participation in the transverse direction, which is 63 %, is significantly smaller than the modal mass participation in the longitudinal direction, which is 77.3 %. Thus other eigenmodes than the governing eigenmode have a more substantial influence on the behaviour of the structure in the transverse direction. The fact that the force-displacement behaviour according to the NLTH analysis can be described by a capacity curve which graphically in between the two capacity curves according to the NLPO method, shows why it is necessary to perform the NLPO analysis using at least two different load distribution patterns.

### 6.2.2 FAILURE MECHANISMS

All analyses have been performed in such a way, that the seismic load has been scaled until one of the NC limit state criteria were met according to NPR 9998. In the longitudinal direction, which is the governing direction, the inter-story drift limit of the first floor was exceeded first according to the NLTH and NLPO method. The first limit state criterion which was met according to the MRS method is the exceedance of the capacity the pier on the fourth floor of wall L2. A flexural failure mechanism occurs in this pier. However, it should be mentioned that the capacity of all piers in wall L2 was also almost exceeded.

In the transverse direction, a failure mechanism was never reached according to the NLTH method. This is due to the fact that while performing the NLTH method, a seismic load is always applied in the transverse, longitudinal and vertical direction at the same time. Thus if the capacity in one of those directions is considerably less, then the capacity is never exceeded in the other direction. The failure mechanism which occurred according to the NLPO method is a strength degradation of 80 % in comparison with the base shear capacity. The failure mechanism according to the MRS method was exceedance of the capacity of pier B in wall T2 on the fourth floor. A flexural failure mechanism occurs in this pier. However, it should be mentioned that the capacity of almost all piers in part B and C of wall 2 were exceeded.

The fact that the location of the failure mechanism is different from the location of the failure mechanism which occurs according to the NLPO and NLTH analyses shows one of the limitations of the MRS method. This limitation is that it is not possible to redistribute forces during an MRS analysis. Thus an exceedance of the capacity of a single element leads to failure of the entire structure. A result of this limitation is that the allowed deformations in a structure are considerably smaller than for the nonlinear methods. This is clearly visible when looking at the inter-story drifts at the moment of failure, as presented in Figure 6.7.

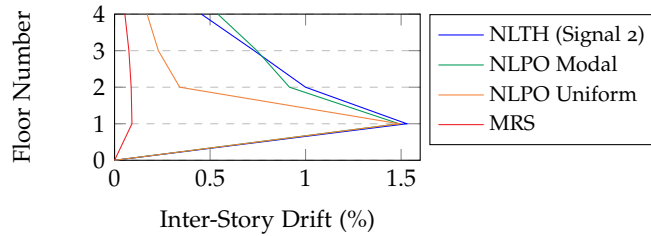


Figure 6.7: Comparison Inter-Story Drifts at Failure

It should be noted that only the inter-story drifts of the governing NLTH are shown, which is signal 2. Furthermore, both the inter-story drifts at failure according to the NLPO method, while applying the uniform and modal load distribution are shown. Another interesting aspect related to Figure 6.7 is that the displacement profile at the moment of failure of the NLTH and NLPO using the modal load distribution are similar. This is as expected because the force-displacement behaviour as presented in Chapter 6.2.1 was also similar.

### 6.2.3 DAMAGE AT FAILURE

The damage in the structure at failure according to the nonlinear methods is presented in this chapter. However, a comparison is made with the failure mechanisms which occurred according to the MRS method, to see if the inelastic mechanism which occurs according to the NLPO and NLTH method are in line with the failure mechanism which occurs according to the MRS method. The crack width at the moment of failure according to the NLTH and NLPO method using the modal pattern, are presented in Figure 6.8. The crack widths according to the NLPO method the uniform load pattern are not presented, because the results of the modal load pattern are more similar to the results of the NLTH method. The maximum crack widths up until the last time step are presented for the NLTH signal 2. For both the NLPO analyses is clearly visible that shear dominated inelastic mechanisms occur. The NLTH analysis shows that the crack widths are way more distributed throughout the structure. However, the diagonal crack patterns indicate that shear-like inelastic mechanisms occur.

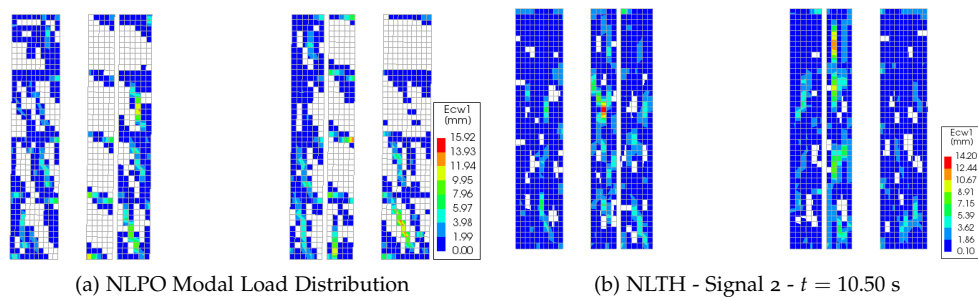


Figure 6.8: Crack Widths at Failure - Wall L1, L2, L3, L4, L5 & L6

The position and type of inelastic mechanisms are not inline with the failure mechanisms which occur according to the MRS method. The first failure mechanisms which would occur according to MRS is flexural failure of one of the piers on the fourth floor. However, initial failure does not always correspond to further crack developments. Thus, it not possible to draw conclusions based on the fact that the most damage according to the nonlinear methods is not in line with the predicted failure mechanisms according to the MRS method.

It is not of interest to compare the damage of the structure in the transverse direction according to the NLTH method with the NLPO method, because the structure is not deforming plastically yet according to the NLTH method. However, it is of interest to compare the inelastic mechanisms which occur according to the NLPO method with the failure mechanisms according to the MRS method. Concerning the NLPO method, a combination of flexural and shear inelastic mechanisms could be seen when looking at the damage parameters, as presented in chapter most substantial presence on the first two floors of wall T2. When comparing these inelastic mechanisms which the failure mechanism according to the MRS method, it can be seen that all the piers in which a considerable amount of damage occurs, also have a unity check according to the MRS method. However, the unity check which is exceeded the most is one which corresponds to a pier on the fourth floor, which is not visible in the results of the NLPO analysis.

#### 6.2.4 MAXIMUM ADMISSIBLE SEISMIC LOAD

The maximum admissible seismic load acting on the structure in terms of the maximum allowed PGA at ground level is determined according to the MRS, NLPO and NLTH method. The maximum admissible load has been determined by incrementally increasing the seismic load until one of the NC limit state criteria according to NPR 9998 was exceeded. The methodology of executing the methods has been done according to NPR 9998. However, two additional methods for the post-processing of the capacity curve and demand for an NPLO have also been applied, namely according to Eurocode 8 and Guerrini. An overview of the maximum admissible seismic load according to the studied methods can be found in Table 6.6. It should be noted that for the NLTH method, only the capacity in the longitudinal direction is given. This is the case because an NLTH analysis is always performed by applying a seismic signal in both horizontal directions simultaneously and the structure always failed in the longitudinal direction before it could fail in the transverse direction.

Table 6.6: Maximum Admissible Seismic Load according to Codes

	<b>MRS</b>	<b>NLPO</b>	<b>NLPO</b>	<b>NLPO</b>	<b>NLTH</b>
	<b>NPR 9998</b>	<b>NPR 9998</b>	<b>Eurocode 8</b>	<b>Guerrini</b>	<b>NPR 9998</b>
Transverse	0.22 g	0.46 g	1.12 g	0.76 g	-
Longitudinal	0.03 g	0.27 g	0.18 g	0.17 g	0.26 g

The first point of interest when looking at the maximum admissible seismic load acting according to the studied methods is that the capacity according to the MRS method is considerably lower compared to the nonlinear methods. A reason for this difference is that when looking at the force-displacement behaviour according to the NLPO and NLPO methods, that a considerable amount of plastic deformation can occur, without failure of the structure. A part of this plastic deformation is taken into account by introducing the behaviour factor. However, this behaviour factor is often conservative. It is possible to determine a more appropriate behaviour factor based on the output of the NLPO method.

Equation 6.1 can be used to determine the behaviour factor  $q$  based on the ductility of a system  $\mu$ . An explanation of the background of this equation can be found in Chapter 3.1.2.

$$q = \sqrt{2\mu - 1} \quad (6.1)$$

This ductility can be determined by performing an NLPO analysis, where the ductility is defined as the ratio of the displacement capacity and yield displacement. The ductility factor and corresponding behaviour factor for the governing load cases in the transverse and longitudinal direction are presented in Table 6.7. It should be noted that the behaviour factors are determined taking into account that the governing natural period in both directions is in the short-period range.

Table 6.7: Behaviour Factor according to NLPO Analysis

	$\mu$	$q$
Longitudinal	3.7	2.5
Transverse	8.4	4.0

The behaviour factor which is specified for unreinforced masonry is 1.5. Thus, it can be concluded that the behaviour as specified in NPR 9998 for this case study is too conservative. However, even if a ductility factor of 2.5 would be applied in the longitudinal direction, then the maximum admissible seismic load would still be significantly lower according to the MRS in comparison with NLPO and NLTH. Nonetheless, when looking at the maximum admissible seismic load in the transverse direction according to the MRS method when using the behaviour factor as determined with the NLPO analysis, then the maximum admissible seismic load is more in line with the NLPO results.

The maximum admissible load according to the NLPO method using the methodology of NPR 9998 and Eurocode 8 are significantly different. Moreover, the maximum admissible seismic load is more conservative in the transverse direction according to NPR 9998 compared to Eurocode 8, while it is the other way around in the longitudinal direction. This difference can be explained by the calculations steps which have to be performed to determine the target displacement according to both methods. Eurocode 8 takes into account the natural period of the idealised SDoF system into account directly, while this is not the case for the method as described in NPR 9998. Thus two structures which have the same displacement capacity but a significantly different natural period could have the same maximum admissible seismic load according to NPR 9998, but the maximum admissible Eurocode 8. A thorough description of the differences in the methods can be found in Chapter H.2. In conclusion, structures which have a capacity curve and natural period similar to the case study in the transverse direction, NPR 9998 is more conservative. However, for structures which behave similar to the structure in the longitudinal direction, Eurocode 8 is more conservative.

When comparing the results of the NLPO and NLTH method, can be seen that the maximum admissible seismic load according to the NLTH method is similar to the capacity according to the NLPO using NPR 9998. However, the NLPO load case using the uniform load pattern is the governing load case, which corresponds to a behaviour of the structure, which was not captured by the NLTH analysis. Thus, even though the maximum admissible seismic load according to the NLTH method is in-line with that of the NLPO using the NPR 9998 target displacement method, both cases represent a different behaviour of the structure. If only the capacity curve according to the modal load pattern would be considered, then the results of the NLTH are more in line with the results of the NLPO using the target displacement method of Eurocode 8. These results are presented in Table 6.8.

Table 6.8: Maximum Admissible Seismic Load when Neglecting Uniform Load Pattern for NLPO

	<b>MRS</b>	<b>NLPO</b>	<b>NLPO</b>	<b>NLPO</b>	<b>NLTH</b>
	<b>NPR 9998</b>	<b>NPR 9998</b>	<b>Eurocode 8</b>	<b>Guerrini</b>	<b>NPR 9998</b>
Transverse	0.22 g	0.46 g	1.12 g	0.76 g	-
Longitudinal	0.03 g	0.45 g	0.25 g	0.21 g	0.26 g



## CONCLUSIONS

### 7.1 CONCLUSIONS

This work aims at answering the following research questions:

- *To what extent can the nonlinear pushover method be used for the seismic assessment of low-rise URM apartment buildings in Groningen?*
- *To what extent is the equivalent frame method applicable as computational discretisation method for the pushover analysis of low-rise URM apartment buildings in Groningen?*

Both objectives are studied by looking into a single case study which is a low-rise apartment building for which the wall configuration on the second floor is presented in Figure 7.1. The behaviour of the structure in the longitudinal direction is characterised by a relatively low stiffness and lateral capacity compared to the transverse direction. The conclusions which are drawn from the case study can generally be applied to low-rise URM apartment buildings in Groningen. However, it must be noted that significant alterations in geometry and building materials might influence the results. For example, higher mode effects could become relevant if the wall configuration is more irregular compared to the case study, which are difficult to capture with an NLPO analysis. Furthermore, the results of the NLPO method generally less reliable for structures with flexible diaphragms, and only rigid diaphragms were considered in the case study.

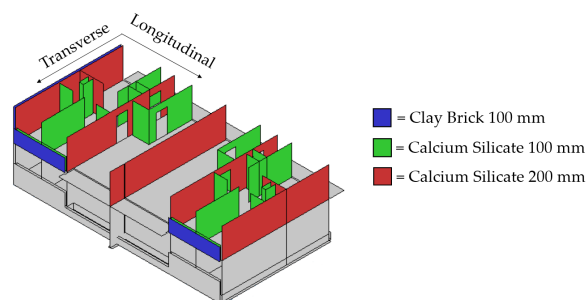


Figure 7.1: Walls Configuration in DIANA

#### 7.1.1 APPLICABILITY OF THE EQUIVALENT FRAME METHOD

The following conclusions are drawn based on the comparison of the results of the NLPO analyses using the DIANA and 3MURI models:

- No significant differences were found between the results of the analyses under static conditions and the modal eigenvalue analyses. Furthermore, the displacement profile at failure, type and position of inelastic mechanisms and the maximum admissible seismic load according to DIANA and 3MURI are similar.
- The base shear capacity in the longitudinal direction according to DIANA is higher compared to 3MURI, while in the transverse direction the base shear capacity is similar in both programs. This difference occurs because 3MURI does not take into account out-of-plane behaviour of walls, which has a significant effect on the behaviour of the structure in the longitudinal direction, due to the fact that this direction is characterised by very short piers and a low in-plane capacity.

- The displacement capacity of the load case in the transverse direction using the uniform load pattern is considerably smaller in 3MURI compared to DIANA, due to the fact numerical instability of the 3MURI model occurs at an earlier stage compared to DIANA. A reason for this difference is that DIANA allows for gradual softening, which helps the post-peak force redistribution.

The fact that the behaviour of the structure according to DIANA and 3MURI is similar, and the fact that the two identified disadvantages of 3MURI can only result in more conservative results, suggests that the macro EFM as implemented in 3MURI is a suitable computational discretisation method for the seismic assessment according to the NLPO method for low-rise residential URM structures in Groningen.

However, several assumptions which were made in the approach might have influenced the results. First, several structural elements which were modelled in DIANA were not modelled in 3MURI due to limitations of the program, which could result in a different behaviour of the structure. Second, the assumption is made that the modelling approach provides accurate results for both the NLPO analysis in DIANA and 3MURI. Extensive research has been performed by VIIA on the effects of the modelling assumptions in the DIANA model, while such research has not been performed concerning 3MURI. Thus, no guarantee can be given that the assumptions in 3MURI are able to describe the behaviour of the structure accurately.

#### 7.1.2 APPLICABILITY OF THE NLPO METHOD

The following conclusions are drawn based on the comparison of the results of the MRS, NLPO and NLTH analyses:

- Very conservative results were found regarding the MRS method. A reason that was found for these conservative results is that the prescribed behaviour factor by NPR 9998 is too low for the case study, when compared to that derived from the NLPO analysis. However, even with a larger behaviour factor, the results according to the MRS method would still be conservative in the longitudinal direction.
- The force-displacement behaviour according to the NLTH analysis is in line with the capacity curve according to the NLPO method using the modal load pattern, as presented in Figure 7.2. However, in the transverse direction, the force-displacement behaviour according to the NLTH analysis is enveloped by the capacity curves according to the NLPO method using the uniform and modal load patterns. A reason for this difference could be that the modal mass percentage of the governing eigenmode in the longitudinal direction is considerably higher compared to the transverse direction.

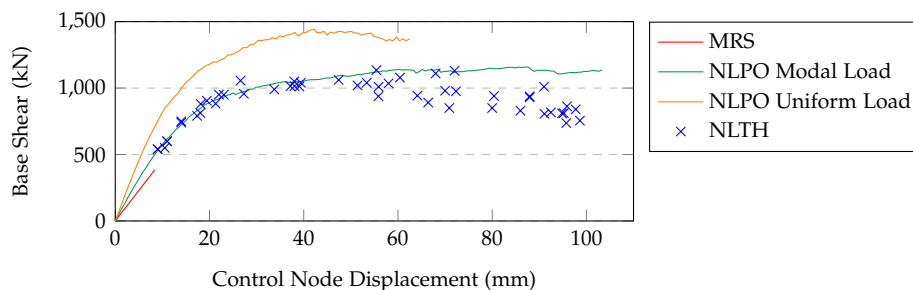


Figure 7.2: Comparison Force-Displacement Behaviour According to DIANA - Longitudinal Direction

- Concerning the longitudinal direction, the predicted failure mechanisms, position and type of inelastic mechanisms and the displacement profile at failure according to the NLTH and NLPO analysis (using the modal load pattern) are similar.

- The target displacement calculation method has a significant influence on the maximum admissible seismic load, as presented in Table 7.1. It was found that NPR 9998 is more conservative in the transverse direction and Eurocode 8 and Guerrini are more conservative in the longitudinal direction. This difference occurs because the target displacement method according to Eurocode 8 takes the natural period of the structure into account directly, while this is not the case in the NPR 9998 method. Concerning the longitudinal direction, the maximum admissible seismic load according to NPR 9998 is the most similar compared to the NLTH analysis.

Table 7.1: Maximum Admissible Seismic Load according to Codes

	MRS	NLPO	NLPO	NLPO	NLTH
	NPR 9998	NPR 9998	Eurocode 8	Guerrini	NPR 9998
Transverse	0.22 g	0.46 g	1.12 g	0.76 g	-
Longitudinal	0.03 g	0.27 g	0.18 g	0.17 g	0.26 g

Given the above, the behaviour of the studied structure is similar according to the NLPO and NLTH method, where maximum admissible seismic load using the target displacement method according to NPR 9998 is in-line with that of the NLTH analysis. However, the governing load case made use of a uniform load pattern, which returns a structural behaviour different than that obtained by NLTH analyses. If only the capacity curve according to the model load pattern would be considered, then the results of the NLTH are more in line with the results of the NLPO using the target displacement method of Eurocode 8.

Several aspects which are taken into account in an NLTH analysis cannot be captured by the other methods. First, the horizontal seismic load applied in the NLTH analysis is of a bilateral nature, while MRS and NLPO consider both loading directions separately. Furthermore, NLTH takes into account a vertical load, which is not considered in the MRS and NLPO analyses. Moreover, hysteretic effects included in the masonry model are taken into account in the NLTH method, which are impossible to capture by the static methods.

Furthermore, several modelling assumptions have been applied, and it is important to note that the possible influence of these assumptions, may partially limit the extent of the conclusions. Three assumptions which might have influenced the results are listed below. First, the seismic signals which are applied for the NLTH analysis are based on seven real earthquake signals, which have been matched and processed in a way that the response spectra at ground level due to these signals match the response spectra as defined in NPR 9998:2015. However, the choice and duration of these signals are not prescribed by the NPR 9998, and a different set of signals could lead to different results. Second, the seismic signals have been scaled at ground level, and SSI effects are not taken into account in the NLTH analysis as a consequence. These SSI effects could have a positive effect on the seismic resistance of a structure according to the NLTH method. Ultimately, the engineering masonry model has been applied to model the masonry for all analyses in DIANA. However, it is not prescribed to use this material model by the NPR 9998, and the use of other material models could have a significant influence on the results.

In conclusion, taken into account the aforementioned limitations of modelling assumptions and the fact that several limitations are inherent to the studied methods, the fact that the behaviour of the structure according to the NLPO and NLTH method is similar, suggests that the NLPO method is a suitable method for the seismic assessment of low-rise URM apartment buildings in Groningen. Furthermore, the NLPO method is greatly recommended over the MRS method for this typology, due to the fact that the maximum admissible seismic load according to the MRS method is significantly lower.

## 7.2 RECOMMENDATIONS

The objective of this study was to find out in which extent the pushover method and equivalent frame method are applicable for the seismic assessment of URM low-rise residential buildings in Groningen. This objective is studied by looking into a single case study. However, it is expected that the conclusions of this study are not applicable if significant alterations in geometry and building materials are made. It is recommended to perform a similar study like the one performed in this report but by looking into variations of the studied building. Variations which are of interest are irregular wall configurations because higher modes will become more relevant, which are difficult to capture with the NLPO analysis. Furthermore, only rigid diaphragms were considered in the case study, and the NLPO method is generally less accurate for more flexible floors. Thus, it is also of interest to study the effect of more flexible floors such as timber.

The two main identified disadvantages of macro EFM are not directly related to the nature of EFM, but to the used material model in 3MURI. These disadvantages are that out-of-plane behaviour and softening are not taken into account. It is of interest to investigate the possibility to include these aspects in a macro EFM model.

In the conclusions is stated the maximum admissible seismic load according to the NLTH method could be higher, if SSI effects were taken into account. An additional study if of interest to see what the magnitude this influence is.

The capacity of the structure according to the studied methods is expressed in terms of the maximum admissible seismic load and conclusions are drawn based on the differences. However, it would also be of interest to describe the capacity of the structure in terms of the amount of retrofitting which is required.

When comparing the force-displacement behaviour according to the NLTH method and the capacity curves according to the NLPO method, could clearly be seen that a more substantial amount of degradation occurs according to the NLTH method. This degradation occurs due to hysteretic effects which are not taken into account in the NLPO method. It could be an option to include these hysteretic effects in the determination of the capacity curves according to the NLPO method. For example, these effects could be included in the material model. Furthermore, it is also possible to capture these hysteretic effects by performing a cyclic pushover. A study into both these options is deemed useful.

The pushover analyses have been performed using vertical distributions of the lateral load which are constant during the loading process. An alternative is an adaptive pushover, in which the load patterns are updated as a function of the response of the structure. A study using the adaptive pushover is especially of interest for structures in which a clear sway-like eigenmode is not visible.

Ultimately, a recommendation to building practice is to only consider the nonlinear methods for the seismic assessment of structures of the studied typology. Advantages which were identified of the nonlinear methods over the MRS method are a considerably higher maximum admissible seismic load, the possibility to trace the sequence of damage and failure on a local level and the use of behaviour factors, which cannot be rigorously assessed, can be avoided. All aforementioned advantages result in a lower amount of required retrofitting according to the nonlinear methods in comparison with MRS.

Part IV

APPENDICES



## DERIVATION EQUATION OF MOTION

This chapter is compromised the derivation of the equation of motion of a single and multiple degree of freedom system. The equations of motion describe the behaviour of a physical structure as a set of mathematical functions in terms of dynamic variables. This derivation is required because the studied seismic assessment methods are all based on the EOM of a system. Firstly, the EOM for a linear single degree of freedom (SDF) system is derived, since this EOM is required for the modal response spectrum method. Secondly, the EOM for a nonlinear multi-degree of freedom (MDF) system is derived, since it used as a basis for the nonlinear pushover and nonlinear time history method.

### A.1 LINEAR SINGLE DEGREE OF FREEDOM SYSTEM

A single degree of freedom system as shown in Figure A.1 is considered. Such a system consists of a mass  $m$  connected to the ground by a spring  $k$  and a viscous damper  $c$ . The spring provides stiffness, and the damper dissipates the energy of the system.

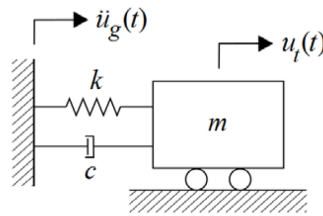


Figure A.1: Single Degree of Freedom System

It should be noted that the total displacement  $x_t$  of the mass is the summation of the ground displacement  $x_g$  due to an earthquake and the relative displacement of the mass with respect to the ground  $x$ , as shown in Equation A.1.

$$x_t(t) = u_g(t) + x(t) \quad (\text{A.1})$$

The relevant forces for determining the response of the mass due to an earthquake excitation are the inertia force  $f_i$ , spring force  $f_s$  and damping force  $f_d$ . The inertia force is related to the total acceleration of the structure and its mass. The internal force due to the spring which resists the displacement of the mass is called the spring force. This force acts in the opposite direction of the displacement. It should be noted that the magnitude of this force is related to the relative displacement of the mass with respect to the ground. The stiffness of the system is denoted with a  $k$ , and this stiffness can be determined by taking into account the material properties of a structure. The process by which free vibration steadily diminishes in amplitude is called damping. The energy of a vibrating system is dissipated by the various mechanism like friction at connections, opening and closing of micro-cracks and friction between the structure itself and non-structural elements. It is a challenge to identify or describe these mechanisms mathematically. As a result, the damping is usually represented highly idealised. The damping force is modelled as an internal force which is related to the velocity. The constant  $c$  is introduced as the viscous damping coefficient. The expressions of the forces are given by:

$$f_i = m\ddot{x}_t(t), \quad f_d = c\dot{x}(t), \quad f_s = kx(t) \quad (\text{A.2})$$

Using Newton's second law of motion results in the following equilibrium equation in the x-direction:

$$f_i + f_d + f_s = 0 \quad (\text{A.3})$$

The forces as shown in Equation A.2 are substituted in equation A.3, taken into account that the inertia force is related to the absolute displacement and the other forces to the relative displacement of the mass with the ground.

$$m\ddot{x}(t) + c\dot{x}(t) + kx(t) = -m\ddot{u}_g(t) \quad (\text{A.4})$$

## A.2 NONLINEAR MULTI DEGREE OF FREEDOM SYSTEM

The derivation of the EOM for an SDoF system is shown in Chapter A.1. A similar derivation is required for MDoF systems since this EOM is used as the basis for the nonlinear methods. The same methodology as for the SDoF system is applied, where the inertia, spring and damping forces are defined first. Then, making use of Newton's second law is the EOM formulated. The EOM for a linear system is first determined, and afterwards this equation is converted into one including nonlinear behaviour.

It is necessary to idealise a structure as an assemblage of elements, which are interconnected at nodes. These elements could be for example beams, columns and walls. The displacement of these nodes are the degrees of freedom. In general, a node in a three-dimensional structure has six degrees of freedom, three translations and three rotations. It is possible to relate these degrees of freedom to the spring, damping and friction forces. Only the fuss derivation of this relation is elaborated for the spring force since the derivation is similar for the inertia and damping force.

The relation between the displacement and the spring force is determined by applying a unit displacement along DOF  $j$ , while holding all other displacements to zero. A force must be applied to maintain these displacements. The stiffness influence coefficient  $k_{ij}$  is the force required along DOF  $i$  due to a unit displacement at DOF  $j$ . The total spring force  $f_s^i$  at DOF  $i$  can be found by the superposition of all components of  $x_j$ .

$$f_{si} = k_{i1}x_1 + k_{i2}x_2 + \dots + k_{ij}x_j + \dots + k_{iN}x_N \quad (\text{A.5})$$

One of these equations exists from  $i = 1$  to  $N$ . This set of equations can be written in matrix form,

$$\begin{bmatrix} f_{S1} \\ f_{S2} \\ \vdots \\ f_{SN} \end{bmatrix} = \begin{bmatrix} k_{11} & k_{12} & \dots & k_{1j} & \dots & k_{1N} \\ k_{21} & k_{22} & \dots & k_{2j} & \dots & k_{2N} \\ \vdots & \vdots & & \vdots & & \vdots \\ k_{N1} & k_{N2} & \dots & k_{Nj} & \dots & k_{NN} \end{bmatrix} \begin{bmatrix} x_1 \\ x_2 \\ \vdots \\ x_N \end{bmatrix} \quad (\text{A.6})$$

$$f_s = \mathbf{K}x \quad (\text{A.7})$$

where  $\mathbf{K}$  is the stiffness matrix. The stiffness matrix is a symmetrical matrix. The most common method to determine the values of the stiffness influence coefficients is the direct stiffness method. In this method, the stiffness matrices of the individual elements are assembled to obtain the structural stiffness matrix.

Exactly the same method can be used to determine the damping and inertia forces. Thus the derivation of these vectors is not shown in this chapter. Keeping this in mind is it possible to relate the damping force vector  $f_d$  with the velocity vector  $\dot{x}$  by introducing damping influence coefficients  $c_{ij}$ . This coefficient is the external force in DOF  $i$  due to a unit velocity in DOF  $j$ . It is impractical to relate these coefficients directly to the properties and dimensions properties of individual structural elements. Therefore these values are mostly based on experimental data for similar structures. It is possible to collect all individual equations for the structural elements in matrix form, where  $C$  is the damping matrix.

$$f_d = C\dot{x} \quad (\text{A.8})$$

Before defining the equations for the inertia forces is it necessary to make a distinction between the global and local displacements. The displacement of the ground is denoted by  $u_g$ , the total displacement of the masses by  $x_{tj}$  and the relative displacement of the masses with respect to the ground by  $x_j$ . These displacements are related by:

$$x_{tj}(t) = u_g(t) + x_j(t) \quad (\text{A.9})$$

If these equations are taken for  $N$  masses it results in the following vector,

$$x_t = ru_g(t) + x \quad (\text{A.10})$$

where  $r$  is the influence vector, which is obtained by displacing the structure as a rigid body, towards the ground motion direction.

The same steps should be taken to determine the inertia forces, only in this case the force is related to the total acceleration of the mass of a node. The mass is distributed throughout a structure. Thus an idealisation is required. This can be done by representing the mass of an element as a point mass at the nodes of an element. Collecting all the equations for the separate nodes results in the following equation, where  $M$  is the mass matrix.

$$f_i = M\ddot{x}_t \quad (\text{A.11})$$

The equation of motion can now be determined by using Newton's second law of motion, taken into account no external dynamic forces.

$$f_i + f_d + f_s = 0 \quad (\text{A.12})$$

Substituting the force vectors as defined in Equation A.7, A.8 and A.11 and taking into account the relation between the displacements as defined in Equation A.10 gives:

$$M\ddot{x} + C\dot{x} + Kx = -Mr\ddot{u}_g(t) \quad (\text{A.13})$$

This equation of motion takes into account the fact that the relative motions with respect to the ground produce spring and damping forces, while the inertia forces are related to the total accelerations. The last step that should be taken is converting the EOM for a linear system, to one for a nonlinear system. For an inelastic system, the relation between the spring forces and node displacements is path depended. This means that the force depends on whether deformation is increasing or decreasing during a time step. This changes the EOM into:

$$M\ddot{x} + C\dot{x} + f_s(x, \text{sign}(\dot{x}), t) = -Mr\ddot{u}_g(t) \quad (\text{A.14})$$



## PROCEDURES FOR NONLINEAR ANALYSIS

---

Several mathematical procedures are required to be able to solve a nonlinear set of equations. This chapter is comprised of an overview and theoretical background the procedures, which are required to analyse a structure with FEM package. These procedures are numerical iteration schemes, convergence criteria and the arc length control. It should be noted that purpose of this chapter is not to provide the reader with an extensive description of each of the methods, but more like an overview of the methods which are available and the advantages and disadvantages of the possible modelling choices.

### B.1 NUMERICAL ITERATION SCHEMES

In the previous chapter was specified that the only unknowns in in Equation 3.55 are the displacement increment  $\delta x_i$  and the nonlinear stiffness relation  $\delta f_s$ . This nonlinear stiffness relation is dependent on the displacement increment. Thus an iterative method is required to solve the system of equations. The general procedure of such methods is first to increase the external load, which is a ground acceleration in the case of an earthquake. Secondly, the out of balance force is determined, by extracting the internal forces from the external forces. The method predicts a displacement increment afterwards, which will result in a change of the internal force. The last step is to check the convergence criteria are met. These criteria could be based on the equilibrium of force or the change in incremental displacement after an iteration. If this convergence limit is not met, the process starts again by predicting another displacement increment. Possible convergence criteria are elaborated in Chapter B.2. In all procedures the goal is to find the total displacement increment  $\delta x_i$ . This total displacement increment is found by adopting the displacement increment by iterative increments  $\delta u$  until equilibrium is reached. This equilibrium is reached if the convergence criterion is met. The incremental displacement at iteration  $i + n$  are calculated from:

$$\delta x_i^{(n+1)} = \delta x_i^{(n)} + \delta u^{n+1} \quad (\text{B.1})$$

where the top right superscript indicates the iteration number. The difference between the several procedures is the way in which  $\delta u$  is determined. In general, this iterative increment is calculated by using stiffness matrix  $K$  which represents the relation of the force vector and displacement vector. In some methods the stiffness can change every iteration. Thus the relation between the out of balance force  $g_i$  and the iterative increment is:

$$\delta u^{(n)} = K^{(n)-1} g_i \quad (\text{B.2})$$

where  $K^{(n)-1}$  is the inverse stiffness matrix at increment  $n$ . The amount of times the stiffness matrix is updated and how this is done depends on the chosen method. In the Regular Newton-Raphson method the stiffness matrix is updated at every iteration, as shown in Figure B.1a. An advantage of this method that it required relatively few iterations, but a disadvantage is that the stiffness matrix has to updated at every iteration and this is a computationally demanding procedure. Another disadvantage is that if the initial prediction is far from the final solution, the method easily fails due to divergence.

The Secant method does not have to update the stiffness matrix at every iteration. This method uses information from earlier determined solution vectors and out of plane balance forces to determine the stiffness after an increment. More iterations are necessary compared to the Regular Newton-Raphson method, but the iterations take less time because it is not required to update the stiffness matrix at every iteration. Ehiwario and Aghamie (2014) have found at that the convergence rate of the Secant method is close to that of the Newton-Raphson method.

Another commonly used method is the Linear Stiffness method. As shown in Figure B.1c, this method solely determines the stiffness matrix at the start of an iteration. This method has the slowest convergence rate. Thus it required the highest amount of iterations, but since the stiffness matrix only needs to be determined once, the iterations take the least amount of time. The method is also very robust.

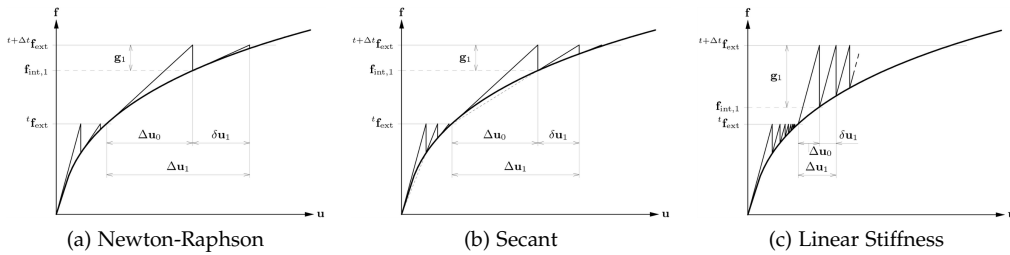


Figure B.1: Commonly used Iteration Methods.  
Source: DIANA FEA BV (2017)

B.2 CONVERGENCE CRITERIA

It is of importance to check the convergence of a numerical analysis. This is done by adopting the displacement increment by iterative increments until equilibrium is reached. The displacement increment is reached if the convergence criterion is met. This convergence criterion can be based on displacements, forces and energies.

The force criterion is a check of the out-of-balance force. The convergence criterion is met if the remaining force imbalance is a small fraction of the total applied force. Because the reference force is known before the first prediction of displacements, it is possible to calculate the force form directly after the first prediction. This means that the behaviour of a system is still linear and no unnecessary iterations have to be performed. The force norm as applied in DIANA is:

$$\epsilon = \frac{\sqrt{g_0^T g_i}}{\sqrt{g_0^T g_0}} \tag{B.3}$$

The displacement norm is a check of the iterative displacement increment. The displacement criterion met if the last update of the displacement increment is a small fraction of the initial displacement increment. Equation B.4 is applied in DIANA to determine the convergence norm. From this equation can be concluded that always one additional iteration is necessary because the norm is equal to 1 for the first prediction.

$$\epsilon = \frac{\sqrt{\delta u_0^T \delta u_i}}{\sqrt{\Delta u_0^T \Delta u_0}} \tag{B.4}$$

The last way to check convergence is the energy norm. This norm contains the internal forces and relative displacements. The last update of the stored energy is a small fraction of the initial stored energy. As for the displacement norm, an additional step is required to detect convergence.

$$\epsilon = \frac{\delta u_0^T (f_{int,i+1} + f_{int,i})}{\Delta u_0^T (f_{int,1} + f_{int,0})} \quad (\text{B.5})$$

### B.3 ARC LENGTH CONTROL

A force-controlled pushover is executed in DIANA. A disadvantage of a force controlled pushover is that it is difficult to find convergence in the nonlinear branch of the pushover curve. This is due to the fact that if a fixed load increment is prescribed, the predictions of the displacement could get very large. This problem could be solved by using the Arc-length method. The arc length method constrains the norm of the incremental displacements to a fixed value. This is done by simultaneously adapting the size of the increment. It should be noted that the size of the increment is adapted within the iteration process and is not fixed at the moment the increment starts. An external force at the start of the increment is defined, where the increment of this external force is indicated as  $\Delta\lambda_i \hat{f}$ , where  $\Delta\lambda_i$  is a load factor which is multiplied with a unit load  $\hat{f}$ . Substitution of these vectors in Equation B.1, results in the following equation for the displacement increment of a single iteration:

$$\delta u_i = K^{-1} \left( \Delta\lambda_i \hat{f} + {}^t f_{int} - f_{int} \right) \quad (\text{B.6})$$

The solution can be divided into two parts:

$$\delta u_i^I = K^{-1} ({}^t f_{int} - f_{int}) \quad \text{and} \quad \delta u_i^{II} = K^{-1} \hat{f} \quad (\text{B.7})$$

By substituting Equation B.7 in Equation B.6 results in the following equation:

$$\delta u_i = \delta u_i^I + \Delta\lambda_i \delta u_i^{II} \quad (\text{B.8})$$

The load factor  $\Delta\lambda_i$  is the only unknown in the equation above, and it can be used to constrain the displacement increment. Two methods can be used in DIANA to determine this load factor. The first method is called the Spherical Path method, which uses a quadratic constraint. The second method, the Updated Normal Plane method, uses a linearised constraint.



## DRAWINGS CASE STUDY

Drawings of the case study structure can be found in this chapter. These drawings include a top view, a front view and a side view of the structure. A legend can also be found underneath each of the figures in which the material properties are indicated.

### C.1 TOP VIEW - GROUND LEVEL

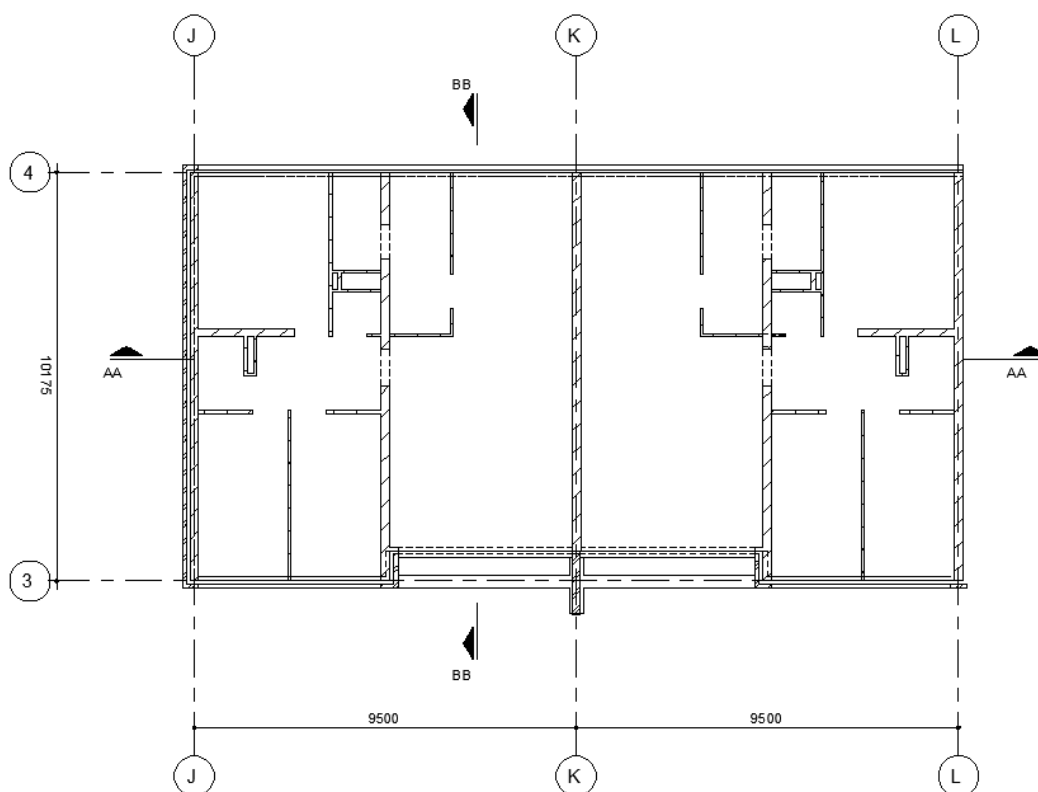
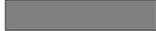


Figure C.1: Top View Ground Floor

	= Insitu Casted Concrete
	= Prefab Concrete
	= Calcium Silicate
	= Clay Brick
	= Wood

C.2 FRONT VIEW - SECTION AA

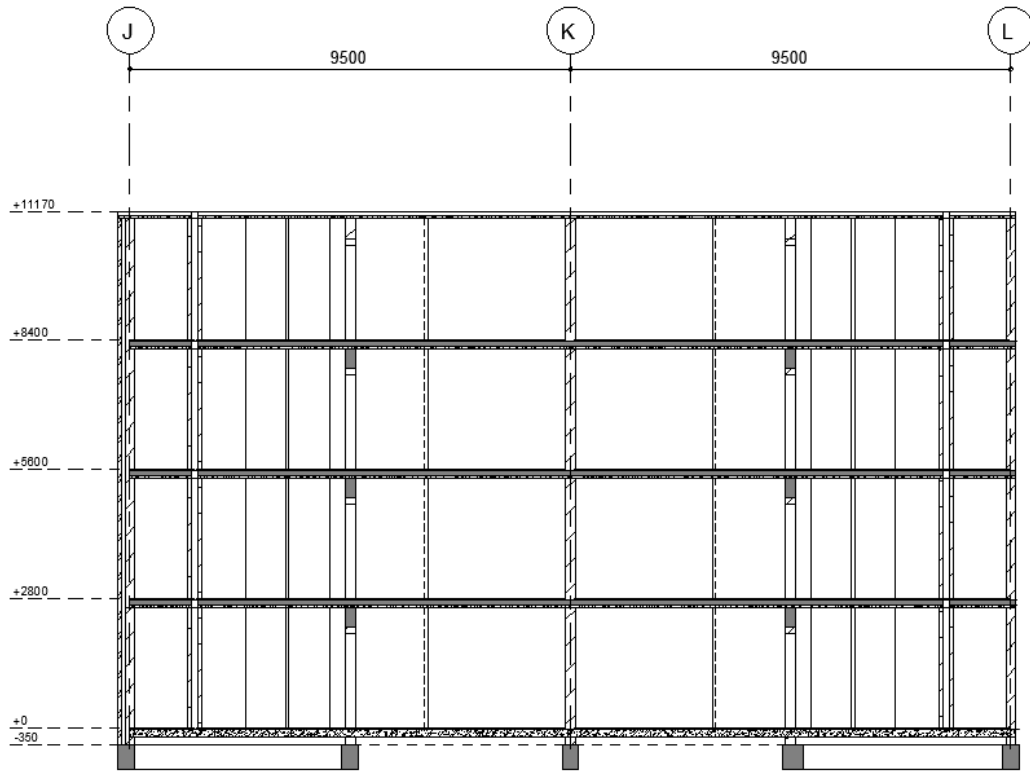
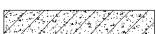


Figure C.2: Front View - Section AA

	= In situ Casted Concrete
	= Prefab Concrete
	= Calcium Silicate
	= Clay Brick
	= Wood

C.3 SIDE VIEW - SECTION BB

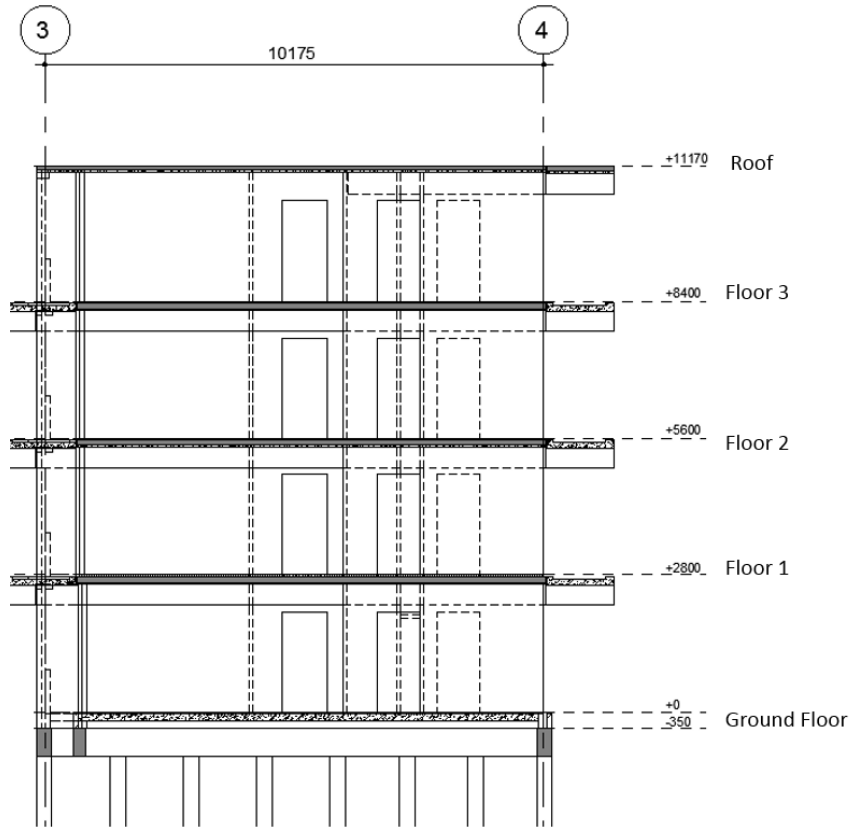
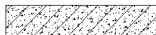


Figure C.3: Side View - Section BB

	= Insitu Casted Concrete
	= Prefab Concrete
	= Calcium Silicate
	= Clay Brick
	= Wood



## MODEL PROPERTIES

This chapter is comprised of an overview of all used material properties and the position and magnitude of additional loads. The chapter is subdivided into three parts: The nonlinear DIANA model, the linear DIANA model and the 3MURI model. All material properties have been taken from NPR 9998:2015 or derived by VIIA by additional studies. The origin of the material properties of each material is mentioned.

### D.1 DIANA MODEL FOR NONLINEAR ANALYSES

The material properties used for the DIANA model which is used for the nonlinear analyses are specified in this hereafter. The material properties of masonry, concrete, the ribbed floor, the foundation piles and the nonlinear interface elements between the walls are presented.

Two different types of masonry can be found in the structure, namely calcium silicate and clay brick. NPR 9998 prescribes material properties for these materials depended on the time of construction the structure. The engineering masonry model as described in Chapter 2.4.1 is used to model masonry. The following material properties have been used for the masonry in DIANA. It should be mentioned that a compressive unloading with  $\lambda = 0$  is assumed. This means that unloading occurs with the initial stiffness until zero compressive stress. Other parameters which require further elaboration are the Rayleigh damping parameters. These have been based on the 2%  $\zeta$  at a frequency of 6 HZ and 15 HZ.

Table D.1: Material Properties Masonry - Nonlinear DIANA Model

Material Property	Calcium Silicate	Clay Brick	Unit
Density	2.00E+03	2.00E+03	kg/m <sup>3</sup>
Young's Modulus (x)	2.33E+09	3.00E+09	N/m <sup>2</sup>
Young's Modulus (y)	3.50E+09	6.00E+09	N/m <sup>2</sup>
Shear modulus	1.22E+09	1.90E+09	N/m <sup>2</sup>
Tensile Strength (x)	3.00E+05	4.50E+05	N/m <sup>2</sup>
Tensile Strength (y)	1.00E+05	2.00E+05	N/m <sup>2</sup>
Residual Tensile Strength	5.00E+03	1.00E+04	N/m <sup>2</sup>
Compressive Strength	7.00E+06	1.00E+07	N/m <sup>2</sup>
Tensile Crack Energy	5.00E+00	1.00E+01	Nm/m <sup>2</sup>
Compressive Crack Energy	1.70E+04	2.00E+04	Nm/m <sup>2</sup>
Shear Crack Energy	1.00E+02	2.00E+02	Nm/m <sup>2</sup>
Cohesion	2.50E+05	4.00E+05	N/m <sup>2</sup>
Friction Angle	5.40E-01	6.44E-01	rad
Damping Parameter a	2.51E-01	2.51E-01	rad/s
Damping Parameter b	7.09E-06	7.09E-06	s/rad

Concrete is modelled with linear material properties. The damping parameters have been based on a  $\zeta$  of 5% at a frequency of 0.1 HZ to 15 HZ. This type of concrete is applied to model the roof, floors, balconies, galleries, foundation strips and the beams which support the balconies. The Young's modulus is based on the cracked stiffness properties of concrete.

Table D.2: Concrete Material Properties - Nonlinear DIANA Model

<b>Material Property</b>	<b>Value</b>	<b>Unit</b>
Density	2.50E+03	kg/m <sup>3</sup>
Young's Modulus	1.50E+10	N/m <sup>2</sup>
Poison Ratio	2.00E-01	-
Damping Parameter a	6.24E-02	rad/s
Damping Parameter b	1.05E-03	s/rad

The bottom floor of the building is a ribbed floor. This floor has orthotropic material properties. These material properties have been defined by VIIA (2017b).

Table D.3: Material Properties Ribbed Floor - Nonlinear DIANA model

<b>Material Property</b>	<b>Value</b>	<b>Unit</b>
Density	1.04E+03	kg/m <sup>3</sup>
Young's Modulus (x)	1.11E+10	N/m <sup>2</sup>
Young's Modulus (y)	2.37E+08	N/m <sup>2</sup>
Young's Modulus (z)	1.06E+11	N/m <sup>2</sup>
Shear Modulus (x)	1.33E+08	N/m <sup>2</sup>
Shear Modulus (y)	1.33E+10	N/m <sup>2</sup>
Shear Modulus (z)	2.51E+10	N/m <sup>2</sup>
Damping Parameter a	6.24E-02	rad/s
Damping Parameter b	1.05E-03	s/rad

The foundation piles have been modelled as one-dimensional beam elements. Both the properties of the pile and the interface between the pile and soil block had to be given as input. These properties have been determined by a geotechnical engineer from VIIA.

Table D.4: Material Properties Foundation Piles - Nonlinear DIANA Model

<b>Material Property</b>	<b>Value</b>	<b>Unit</b>
Density	2.50E+03	kg/m <sup>3</sup>
Young's Modulus	3.00E+10	N/m <sup>2</sup>
Lateral Stiffness between Pile and Soil	1.00E+10	N/m <sup>3</sup>
Parallel Stiffness between Pile and Soil	1.00E+10	N/m <sup>3</sup>
Damping Parameter a	6.24E-02	rad/s
Damping Parameter b	1.05E-03	s/rad

Nonlinear interface elements are used to model the connections between certain walls. The elements are not able to transfer shear or tensional forces.

Table D.5: Material Properties Nonlinear Interface Elements - Nonlinear DIANA Model

<b>Material Property</b>	<b>Value</b>	<b>Unit</b>
Normal Stiffness modulus-y	1.00E+9	N/m <sup>3</sup>
Normal Stiffness modulus-x	1.00E+0	N/m <sup>3</sup>
Normal Stiffness modulus-z	1.00E+0	N/m <sup>3</sup>
Damping Parameter a	1.00E+0	rad/s
Damping Parameter b	1.00E-5	s/rad

Surface loads acting on the floors are taken into account by increasing the density of the floors on which the load is acting. The applied densities in DIANA are shown in Table D.6.

Table D.6: Applied Densities in DIANA

	<b>Density Material (kN/m<sup>2</sup>)</b>	<b>Design Load (kN/m<sup>2</sup>)</b>	<b>Thickness (mm)</b>	<b>Density in DIANA (kN/m<sup>3</sup>)</b>
Roof	25.0	0.60	0.15	29.0
Floor 2,3,4	25.0	1.32	0.15	33.8
Gallery	25.0	1.36	0.15	34.1
First Floor	10.0	1.32	0.26	15.0

## D.2 DIANA MODEL FOR MRS ANALYSIS

The material properties that are used for the linear model used for the MRS analyses are described hereafter. The only material properties which differ from the nonlinear model, are those of the masonry and the interface elements.

NPR 9998 prescribed that the cracked properties of masonry should be applied for a linear model. It is also specified that the stiffness properties of cracked masonry, may be taken as half of the untracked masonry properties.

Table D.7: Material Properties Masonry - Linear DIANA Model

<b>Material Property</b>	<b>Calcium Silicate</b>	<b>Clay Brick</b>	<b>Unit</b>
Density	2.00E+03	2.00E+03	kg/m <sup>3</sup>
Young's Modulus (x)	1.17E+09	1.5E+09	N/m <sup>2</sup>
Young's Modulus (y)	1.75E+09	3.00E+09	N/m <sup>2</sup>
Shear modulus	0.61E+09	0.85E+09	N/m <sup>2</sup>

The line interface between the walls is defined in such a way that its stiffness is considerably smaller than the stiffness of the walls. Thus forces will not be transferred through the interface elements.

Table D.8: Material Properties Interface Elements - Linear DIANA Model

<b>Material Property</b>	<b>Value</b>	<b>Unit</b>
Normal Stiffness modulus-y	1.00E+0	N/m <sup>3</sup>
Normal Stiffness modulus-x	1.00E+0	N/m <sup>3</sup>
Normal Stiffness modulus-z	1.00E+0	N/m <sup>3</sup>

### D.3 3MURI MODEL

#### D.3.1 MATERIAL PROPERTIES

The material properties used for the 3MURI model are specified hereafter. The material properties which are described are the those of the masonry, concrete, the ribbed floor and the dummy walls.

Masonry is modelled in 3MURI using macro elements. The material properties are prescribed in NPR 9998.

Table D.9: Material Properties Masonry - 3MURI Model

<b>Material Property</b>	<b>Value</b>	<b>Unit</b>
Density	2.00E+03	kg/m <sup>3</sup>
Young's Modulus	3.50E+09	N/m <sup>2</sup>
Shear modulus	1.22E+09	N/m <sup>2</sup>
Compressive Strength	7.00E+06	N/m <sup>2</sup>
Initial Bed Joints Shear Strength	2.50E+05	N/m <sup>2</sup>
Limit Shear Strength	9.10E+05	n/m <sup>2</sup>
Characteristic Compressive Strength	4.20E+06	n/m <sup>2</sup>

Dummy walls are applied in 3MURI because without them the program had numerical stability problems. The properties of the dummy walls have been chosen in such a way, that they do not influence the global behaviour of the structure.

Table D.10: Material Properties Dummy Walls - 3MURI Model

<b>Material Property</b>	<b>Value</b>	<b>Unit</b>
Density	1.00E-1	kg/m <sup>3</sup>
Young's Modulus	0.75E-1	N/m <sup>2</sup>
Shear modulus	0.29E-1	N/m <sup>2</sup>
Compressive Strength	9.99E+2	N/m <sup>2</sup>
Initial Bed Joints Shear Strength	9.99E+2	N/m <sup>2</sup>
Limit Shear Strength	4.99E-1	N/m <sup>2</sup>
Characteristic Compressive Strength	9.99E+2	n/m <sup>2</sup>

All floors are concrete, except for the floor on ground level. Linear material properties are used to model the concrete.

Table D.11: Material Properties Concrete - 3MURI Model

<b>Material Property</b>	<b>Value</b>	<b>Unit</b>
Young's Modulus	1.50E+10	N/m <sup>2</sup>
Shear Modulus	6.25E+09	N/mc
Poison Ratio	2.00E-01	-

The wall on the ground floor is a ribbed floor. This floor has been modelled with linear properties, which are the same as the material properties used for the ribbed floor in DIANA.

Table D.12: Material Properties Ribbed Floor - 3MURI

Material Property	Value	Unit
Young's Modulus (x)	1.11E+10	N/m <sup>2</sup>
Young's Modulus (y)	2.37E+08	N/m <sup>2</sup>
Shear Modulus	1.33E+10	N/mc
Poison Ratio	2.00E-01	-

### D.3.2 EQUIVALENT STATIC LOADS

It is not possible to model several elements in 3MURI, which were modelled in DIANA, due to the limitations of the program. The elements which could not be taken into account are the outer leaves of the cavity wall in the façade, the galleries, the extension of the roof above the galleries, the balconies and the concrete beams. All of these elements do not contribute to the global seismic capacity of the structure, but the mass of these elements has to be taken into account for determining the seismic response of the structure. The mass these elements is calculated first and subsequently applied to the structure in 3MURI. The mass of the concrete beams is added as a line load, acting on the walls. All other loads are applied as point loads acting on the edge of the walls. Some of these loads would have normally be applied to the floor, but it only possible in 3MURI to apply point loads directly to the walls. The positions of where the additional loads have been applied have been assigned with an identification number, as shown in Figure D.1.

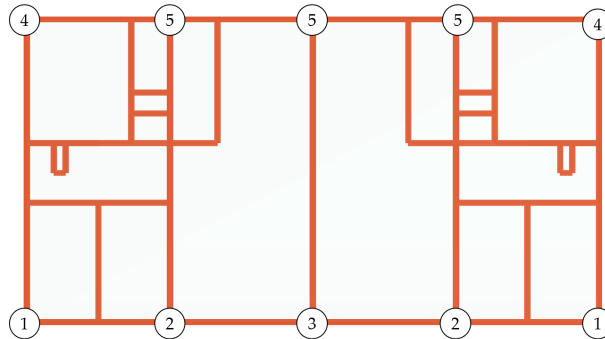


Figure D.1: Equivalent loads in 3MURI

This results in the following loads which are applied in the 3MURI model.

Table D.13: Equivalent Loads acting on the Ground Floor

Position	Facade	Cavity Wall	Total	Unit
1	1.65	5.65	7.30	kN
2	3.30	5.65	8.95	kN
3	3.30	0.00	3.30	kN
4	1.65	0.00	1.65	kN
5	3.30	0.00	3.30	kN

Table D.14: Equivalent Loads acting on Floor 2,3 and 4

Position	Facade	Cavity Walls	Balconies	Galleries	Total	Unit
1	1.65	5.65	0.00	0.00	7.30	kN
2	3.30	5.65	16.7	0.00	25.7	kN
3	3.30	0.00	33.4	0.00	36.7	kN
4	1.65	0.00	0.00	16.9	18.5	kN
5	3.30	0.00	0.00	33.7	37.0	kN

Table D.15: Equivalent Loads acting on the Roof

Position	Facade	Roof	Total	Unit
1	1.65	0.00	1.70	kN
2	3.30	0.00	3.30	kN
3	3.30	0.00	3.30	kN
4	1.65	14.5	16.1	kN
5	3.30	28.9	32.2	kN



## MASONRY STATE PARAMETER

This chapter is comprised of a description of the masonry damage state parameter from the engineering masonry model. DIANA FEA has included a masonry state parameter output in their software. This masonry state parameter (STATUS EMASON) returns a number corresponding to the branch of the stress-strain curve on which the node is currently located. This is provided for the normal stress behaviour of bed and head joints and the shear behaviour of the masonry. It should be noted that the descriptions and the images hereafter are directly taken from VIIA (2018).

### BED AND HEAD JOINT PARAMETER

The possible status values and their definitions for the head and bed joint are presented in Table E.1 and Figure E.1.

Table E.1: Definition of Head and Bed Joint Failure Status Parameter

Parameter	Description
-3	Ultimate branch of the compressive stress-strain curve
-2	softening branch of the compressive stress-strain curve
-1	unloading/reloading section of the compressive stress-strain curve
0	no crack and no compressive failure
1	unloading/reloading section of the tensile stress-strain curve
2	partially open crack loading
3	fully open crack loading

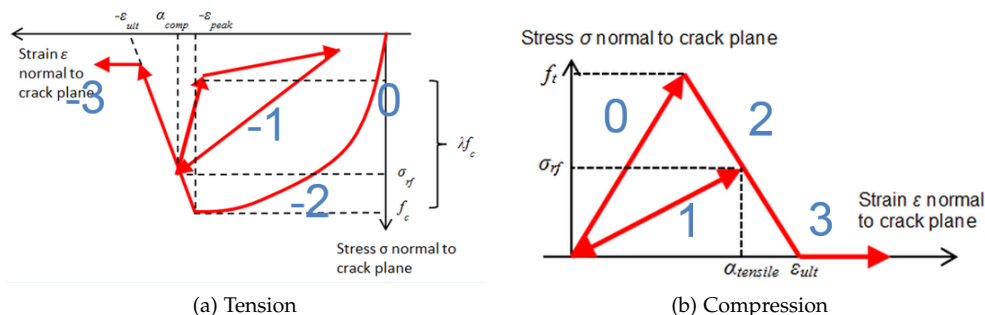


Figure E.1: Numbered Stress-Strain Curve

Source: VIIA (2018)

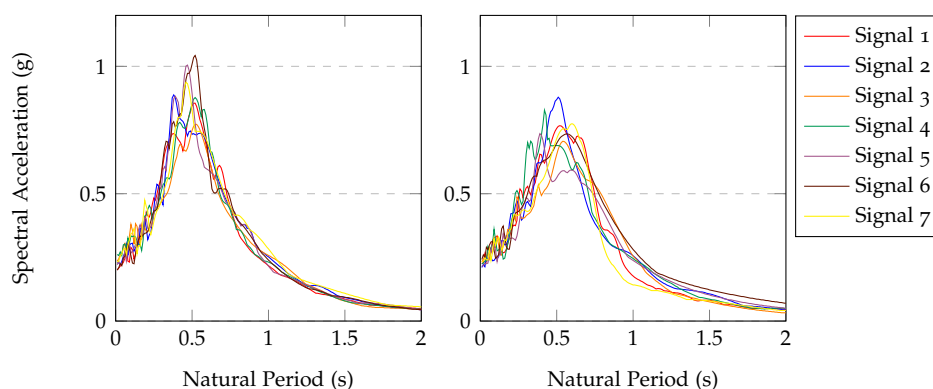


## RESPONSE SPECTRA

This response spectra which are used for the MRS and NLPO analyses are presented in this chapter. These chapters have been determined based on NLTH analysis of the soil column. Furthermore, the effect of scaling the signal at ground level on the applied response spectra is also presented.

### F.1 DESIGN SPECTRA

The response spectra which are used for the MRS and NLPO analyses are derived from the NLTH analyses of the soil column. The method of how this is done is explained in Chapter 4.3.4. The response spectra for each signal are shown in Figure F.1.



(a) Transversal Direction (b) Longitudinal Direction  
Figure F.1: Response Spectra Derived from NLTH Analyses

The outer envelope of these spectra is used as input for the MRS and NLPO analyses. These outer envelopes are shown in Figure F.2. The response spectra have been scaled in such a way that the PGA which corresponds to each response spectrum are equal.

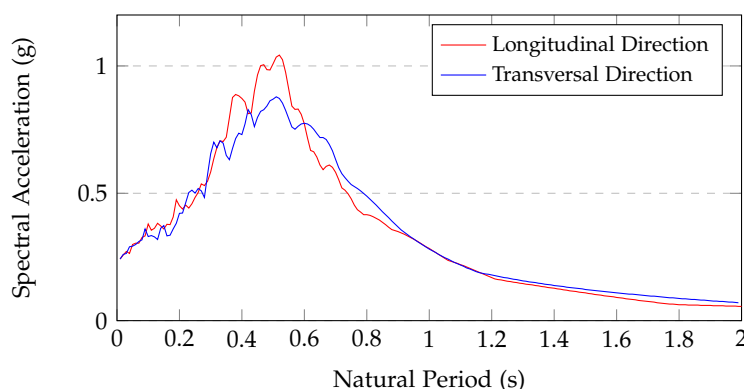


Figure F.2: Outer Envelope of Derived Response Spectra

It should be noted that usually when evaluating a structure according to NPR:9998:2018 using a location-specific spectrum, a minimum value of the spectral acceleration is given for each natural period, based on the response spectra which are prescribed in the code. It is prescribed that the minimum value of the spectral acceleration at a particular natural period, is 80% of the spectral acceleration at that period as prescribed in the NPR 9998. This criterion is not applied for this study, because the design spectrum which is prescribed for this case study in NPR 9998:2015 is significantly higher than the location-specific spectrum which resulted from the NLTH analyses, which would result in that the NPR 9998:2015 spectrum would be governing for all natural periods.

## F.2 EFFECT SCALING SIGNAL AT GROUND LEVEL

The seismic signals are scaled linearly at ground level for all analysis methods. Thus the material properties of the soil are only taken into account once. A consequence of this is that the applied seismic signals are different than as they would be if the signals were scaled at a depth of 30 meters, as is prescribed in the NPR 9998. The effect of this modelling assumption is elaborated hereafter.

An additional study has been performed to show the effect of scaling the signal at a ground level. Signal 2 is used as an example to show this effect. Several NLTH analyses of the soil column have been performed, where the signal is scaled at a depth of 30 meters. The accelerations are measured at ground level, and response spectra have been determined based on these accelerations. These response spectra are presented in Figure F.3. It can clearly be seen that if the response is scaled at ground level linearly, that this not result in a linear change of the response spectra at ground level. The signal which corresponds to the PGA at ground level of 0.23 g is used as the basis signal, which is linearly scaled.

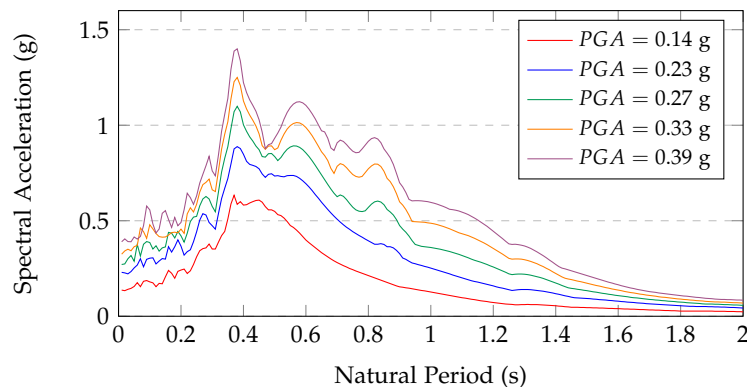


Figure F.3: Influence Non Linear Soil Properties on Response Spectrum

The difference between the real spectra and the scaled spectra can be seen even more clearly in Figure F.3. The real spectrum is the spectrum which has been determined by applying a signal at a depth of 30 meters. The scaled spectrum is the spectrum which has been determined by linearly scaling the basis signal, which is the spectrum which corresponds to a PGA at ground level of 0.23 g.

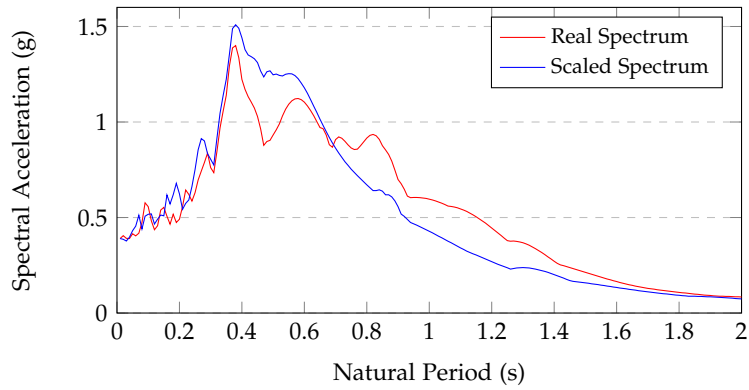


Figure F.4: Comparison Real and Scaled Spectrum for  $PGA = 0.39$  g



## RESULTS: MODAL RESPONSE SPECTRUM ANALYSIS

The results of the MRS analysis are presented in this chapter, which are evaluated according to NPR 9998. The chapter is subdivided into three parts. First, the response spectra which are used as input are linearised, to make them suitable for the MRS method. Second, the results of a modal eigenvalue analysis are presented. Ultimately, the maximum admissible seismic load is determined.

### G.1 LINEARISED RESPONSE SPECTRUM

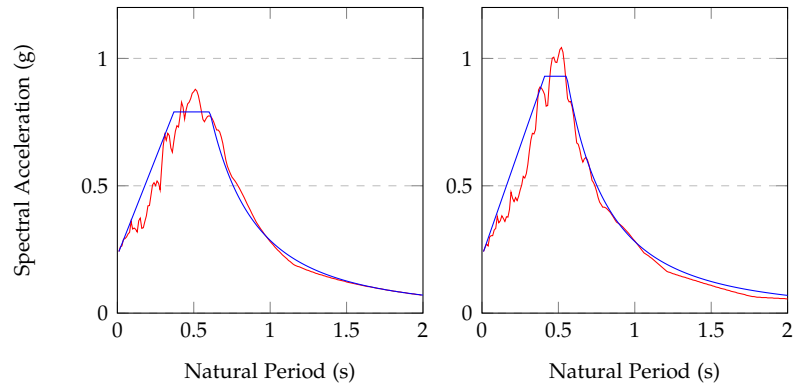
The seismic load is introduced in an MRS analysis by introduced by applying a base excitation, which is amplified by the shapes of the eigenmodes and a factor which is based on a response spectrum. The response spectrum as defined in Appendix F is used as input, which is defined on the outer envelope of the results of NLTH analyses of the soil column. A disadvantage of using the maximum envelope of the response spectra is that a small change in the natural period could lead to a significant change in spectral acceleration. This could have a significant effect on the results of the MRS analyses. Thus the decision has been made the linearise the response spectra for the MRS analyses. This is done by applying the method as is described in NPR 9998:2015. The parameters which define this linearised spectrum are  $S_{MS}$ , the design acceleration in the short period range and  $S_{M1}$ , the design acceleration in the long period range.  $S_{MS}$  is equal to the spectral acceleration at a natural period of 0.2 seconds. It is not allowed to apply a value of  $S_{MS}$  which is lower than 90 % of the spectral acceleration for each natural period higher than 0.2 s. The parameter  $S_{M1}$  is equal to the spectral acceleration at a natural period of 1 second or to twice the spectral acceleration at a natural period of 2 seconds. Equation G.1 can be used subsequently to determine the corner period  $T_c$ , based on these parameters. This corner period is also used as input during the NLPO analyses according to Eurocode 8 and Guerrini. The values of the spectrum parameters in the longitudinal and transverse direction are presented in Table G.1.

$$T_c = \frac{S_{M1}}{S_{MS}} \quad (\text{G.1})$$

Table G.1: Calculation of Parameters for Location-Specific Spectrum

	$S_e(0.2 \text{ s})$	$\max(0.9S_e)$	$S_e(1 \text{ s})$	$2S_e(2 \text{ s})$	$S_{MS}$	$S_{M1}$	$T_c$
Longitudinal	0.42 g	0.79 g	0.28 g	0.11 g	0.79 g	0.28 g	0.60 s
Transverse	0.45 g	0.94 g	0.28 g	0.14 g	0.94 g	0.28 g	0.55 s

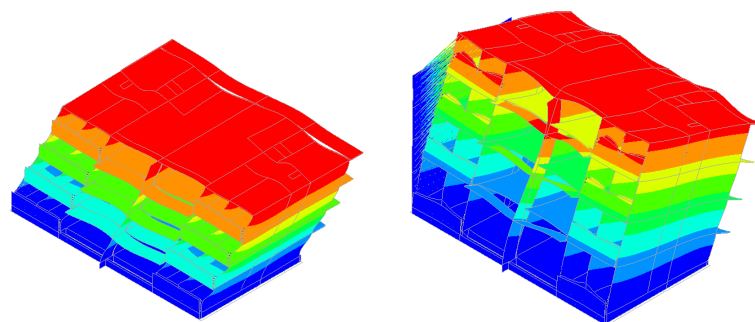
The position of the left corner period of a location-specific spectrum is not specified in NPR 9998:2015. Thus the decision has been made to choose a value for the corner period in such a way, that the outer envelope of the spectra is always smaller than the linearised spectrum. The linearised spectra are presented in Figure G.1.



(a) Transversal Direction (b) Longitudinal Direction  
 Figure G.1: Response Spectra derived from NLTH analyses

G.2 MODAL EIGENVALUE ANALYSIS

The model used for the MRS analysis is different compared to the model used for the NLPO and NLTH analysis because the masonry is modelled using a smaller Young’s modulus. For this reason, the MRS model behaves less stiff compared to the model used for the nonlinear analyses. It is thus required to perform an additional model eigenvalue analysis because due to the change in stiffness, the results will be different compared to the results of the model eigenvalue analysis of the nonlinear model, as described in Chapter 5.3.1. The displacements according to the governing eigenmodes are presented in Figure G.2. The first aspect which can be noted is that the shape of the eigenmodes is almost exactly the same as according to the model eigenvalue analysis of the nonlinear model. However, some significant differences can be seen when looking at the magnitude of the natural periods. The natural period in the longitudinal direction increased from 0.53 second to 0.67 second and the natural period in the transverse direction increased from 0.20 seconds to 0.28 seconds. The linear model behaves less stiff compared to the nonlinear model, which is as expected.



(a) Governing Mode in Longitudinal Direction 0.67 s (72.2%) (b) Governing Mode in Transversal Direction 0.28 s (64.2%)  
 Figure G.2: Governing Modes Part of DIANA Model

Another aspect which is of importance is the cumulative modal mass participation, as presented in Figure G.3. The modal mass participation indicates the significance of eigenmode on the total response of the structure. NPR 9998 states that the sum of the participating mass of the considered eigenmodes during an MRS analysis should be larger than 90 %. The minimum amount of 90 % is exceeded for 248 eigenmodes in the transverse direction and 450 eigenmodes in the longitudinal direction.

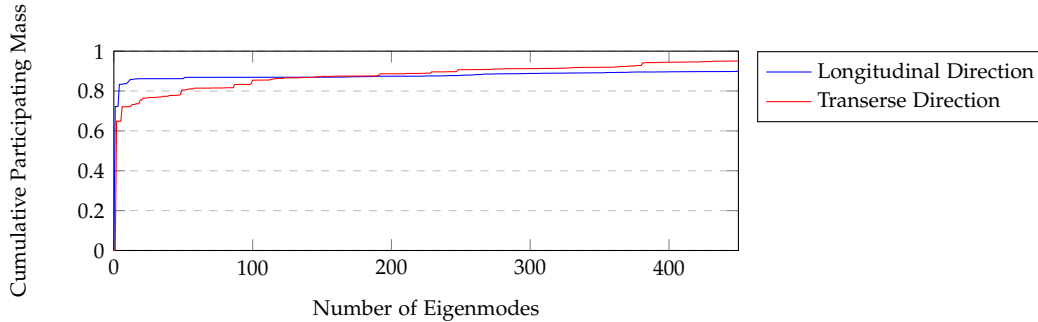


Figure G.3: Cumulative Modal Mass Participation

### G.3 MAXIMUM ADMISSIBLE SEISMIC LOAD

The maximum admissible seismic load is found, by incrementally the demand, until one of the NC limit state criteria are exceeded. The seismic resistance of the structure according to the MRS method will be expressed in terms of the maximum admissible seismic load in terms of PGA at ground level. It should be noted that when checking a structure according to the MRS method for a characteristic load  $E_k$ , that a design load  $E_d$  has to be applied, which can be determined using Equation G.2. The behaviour factor  $q$  takes into account that nonlinear effects are not included in the model. The behaviour factor for unreinforced masonry is defined to be 1.5 in NPR 9998. However, it is allowed to multiply this factor by 4/3 because the NC limit state is studied.

$$E_k = E_d \times q \quad (\text{G.2})$$

In NPR 9998 is defined that primary seismic elements may not fail for the NC limit state criterion. Redistribution of forces is not possible, because MRS is a linear method. Thus exceedance of the force capacity of one of the primary seismic elements results into exceedance of the limit state criteria. Equations are given in NPR 9998 for the force capacity of piers. A more thorough description of these equations can be found in Chapter 4.3.1. Both shear and flexural failure are taken into account by these limit state criteria.

The shear force is determined by determining the maximum average distributed shear force over the height of the pier, and subsequently multiplying this average distributed shear force by the width of the pier. The axial force is determined at the bottom of the pier by determining the distributed axial force in the compressive zone, and subsequently multiplying it by the width of the compressive zone. The shear force is subsequently divided by the capacity of the piers and the results of these calculations are presented using unity checks, which have to be smaller than 1.0, to fulfil the limit state criteria. Several MRS analyses are performed where the seismic demand is scaled until all unity checks are smaller than 1.0.

From the MRS analysis was found that the walls in which the capacity was exceeded the first are wall T2 in the transverse direction and wall L1 in the longitudinal direction. The same wall numbering convention is used as in Chapter 5.3.2, however additional symbols have been added, to indicate the different piers of wall T2. These additional symbols are presented in figure G.4. All performed calculations to determine the capacity according to the MRS method in the transverse and longitudinal direction are presented hereafter. However, the performed calculation steps are only presented for the case in the transverse direction, but the performed calculation steps in the longitudinal direction are exactly the same.

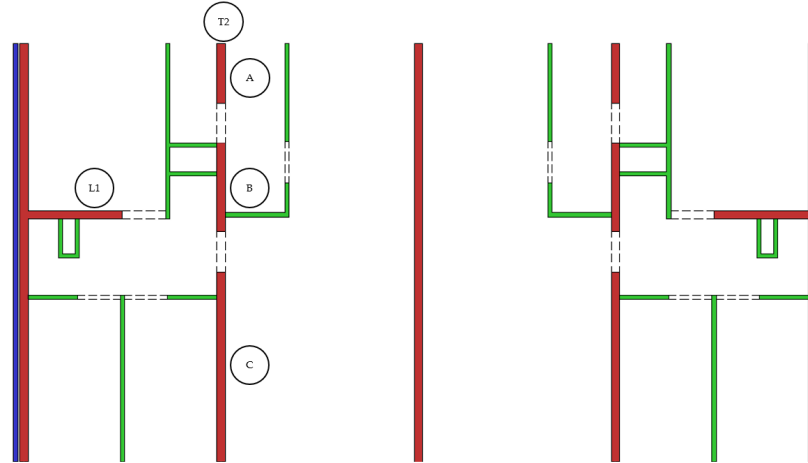


Figure G.4: Wall Numbering

TRANSVERSE DIRECTION

The seismic demand has been scaled until one of the limit state criteria was met. The first limit state criterion was exceeded for a design load of 0.11 g. The characteristic load can be determined subsequently by multiplying the design load with the behaviour factor.

$$E_k = E_d \times q = 0.11 \times 2 = 0.22 \text{ g} \tag{G.3}$$

The output of DIANA which was used to determine the capacity of all the piers is presented in Figure G.5. The axial force is presented twice, using different contour plot settings. This is done because Figure G.5a is required to determine the magnitude of the axial force in the piers and Figure G.5b is required to determine the compressive width of each pier.

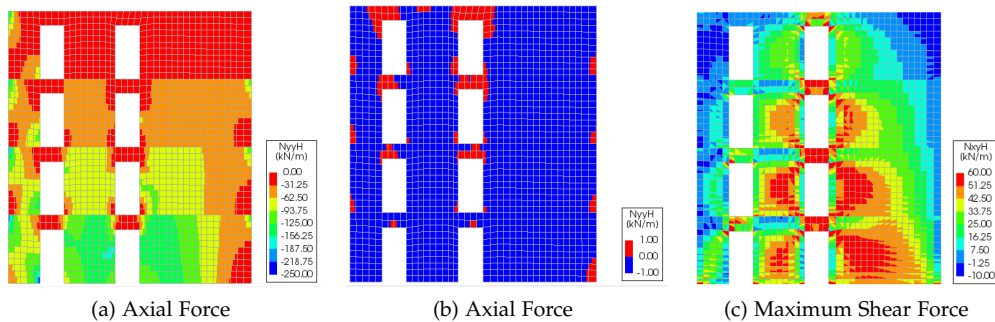


Figure G.5: Distributed Forces - Transverse Direction - Wall T2

The pier in which the limit state criteria are exceeded the first is pier B of wall T2 on the fourth floor. All calculation steps which were taken to determine the capacity of this pier are presented hereafter, as an example. The calculation steps are exactly the same for all other piers. The properties of the governing pier are presented in Table G.2.

Table G.2: Properties Pier 4th Floor Part A

Properties Pier	Symbol	Value	Unit
Width	$D$	2200	mm
Effective Height	$H_{eff}$	2100	mm
Thickness	$t$	200	mm
Cohesion	$c$	0.25	N/mm <sup>2</sup>
Mean compressive Strength	$f_m$	7	N/mm <sup>2</sup>
Material Factor	$\gamma_m$	1.5	-

The first step is to determine the width of the compressive zone because shear can only be transferred through this width. The width of the compressive zone can be determined from Figure G.5b. Tensile forces are presented by the red colour and compressive forces by blue. Thus the compressive zone of the pier is equal to:

$$D' = 2100 \text{ mm} \quad (\text{G.4})$$

The axial and shear force in the pier are determined next. The shear force is determined by determining the maximum average distributed shear force over the height of the pier, and subsequently multiplying this average distributed shear force by the width of the pier. The axial force is determined at the bottom of the pier by determining the distributed axial force in the compressive zone, and subsequently multiplying it by the width of the compressive zone. This results in the following values of the shear and axial force in the pier:

$$V_{Ed} = 40 \text{ kN} \quad \text{and} \quad N_{Ed} = 86 \text{ kN} \quad (\text{G.5})$$

It is required for the shear check to determine the masonry shear strength  $f_{vd}$ , which takes into account the presence of the axial load. The masonry shear strength may not exceed  $0.065f_m/\gamma_m$ .

$$f_{vd} = \frac{c}{\gamma_m} + 0.4 \frac{N}{D't} = \frac{0.25}{1.5} + 0.4 \frac{86}{1200 \times 200} = 0.25 \text{ N/mm}^2 \quad (\text{G.6})$$

The maximum allowed shear force based on the shear failure criterion can subsequently be determined by using:

$$V_{Rd,s} = f_{vd}D't = 0.25 \times 2100 \times 200 = 101 \text{ kN} \quad (\text{G.7})$$

It is required for the flexural check to determine the normalised axial load  $v_d$ .

$$v_d = \frac{N}{Dt f_m} = \frac{86}{2100 \times 200 \times 7} = 0.03 \quad (\text{G.8})$$

The maximum allowed shear force based on the flexural failure check is determined using:

$$V_{Rd,f} = \frac{DN}{2H_0}(1 - 1.15v_d) = \frac{2100 \times 86}{2 \times 2200}(1 - 1.15 \times 0.03) = 40 \text{ kN} \quad (\text{G.9})$$

The maximum allowed shear force for the flexure controlled failure mechanism is lower. Thus this is the governing failure mechanism for this pier. The unity check can be determined by dividing the design load by the capacity of the pier:

$$UC = \frac{V_{Ed}}{V_{f,f}} = \frac{40}{40} = 1.0 \quad (\text{G.10})$$

The calculations steps as described above have been performed for all piers in wall T2. The results of these calculations steps are presented in Table G.3. The first point of interest is that for several piers a flexural failure mechanism would occur and for some a shear-like failure mechanism would occur. It can clearly be seen that a higher axial force would lead to a shear-like failure mechanism. The first failure mechanism which occurs at the smallest load is flexural failure of the pier on the fourth floor of part B. However, the next failure mechanism which occurs is a shear-like failure mechanism of part C of the first floor. This gives an indication that damage in the structure will not be localised on one floor, but it is distributed throughout the structure.

Table G.3: Design Checks MRS - Wall T2

<b>Part</b> <b>(-)</b>	<b>Floor</b> <b>(-)</b>	<b><math>D'</math></b> <b>(mm)</b>	<b><math>V_{Ed}</math></b> <b>(kN)</b>	<b><math>N_{Ed}</math></b> <b>(kN)</b>	<b><math>V_{Rd,s}</math></b> <b>(kN)</b>	<b><math>V_{Rd,f}</math></b> <b>(kN)</b>	<b><math>UC</math></b> <b>(-)</b>
A	4	1200	2	62	65	18	0.1
A	3	1200	11	127	73	35	0.3
A	2	1200	17	191	73	50	0.3
A	1	1300	29	259	79	64	0.4
B	4	2000	40	86	101	40	1.0
B	3	2000	72	174	121	78	0.9
B	2	2100	86	254	127	109	0.8
B	1	2100	101	342	127	141	0.8
C	4	4400	81	152	207	154	0.5
C	3	4400	157	317	267	313	0.6
C	2	4400	205	474	267	453	0.8
C	1	4300	238	616	261	573	0.9

LONGITUDINAL DIRECTION

The same steps as described for the transverse direction are taken to determine the capacity in the transverse direction. The seismic demand has been scaled until one of the limit state criteria are met. The first limit state criterion is exceeded for a design load of 0.015 g. The characteristic load can be determined subsequently by multiplying the design load with the behaviour factor.

$$E_k = E_d \times q = 0.015 \times 2 = 0.03 \text{ g} \tag{G.11}$$

The relevant output of DIANA which is required to perform the limit state checks is presented in Figure G.6. The axial force is presented twice, using different contour plot settings. This is done because Figure G.6a is required to determine the magnitude of the axial force in the pier and Figure G.6b is required to determine the compressive zone of each pier.

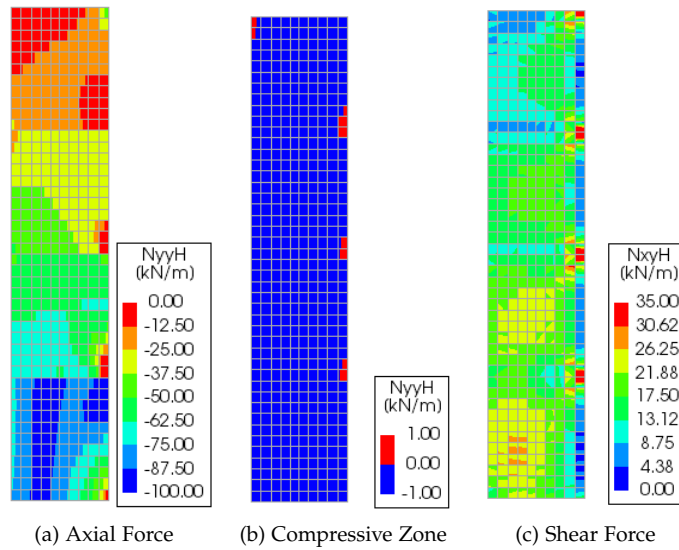


Figure G.6: Distributed Forces - Longitudinal Direction - Wall L2

The pier in which the limit state criteria are exceeded the first is the pier on the fourth floor of wall L1. The unity checks of all the pier in wall L1 are presented in Appendix G.4. It can clearly be seen that a flexural type of failure mechanism occurs before a bed joint sliding failure mechanism would occur.

Table G.4: Design Checks MRS - Wall L1

Floor (-)	$D'$ (mm)	$V_{Ed}$ (kN)	$N_{Ed}$ (kN)	$V_{Rd,s}$ (kN)	$V_{Rd,f}$ (kN)	$UC$ (-)
4	2000	20	46	85	20	1.0
3	2000	33	95	104	38	0.9
2	2000	46	142	121	55	0.8
1	2200	59	202	133	77	0.8



## RESULTS: NONLINEAR PUSHOVER ANALYSIS

The results of the nonlinear pushover analyses are presented in this chapter. The capacity curves are shown first, which will be evaluated according to NPR 9998, Eurocode 8 and Guerrini subsequently. The maximum admissible seismic load is determined next. Furthermore, the inter-story drifts during the pushover analyses are presented. The section closes with an overview of the damage parameters at failure.

### H.1 CAPACITY CURVES

The first step in performing an NLPO analysis is determining the capacity curves of a structure. These capacity curves are determined by applying a lateral load to the structure using a particular vertical distribution of the loads. It is specified in the NPR 9998 that at least two vertical distributions of the vertical load have to be applied. Furthermore, an individual capacity curve has to be determined in each of the four directions. These directions are the positive longitudinal direction, negative longitudinal direction, positive transverse direction and negative transverse direction. Thus in total eight capacity curves have to be performed for a single NLPO analysis. However, only the governing case of the positive and negative direction has to be studied. Thus also only the governing load case of these two is presented. Furthermore, the capacity curves are determined according to DIANA and 3MURI. These capacity curves are presented in Figure H.1.

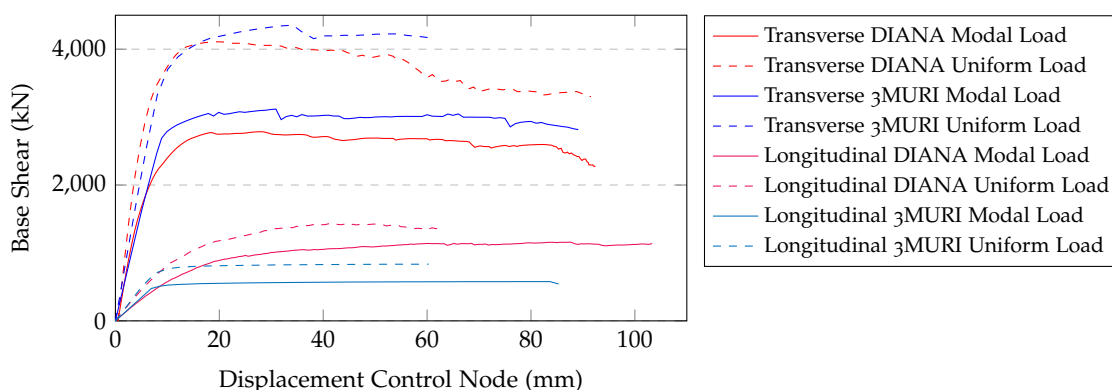


Figure H.1: Pushover Curves

The structure is incrementally loaded until one of the limit state criteria according to NPR 9998 are met. These limit state criteria are the following: Dynamic instability of the structure, a strength degradation of 80 % in comparison with the maximum base shear or exceedance of the inter-story drift limit criteria. Each capacity curve has also been determined twice in 3MURI, once taken into account failure according to the Mohr-Coulomb criterion and once using the one as formulated by Turnsec-Cacovic. It turned out that the capacity curve of the Mohr-Coulomb criterion had a lower capacity in all cases. Thus only the results of these analyses are shown.

An overview can be found in Table H.1 of the limit state criteria, which were exceeded first per load case. A more thorough description of which elements are failed in case of numerical instability or in which elements the most damage occurred is presented in Chapter H.4. The inter-story drifts during the analyses are presented in Chapter H.3.

Table H.1: Overview Characteristics Capacity Curves

Direction	Load Pattern	Program	$k_{init}$ (kN/mm)	$V_b$ (kN)	$u_{cap}$ (mm)	Violated Criterion
Transverse	Modal	DIANA	309	2785	99.7	Strength Degredation
Transverse	Modal	3MURI	281	2994	89.1	Dynamic Instability
Transverse	Uniform	DIANA	489	4109	91.6	Strength Degredation
Transverse	Uniform	3MURI	435	4353	60.2	Dynamic Instability
Longitudinal	Modal	DIANA	66	1159	103.4	Drift Limits
Longitudinal	Modal	3MURI	69	576	85.3	Dynamic Instability
Longitudinal	Uniform	DIANA	95	1443	62.5	Drift Limits
Longitudinal	Uniform	3MURI	99	835	60.3	Dynamic Instability

## H.2 MAXIMUM ADMISSIBLE SEISMIC LOAD

The maximum admissible seismic load according to the NC limit state criteria is determined for all the load cases. This maximum admissible seismic load is expressed in terms of the PGA at ground level. Three methods are used to determine the maximum admissible seismic load: NPR 9998, Eurocode 8 and Guerrini. All methods are presented hereafter by showing all the calculations steps taken for one of the load cases. The load case that is used as an example is the uniform lateral load pattern in the transverse direction using DIANA. The first calculation steps are exactly the same for all methods, and it is noted where the methods start to differ from each other.

The first step according to all methods is to transform the capacity curve of the MDoF system into an equivalent SDoF system. This is done by dividing the base shear  $F_b$  and displacement of the control node  $d_n$  by the transformation factor  $\Gamma$ . The transformation factor depends on the distribution of mass throughout the structure and the displacements which correspond to the governing modal eigenmode. The following equations are used to determine the transformation factor:

$$\Gamma = \frac{m_{eff}}{\sum m_i \phi_i^2} \quad \text{and} \quad m_{eff} = \sum m_i \phi_i \quad (\text{H.1})$$

where  $m_i$  is  $\phi_i$  are the mass and displacement of each floor respectively.  $m_{eff}$  is the effective mass of the structure. The mass of each floor is determined by adding up the dead weight of the elements which are connected to the floor and the dead weight of the floor itself. The mass of the walls is taken into account by adding half of the mass to the floor which is on top of it, and the half to the floor underneath it. An overview of the mass per floor is shown in Table H.2.

Table H.2: Overview Mass per Floor

	Floors	Balconies	Galleries	Walls	Beams	Line Loads	Total	Unit
<b>Roof</b>	934	0	0	433	90	25	1481.0	kN
<b>Floor 3</b>	955	67	139	911	90	41	2198	kN
<b>Floor 2</b>	955	67	139	911	90	41	2198	kN
<b>Floor 1</b>	955	67	139	911	90	41	2198	kN
<b>Ground Floor</b>	769	0	0	478	0	25	1272	kN

The effective mass can subsequently be calculated by multiplying the mass of each floor with the corresponding displacement of that floor of the governing eigenmode. The displacements are normalised in such a way that the displacement of the roof is equal to 1. The calculation of the effective mass is shown for the governing pushover case.

Table H.3: Example Effective Mass Calculation

	$m_i$ (kN)	$\phi_i$ (-)	$m_i\phi_i$ (kN)	$m_i\phi_i^2$ (kN)
<b>Roof</b>	1481.0	1.00	1481.0	1481.0
<b>Floor 3</b>	2198.0	0.80	1766.6	1419.9
<b>Floor 2</b>	2198.0	0.54	1195.8	650.6
<b>Floor 1</b>	2198.0	0.25	559.5	142.4
<b>Ground Floor</b>	1271.9	0.00	0	0

The effective mass and the transformation factor can be calculated subsequently by applying Equation H.2. The effective mass is determined in the same way, for all the other load cases. These results are summarized in Table H.4.

$$m_{eff} = \sum m_i\phi_i = 5003 \text{ (kN)} \quad \Gamma = \frac{m_{eff}}{\sum m_i\phi_i^2} = 1.35 \quad (\text{H.2})$$

Table H.4: Effective Mass and Transformation Factor per Load Case

	Effective Mass (kN)	$\Gamma$ (-)
DIANA Longitudinal	5003	1.35
3MURI Longitudinal	5216	1.31
DIANA Transverse	4717	1.39
3MURI Transverse	4650	1.39

The second step is to transform the capacity curves of the MDoF systems to the capacity curves of their equivalent SDoF systems. The equivalent capacity curve for the pushover in the longitudinal direction with a uniform lateral load pattern in DIANA is presented as an example in Figure H.2.

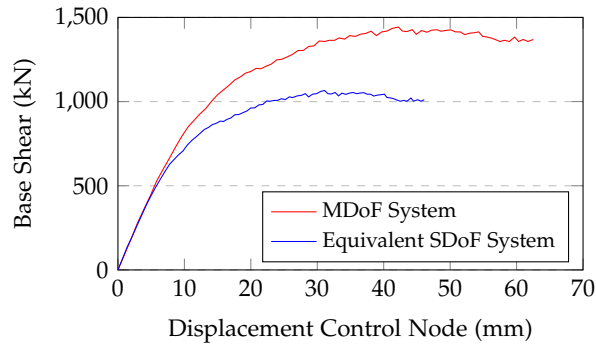


Figure H.2: Example Transformation Capacity Curve

The capacity curve of this equivalent SDoF system should subsequently be bi-linearised. Eurocode 8 and NPR 9998 prescribe different methods for doing this. The bi-linearised curve according to the NPR 9998 method is formulated in such a way that the deformation energy of the original curve should be the same as the bi-linearised curve. This is different in comparison with Eurocode 8 because there is stated that only the deformation energy up until the formulation of the plastic mechanism in both curves should be equal. Another difference is that the yield force of the bi-linearised system in Eurocode 8 is specified as the ultimate strength of the generalised system. In NPR 9998 this yield force is determined based on the initial system of the bi-linearised system, which in its part is determined using displacement of the control node at 60 % of the maximum load capacity. Thus in Eurocode 8 the yield force is given, and the yield displacement has to be determined accordingly, and for the NPR the yield displacement if given and the yield force has to be determined accordingly. Both methods are described thoroughly in Chapter 3.3. Both the bi-linearised curves according to the NPR 9998 and Eurocode 8 are presented in Figure H.3. The next step is to evaluate the capacity of the bi-linearised pushover curves with the demand. The demand is defined differently according to the three studied methods.

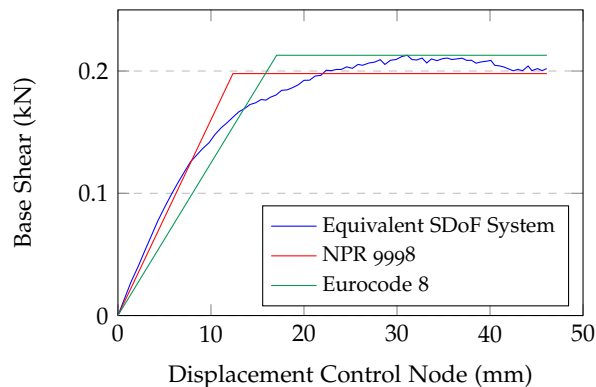


Figure H.3: Bi-Linearisation of Equivalent SDoF Pushover Curve

H.2.1 NPR 9998

The demand, which is represented by a response spectrum, is scaled until the capacity and the demand are equal. This equilibrium situation is presented in Figure H.4. The capacity of a structure is evaluated according to NPR 9998 by comparing the bi-linearised curve with a nonlinear acceleration displacement response spectrum (ADRS). This nonlinear ADRS is determined by reducing the elastic spectrum by introducing a spectral reduction factor  $\eta_{\xi}$ . This reduction factor takes into account, hysteretic, inherent and soil damping. Soil damping does not have to be taken into account, because it is also excluded in the NLTH analyses, because the signal is scaled at ground level. The inherent damping is prescribed to be 5% in the NPR 9998. A description of all the parameters and explanation of the formulas can be found in Chapter 3.3. The following equations are used to determine the hysteresis damping:

$$\mu_{sys} = \frac{u_{cap,sys}}{d_y^*} = \frac{46.1}{12.4} = 3.73 \tag{H.3}$$

$$\xi_{hys} = 0.42 \left( 1 - \frac{0.9}{\sqrt{\mu_{sys}}} - 0.1\sqrt{\mu_{sys}} \right) = 14.3\% \tag{H.4}$$

Thus the equivalent viscous damping  $\xi_{sys}$  can be determined using:

$$\xi_{sys} = \xi_{inherent} + \xi_{hysteric} = 5\% + 14.3\% = 19.3\% \tag{H.5}$$

And subsequently the reduction factor can be determined:

$$\eta_{\xi} = \sqrt{\frac{10}{5 + 19.3}} > 57.3\% \tag{H.6}$$

The following step is to draw the elastic spectrum, nonlinear spectrum and the bi-linearised pushover curve drawn in the same graph. The elastic spectrum is subsequently scaled until the nonlinear spectrum crosses the pushover curve. The demand and capacity are equal when the two lines cross. This situation is presented in Figure H.4.

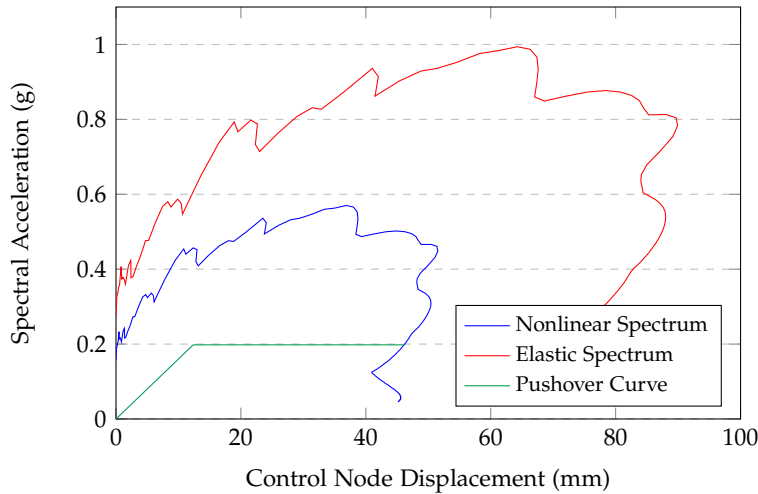


Figure H.4: Comparison Capacity and Demand according to NPR 9998

The situation in which the capacity and the demand are equal is shown in Figure H.4. The peak ground acceleration, in this case, is equal to the spectral acceleration of the elastic spectrum at a control node displacement of zero. Thus, in this case, the maximum admissible seismic load is equal to a PGA of 0.27 g. An overview of the maximum admissible seismic load according to the other load cases can be found in Table H.5 and H.6.

## H.2.2 EUROCODE 8

The demand is scaled until the capacity and the demand are equal, according to Eurocode 8. This equilibrium situation is presented in Figure H.5. The capacity of a structure is evaluated according to Eurocode 8 by comparing the bi-linearised curve with the elastic ADRS. A description of all the parameters and explanation of the formulas can be found in Chapter 3.3. The first step of the method according to Eurocode 8 is to determine the period of the idealised equivalent SDoF system.

$$T^* = 2\pi \sqrt{\frac{m^* d_y^*}{F_y^*}} = 2\pi \sqrt{\frac{509,987 \times 0.017}{1,065,585}} = 0.57 \text{ s} \quad (\text{H.7})$$

The elastic acceleration response  $S_e$  at period  $T^*$  and the corresponding target displacement of the structure assuming unlimited elastic behaviour  $d_{el}^*$  can now be determined using:

$$S_e(T^*) = 0.56 \text{ g} \quad \text{and} \quad d_{el}^* = S_e(T^*) \left(\frac{T^*}{2\pi}\right)^2 = 0.56 \left(\frac{0.57}{2\pi}\right)^2 = 44.6 \text{ mm} \quad (\text{H.8})$$

For the determination of the target displacement  $d^*$  should be checked if the period of the SDoF system is larger or smaller compared to the corner period.

$$T_c = 0.60 \text{ s} \quad \text{and} \quad T^* = 0.57 \text{ s} \quad \text{thus} \quad T^* < T_c \quad (\text{H.9})$$

Subsequently has to be checked if the response is elastic or nonlinear by using:

$$\frac{F_y^*}{m^*} = \frac{1,066,000}{509,9879} = 0.21 \text{ g} \quad \text{and} \quad S_c(T^*) = 0.56 \text{ g} \quad \text{thus} \quad \frac{F_y^*}{m^*} < S_c(T^*) \quad (\text{H.10})$$

thus the response is nonlinear. The ratio  $q_u$  between the capacity of the structure assuming unlimited elastic behaviour and the nonlinear capacity has to be determined subsequently:

$$q_u = \frac{S_c(T^*) m^*}{F_y^*} = \frac{0.56 \times 509,987}{1,065,585} = 2.61 \quad (\text{H.11})$$

The target displacement can be determined subsequently using:

$$d_t^* = \frac{d_{el}^*}{q_u} \left(1 + (q_u - 1) \frac{T_c}{T^*}\right) = \frac{0.0446}{2.61} \left(1 + (2.61 - 1) \frac{0.60}{0.57}\right) = 46.1 \text{ mm} \quad (\text{H.12})$$

The last step is to transform the target displacement of the equivalent SDoF system back to the MDoF system.

$$d_t = \Gamma d_t^* = 1.35 \times 46.1 = 62.5 \quad (\text{H.13})$$

Thus in the situation as described above, the capacity  $d_{cap}$  is equal to the demand  $d_t$ . The situation in which the capacity and the demand are equal is shown in Figure H.5. The seismic load, in this case, is equal to the spectral acceleration of the elastic spectrum at a control node displacement of zero. Thus, in this case, the maximum admissible seismic load is equal to a PGA at ground level of 0.18 g. An overview of the PGA at NC for the other load cases can be found in Table H.5 and H.6.

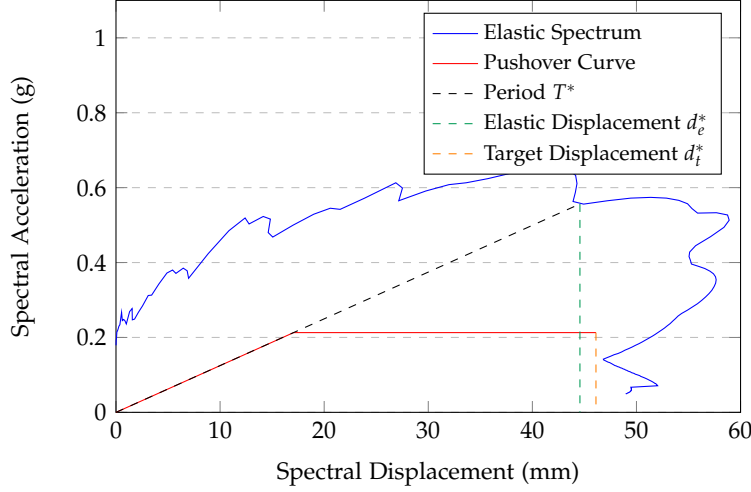


Figure H.5: Comparison Capacity and Demand according to Eurocode 8

### H.2.3 GUERRINI

The demand is scaled until the capacity and the demand are equal, according to Guerrini. This equilibrium situation is presented below. The same bi-linearised capacity curve has to be used as was used for the Eurocode 8 assessment. The only difference between the methods is the equation that is used to relate the elastic and inelastic demands of the equivalent SDoF system. Thus the same natural period as determined in Equation H.7 can be used. This results in the following values of the elastic acceleration response  $S_e$  and the target displacement  $t_d^*$ :

$$S_e(T^*) = 0.53 \text{ g} \quad \text{and} \quad d_{el}^* = S_e(T^*) \left( \frac{T^*}{2\pi} \right)^2 = 0.53 \left( \frac{0.57}{2\pi} \right)^2 = 42.2 \text{ mm} \quad (\text{H.14})$$

The ratio  $q_u$  between the capacity of the structure assuming unlimited elastic behaviour and the nonlinear capacity has to be determined subsequently:

$$q_u = \frac{S_c(T^*) m^*}{F_y^*} = \frac{0.53 \times 509,987}{1,065,585} = 2.47 \quad (\text{H.15})$$

The target displacement can be determined by using Equation H.16 which is proposed by Guerrini. This equation replaces Equation H.12 which is used to relate the inelastic and elastic displacement demands.

$$d_t^* = \frac{d_{el}^*}{q_u} \left( \frac{(q_u - 1)^c}{\left( \frac{T}{T_{hyst}} + \alpha_{hyst} \right) \left( \frac{T}{T_C} \right)^b} + q_u \right) \quad (\text{H.16})$$

An explanation of all parameters required in this formula can be found in Chapter 3.3. The parameters  $b$ ,  $c$ ,  $\alpha_{hyst}$  and  $T_{hyst}$  depend on the amount of hysteretic dissipation in a structure. This hysteretic dissipation was already calculated for the NPR 9998 assessment. In the NPR 9998 is prescribed that the hysteretic damping in a URM structure is always smaller than 15 %. The decision has been made, given this information, that a hysteretic damping of 15% is also taken as a maximum for the assessment according to Guerrini. A consequence of this assumption is that the most conservative values are used for the parameters  $b$ ,  $c$ ,  $\alpha_{hyst}$  and  $T_{hyst}$ . Thus the following parameters have to be used in Equation H.16:

$$b = 2.3 \quad c = 2.1 \quad \alpha_{hyst} = 0.7 \quad T_{hyst} = 0.055 \text{ s} \quad (\text{H.17})$$

The target displacement can be determined subsequently:

$$d_t^* = \frac{42.4}{2.47} \left( \frac{(2.47 - 1)^{2.1}}{\left(\frac{0.57}{0.055} + 0.7\right) \left(\frac{0.57}{0.6}\right)^{2.3}} + 2.46 \right) = 46.1 \quad (\text{H.18})$$

The last step is to transform the target displacement of the equivalent SDoF system back to the MDoF system.

$$d_t = \Gamma d_t^* = 1.35 \times 46.1 = 62.5 \quad (\text{H.19})$$

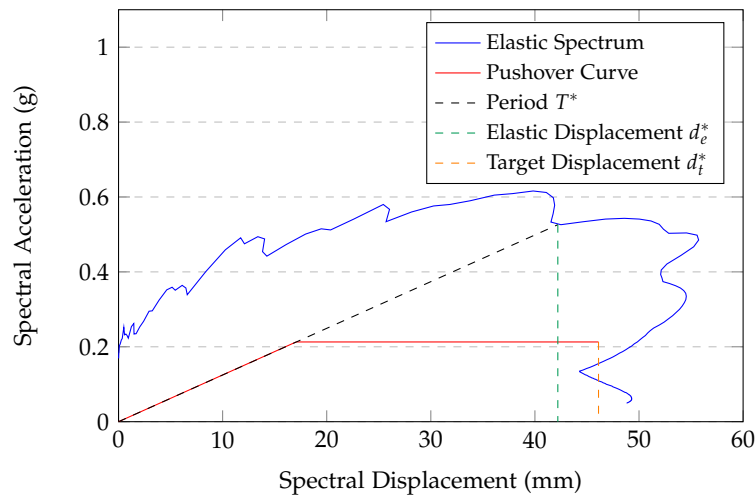


Figure H.6: Comparison Capacity and Demand according to Guerrini

The situation in which the capacity and the demand are equal is shown in figure H.6. The seismic load, in this case, is equal to the spectral acceleration of the elastic spectrum at a control node displacement of zero. Thus, in this case, the maximum admissible seismic load is equal to 0.17 g. An overview maximum admissible seismic load according to the other load cases can be found in table H.5 and H.6.

## H.2.4 OVERVIEW RESULTS

An overview of the maximum admissible seismic load according to all load cases and target displacement calculation methods is presented in Table H.5 and H.6. Both the maximum PGA which correspond to the 0.6 and 1.5 % drift limit criteria are presented. Which one of the inter-story drift limits is governing depends on if a ductile or brittle inelastic mechanisms are occurring. This is elaborated more thoroughly in the discussion of the results.

Table H.5: Maximum Admissible Seismic Load according to 0.6 % Drift Limit

Direction	Load Pattern	Program	Displacement Capacity (mm)	Max PGA NPR 9998 (g)	Max PGA Eurocode 8 (g)	Max PGA Guerrini (g)
Transverse	Modal	DIANA	61.1	<b>0.31</b>	0.78	0.63
Transverse	Modal	3MURI	53.0	<b>0.27</b>	0.59	0.56
Transverse	Uniform	DIANA	41.7	<b>0.28</b>	0.89	0.78
Transverse	Uniform	3MURI	35.2	<b>0.30</b>	0.73	0.71
Longitudinal	Modal	DIANA	48.0	0.20	0.11	<b>0.11</b>
Longitudinal	Modal	3MURI	53.0	0.25	0.13	<b>0.13</b>
Longitudinal	Uniform	DIANA	32.6	0.12	0.09	<b>0.09</b>
Longitudinal	Uniform	3MURI	37.0	0.14	0.11	<b>0.11</b>

Table H.6: Maximum Admissible Seismic Load according to 1.5 % Drift Limit

Direction	Load Pattern	Program	Displacement Capacity (mm)	Max PGA NPR 9998 (g)	Max PGA Eurocode 8 (g)	Max PGA Guerrini (g)
Transverse	Modal	DIANA	99.7	<b>0.46</b>	1.12	0.76
Transverse	Modal	3MURI	89.1	<b>0.44</b>	0.91	0.72
Transverse	Uniform	DIANA	91.6	<b>0.47</b>	1.67	1.00
Transverse	Uniform	3MURI	60.2	<b>0.30</b>	1.06	0.95
Longitudinal	Modal	DIANA	103.4	0.45	0.25	<b>0.25</b>
Longitudinal	Modal	3MURI	85.3	0.40	0.21	<b>0.21</b>
Longitudinal	Uniform	DIANA	62.5	0.27	0.18	<b>0.17</b>
Longitudinal	Uniform	3MURI	60.3	0.30	0.17	<b>0.14</b>

The first point of interest when looking at the assessment of the capacity curves is that maximum admissible seismic load of the structure according to Guerrini is always lower or the same as the maximum admissible seismic load according to Eurocode 8. This is as expected because Guerrini developed his method because he found out that the demand of low period structures was often underestimated when applying the regular N2-method.

Another point of interest is the difference in the maximum admissible seismic load according to the NPR 9998 and Eurocode 8. It can be seen that the maximum admissible seismic load is higher according to NPR 9998 for the longitudinal cases while it is smaller for the transverse cases, in comparison with Eurocode 8. This difference can be explained by looking into the different calculations methods for determining the target displacement and the properties of the capacity curves in the different loading directions.

First of all, it should be noted that the displacement capacity in both directions is comparable. Thus it could not be a reason for the difference in results. Also should be noted that the capacity in terms of displacement was governing in all cases. Thus the capacity in terms of base shear is also not the reason for the difference in results. A parameter which could explain the difference is the natural period of the idealised equivalent SDoF systems. These natural periods are presented in Table H.7.

Table H.7: Natural Periods of Idealized Equivalent SDoF System

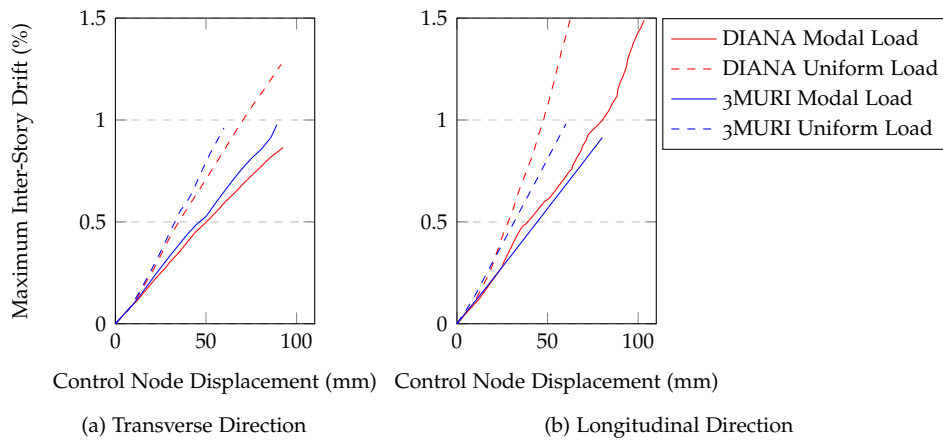
Direction	Load Pattern	Program	Natural Period	Natural Period
			NPR 9998 (s)	Eurocode 8 (s)
Transverse	Modal	DIANA	0.23	0.26
Transverse	Modal	3MURI	0.26	0.29
Transverse	Uniform	DIANA	0.18	0.20
Transverse	Uniform	3MURI	0.21	0.23
Longitudinal	Modal	DIANA	0.61	0.73
Longitudinal	Modal	3MURI	0.54	0.64
Longitudinal	Uniform	DIANA	0.50	0.57
Longitudinal	Uniform	3MURI	0.45	0.51

It can be seen that the natural periods of the equivalent SDoF systems are considerably lower in the transverse direction compared to the longitudinal direction. This is due to the fact that the structure behaves significantly stiffer in the transverse direction. This difference in natural period could be related to the difference in results between Eurocode 8 and NPR 9998. Eurocode 8 uses the natural period as input for the determination of the target displacement, while this parameter is not taken into account directly in the method as described in the NPR 9998. However, it should be noted that the natural period of the structure is taken into account indirectly in the NPR 9998 method. Because if the assumption is made that the displacement and force capacity of a capacity curve are kept constant, then a change of the natural period would lead in a change in the ductility of the structure. Furthermore, a change in ductility would lead to a change in the amount of hysteretic damping which could be taken into account, which has an effect on the reduction factor which is used to transform the elastic demand to the nonlinear demand. It should be noted though that a change in ductility only affects the target displacement if the ductility is smaller than 4. The effect that a change of the natural period has, while all other parameters are kept constant, has a more substantial effect on the target displacement according to Eurocode 8 than NPR 9998.

Thus the results indicate that the NPR 9998 is more conservative for structures which behave with a comparable stiffness and displacement capacity in the transverse direction and Eurocode 8 is more conservative for structures which behave with a comparable stiffness and displacement capacity in the longitudinal direction. More research should be performed to support this hypothesis, but this research is considered to be outside of the scope of this study. However, one aspect that is studied in this report is which of the building codes predicts the same capacity as is determined by an NLTH analysis. This topic is elaborated in Chapter 6.2.4.

H.3 INTER-STORY DRIFTS

The inter-story drifts are one of the limit state criteria which are given by the NPR 9998. Furthermore, the inter-story drifts also indicate where in the structure damage is most likely occurring. NPR-9998 specifies an inter-story drift limit of 1.5 % for ductile inelastic mechanisms and an inter-story drift limit of 0.6 % for brittle inelastic mechanisms. In Chapter H.1, was specified that the 1.5 % drift limit was only met for the load cases in the longitudinal direction using the DIANA model. The evolution of the inter-story drifts during the loading of the structure according to the different load cases is presented in Figure H.7. The maximum inter-story drifts are shown during the pushover analyses. It can first be seen that during all load cases, the 0.6% drift limit is exceeded before any other limit state criterion is met. Secondly, it can be seen that the 1.5% drift limit is only exceeded for the NLPO analyses in DIANA in the longitudinal direction. In all other cases, other limit state criteria are met, before the 1.5 % drift limit is met. Another interesting aspect of the graph is that the behaviour of the structure in terms of maximum occurring inter-story drift in DIANA and 3MURI is similar.



(a) Transverse Direction (b) Longitudinal Direction  
 Figure H.7: Maximum Inter-Story Drift vs Control Node Displacement

The next step is to look into the displacement profile at the moment of failure. This is done by plotting the normalised displacement of each floor. The normalised displacement is determined by dividing the displacement of each floor, by the displacement of the roof. This is shown in Figure H.8.

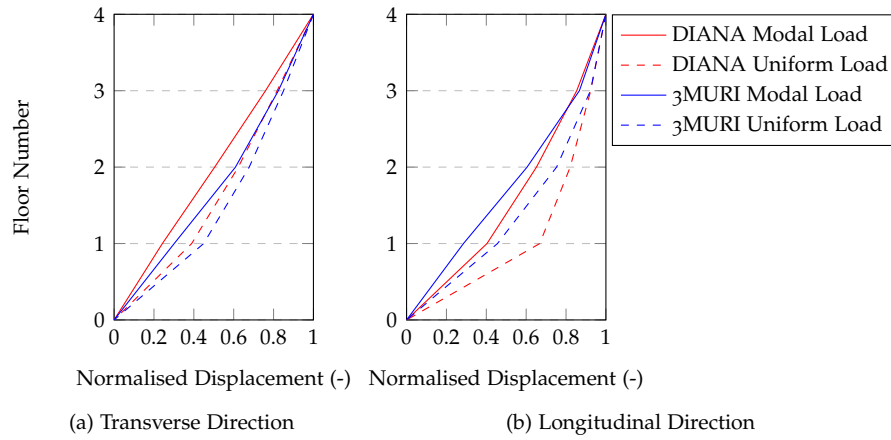


Figure H.8: Displacement Profile

An interesting aspect of Figure H.8 is that in both directions, the deformation of the uniform load patterns is more concentrated in the lower floors. This becomes even more clear when looking at the inter-story drift per floor at the moment of failure, which is plotted in Figure H.9.

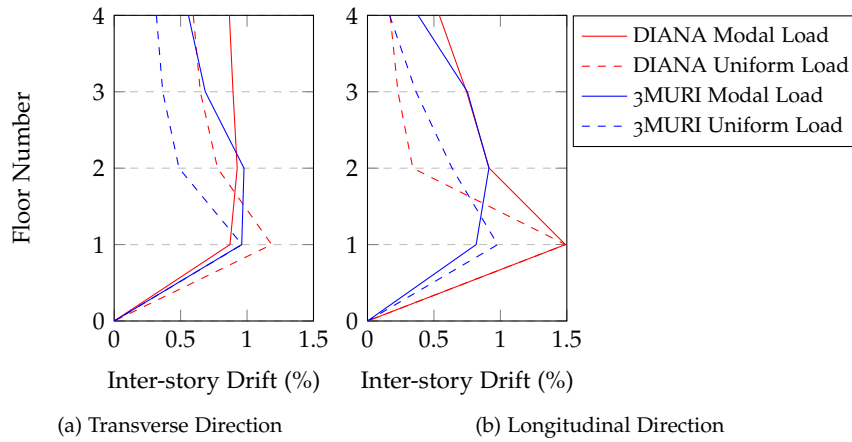


Figure H.9: Interstory Drift per Floor at Failure

It can clearly be seen that in almost all load cases, the inter-story drifts of the first floor are governing, except for the modal load distributions in the transverse direction and the modal load distribution in the longitudinal direction in 3MURI. Another interesting aspect is that the inter-story drifts of the first floor for the uniform load distributions are significantly higher than those of the other floors.

#### H.4 DAMAGE PARAMETERS AT FAILURE

The damage parameters at the failure of all load cases are presented in this section. The output of DIANA which is presented are the crack widths, bed joint state parameter and head joint state parameter. A description of the masonry damage status parameters can be found in Appendix E.

3MURI is not able to plot a similar output. The only output from 3MURI which is available is an indication of each element what kind of damage is occurring and if the element has failed due to that kind of damage. An element which is damaged is defined as an element in which the force capacity has been reached, but the element still has displacement capacity. An element is defined to be failed if the displacement capacity has been reached. The decision has been made to not show the output of all walls in the same image, to keep the output as clear as possible. The output of all walls has been studied first and afterwards a selection of walls is made in which the most damage occurred at failure. The same wall numbering is used as was done in Chapter 5.3. The wall numbering configuration is presented in Figure H.10 for convenience.

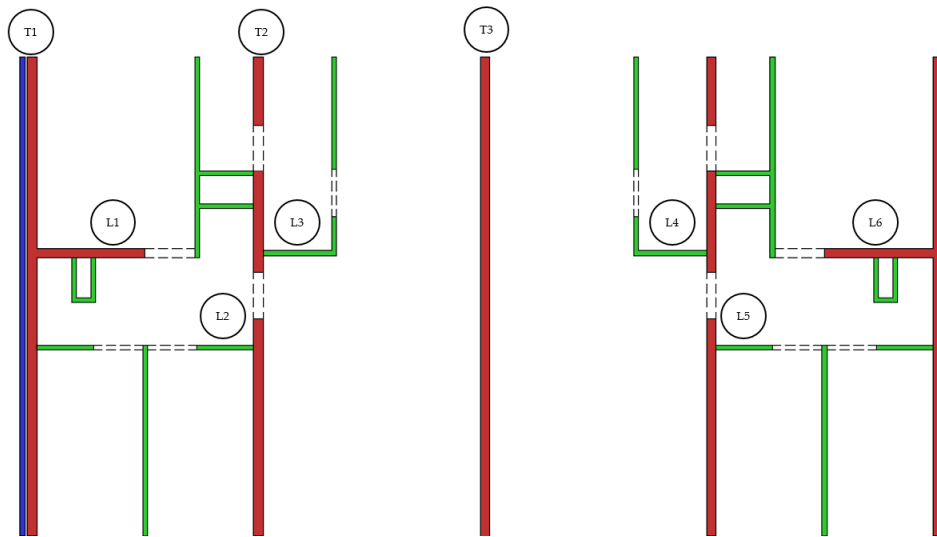


Figure H.10: Wall Numbering

From the results of the analyses can be seen that for the load cases in the longitudinal direction, most damage was concentrated in walls L<sub>1</sub>, L<sub>2</sub>, L<sub>3</sub>, L<sub>4</sub>, L<sub>5</sub> and L<sub>6</sub>. For the load cases in the transverse direction, the most damage is found in wall T<sub>2</sub>. Thus only these walls will be shown in the elaboration of the damage at failure hereafter.

LONGITUDINAL DIRECTION - UNIFORM LOAD DISTRIBUTION

The capacity curves of this load case are characterised by failure due to the exceedance of the 1.5% drift limit of the first floor according to DIANA and numerical instability according to 3MURI. From the inter-story drifts which are presented in Figure H.9 can be seen that the inter-story drifts of the first floor are significantly higher in comparison with the other floors. Thus the most damage can also be observed in this floor. This is supported by the crack widths which are shown in Figure H.11a. It can clearly be seen that the only significant cracks are developed on the first floor. The cracks in the left bottom corner indicate that some rocking behaviour is occurring. When looking at the bed shear parameter, can be seen that in the right bottom corner some crushing failure occurs, but the parameter 3 is not reached yet, which means that the compression is stiff in its softening phase. Some diagonal cracks can also be seen, which goes together with the failure of the head joints, as shown in Figure H.11c. Based on the fact that no clear crushing behaviour can be found, and clear diagonal cracks are developing, it can be concluded that a shear dominated failure mechanism occurred.

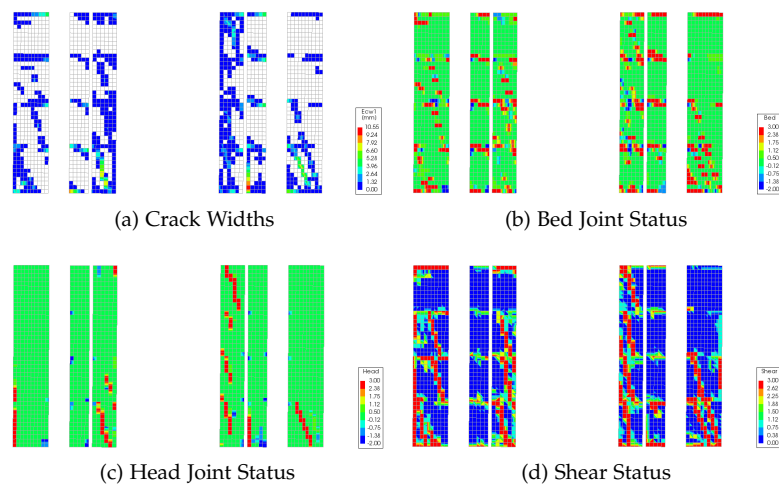


Figure H.11: DIANA Damage Parameters at Failure - Uniform Load Distribution

The output of 3MURI is not as specific as in DIANA. The only damage parameter available indicates that a shear governed mechanism is occurring. This is a sliding shear mechanism, due to the choice of the masonry model in 3MURI, which is explained in Chapter H.1. An interesting aspect is that only damage occurred in the elements and none of the elements in the entire model has failed, even though the program was still not able to find numerical stability.

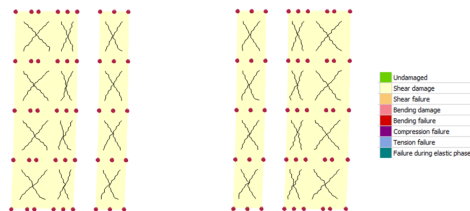


Figure H.12: 3MURI Damage Parameter at Failure - Uniform Load Distribution

LONGITUDINAL DIRECTION - MODAL LOAD DISTRIBUTION

The capacity of the pushover curve was reached when the inter-story drift limits of the second floor were exceeded. This is partly visible by looking at the distribution of the crack widths throughout the structure. It can clearly be seen that diagonal cracks have developed on the first, second and third floor. This was not the case for the uniform load distribution, where only significant cracks occurred on the first floor. That the damage is way better distributed over the structure is even more clear when looking at the head and bed joint failure parameters, where tensional failure is visible on all floors. An interesting aspect is that compressional failure of the bed joints can be observed which was not the case for the uniform load distribution. Even though some crushing behaviour can be found, is it more like that the structure would fail due to its shear behaviour, which is clearly visible on wall 1, 2 and 3.

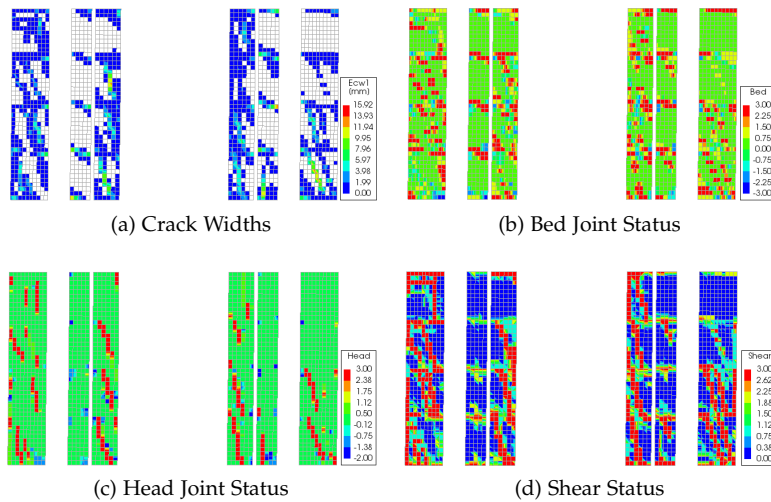


Figure H.13: DIANA Damage Parameters at Failure - Modal Load Distribution

The output of 3MURI of the uniform load distribution and modal load distribution in terms of the damage parameter is exactly the same. A shear governed type of behaviour can be found over the entire height of the structure, but it does not result in the failure of a single element.

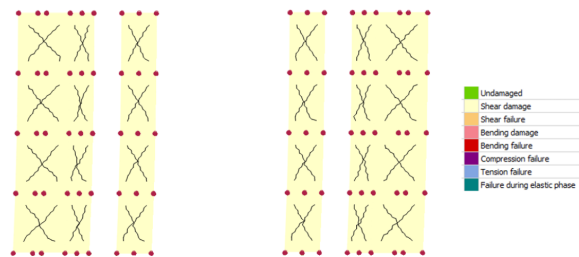


Figure H.14: 3MURI Damage Parameter at Failure - Modal Load Distribution

TRANSVERSE DIRECTION - UNIFORM LOAD DISTRIBUTION

Failure of the structure was reached for the DIANA load case due to the strength degradation limit state criteria of 80 % and in 3MURI due to numerical instability. When looking at the crack widths, it is visible that the crack widths are way more evenly distributed over the walls than in comparison with the longitudinal load cases. This is an indication that a kind of flexural failure is occurring. This is also confirmed by that the highest crack widths are occurring in the left bottom corner of the wall. High crack widths, bed joint failure and head joint failure can also be observed at the connection of the piers and spandrels. The pier in the middle appears to behave more in a shear-like mechanism, as can be seen by the diagonal cracks and diagonal pattern of the head joint status parameter. Hardly any damage is occurring in the most right pier of the wall.

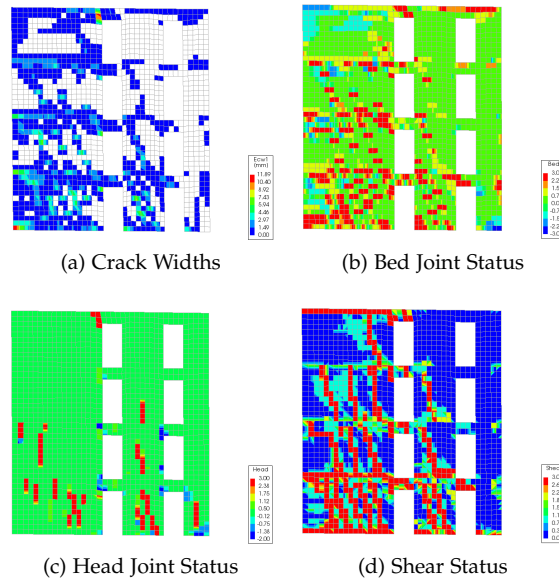


Figure H.15: DIANA Damage Parameters at Failure - Uniform Load Distribution

Two types of failure are occurring according to 3MURI. First, the middle pier is failing due to shear sliding, which was also visible in DIANA. Second, the spandrels are failing due to shear. This is also visible in DIANA, as can be seen by the head joint failure around the connection of the pier and the spandrels. Damage seems not to occur in the most right pier, which was also visible in DIANA.

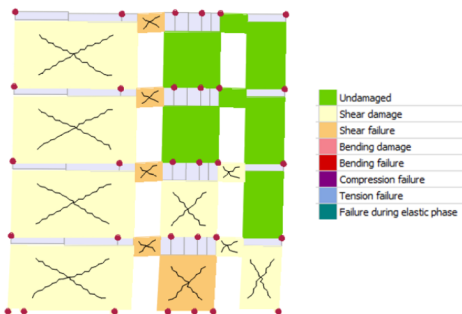


Figure H.16: 3MURI Damage Parameters at Failure - Uniform Load Distribution

TRANSVERSE DIRECTION - MODAL LOAD DISTRIBUTION

The first aspect which is clearly visible are the high crack widths at the connection of the piers and the spandrels. Another interesting aspect at the crack widths which develop at the left bottom of each floor in the most left pier. This indicates a flexural type of failure mechanism. The compressive failure of the head and bed joints in the most right pier is also clearly visible. Diagonal cracks are not visible for this load case. When comparing the results with the results of the uniform load distribution, then can be seen that the damage is divided more equally throughout the structure, while damage is mostly located on the first floor for the uniform load distribution.

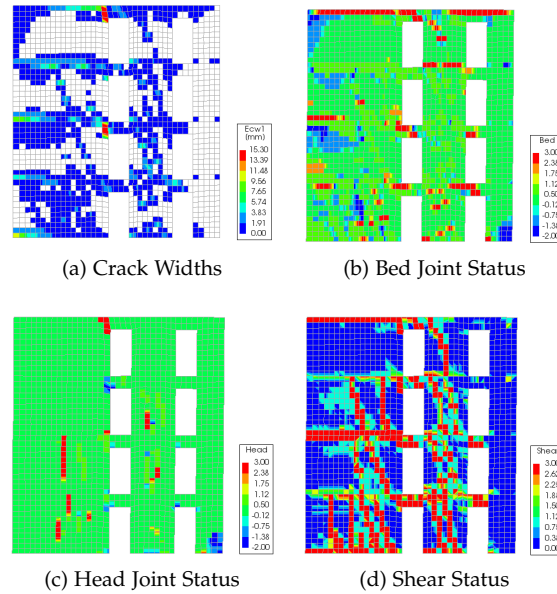


Figure H.17: DIANA Damage Parameters at Failure - Modal Load Distribution

The different failure mechanisms can be seen in the results of the DIANA model. First, flexural failure of the most right pier, which is visible in DIANA by the failure of the head and bed joints in the corner of the element. Second, flexural failure of the most left joint, which could also be observed in the DIANA model. Third, the failure of the spandrels, which is also visible in DIANA, as can be seen by the high crack widths at the connection of the spandrels and the piers.

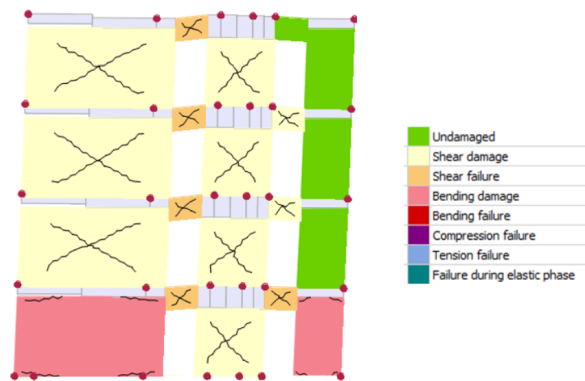


Figure H.18: 3MURI Damage Parameter at Failure - Modal Load Distribution



## RESULTS: NONLINEAR TIME HISTORY ANALYSIS

The results of the nonlinear time history analyses are presented in this chapter. The results of the incremental dynamic approach will be shown first. Furthermore, a description of the force-displacement behaviour according to the seven signals is presented. The displacement profile of the structure is studied next. Ultimately, the damage at the moment of failure is presented.

### 1.1 MAXIMUM ADMISSIBLE SEISMIC LOAD

An incremental dynamic analysis (IDA) is performed. This involves performing multiple NLTH analysis, each for a different seismic intensity. The seismic load has been incrementally scaled until one of the failure criteria according to the NPR 9998 was met. The inter-story drift criterion of 1.5 % in the longitudinal direction was met first for all signals before any other failure criteria were met. The overall behaviour of the structure according to the IDA is presented in Figure I.1. It should be noted that even though for an NLTH analysis a seismic load is applied simultaneously in the transverse and longitudinal direction, only the results in the longitudinal direction are presented hereafter. This decision has been made because the structure is considerably more flexible in the longitudinal direction, compared to the transverse direction. It was found that failure in the longitudinal direction occurs for a particular seismic load, while at that point the structure did not start to deform plastically in the transverse direction.

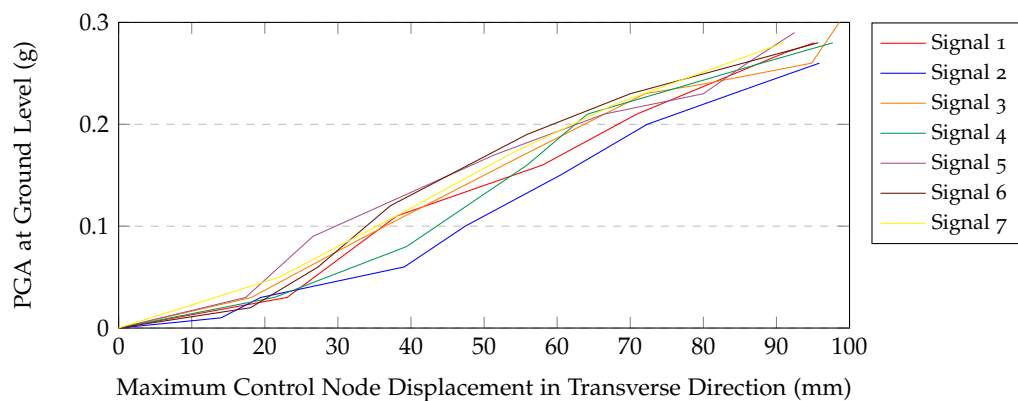


Figure I.1: Incremental Dynamic Analysis Curve

From Figure I.1 can be seen that the highest deformations of the control node occur for signal 2 while comparing the deformations with the deformations that occurred due to the other signals with the same PGA. This is an indication that also the highest inter-story drifts also occur for this signal. The maximum inter-story drift that occurred during each of the signals is presented in Figure I.2 to support the assumption.

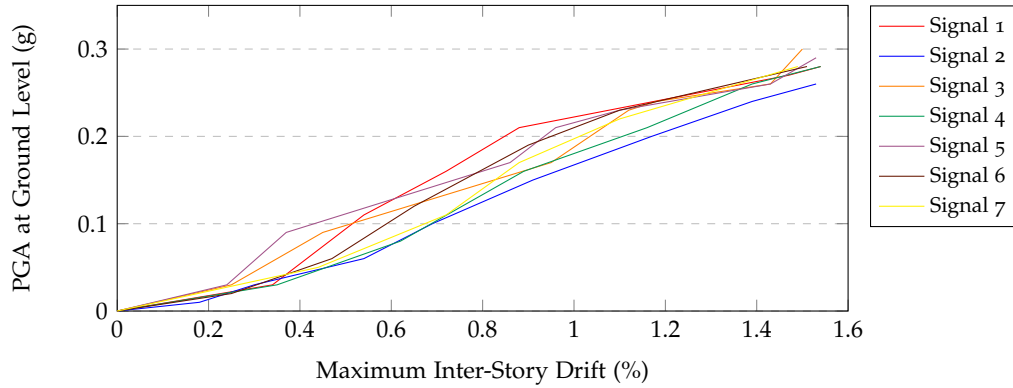


Figure I.2: Maximum Inter-Story Drift during IDA

It should be noted that the PGA at ground level which is shown in Figure I.2 is the design load. It is required to transform this design load to the characteristic load. If a structure has to be checked for a characteristic load  $E_k$ , than a design load  $E_d$  has to be applied. The difference in the characteristic and design load is introduced in the NPR 9998, to take into account if an explicit or indirect check is performed, and to take into account how many signals are applied. The characteristic load can be determined using:

$$E_k = \frac{E_d}{\gamma_n} \quad (\text{I.1})$$

where  $\gamma_n$  is equal to 1.1 because an indirect check is performed and the seven seismic signals are taken into account. The design load is equal to the mean value of the PGA at ground level of the seven signals at the inter-story drift limit. The characteristic load at the limit state criteria is equal to the maximum admissible seismic load according to the NLTH method, which is presented in Table I.1. Both the maximum admissible seismic load is shown if a ductile or a brittle inelastic failure mechanism occurs.

Table I.1: Maximum Admissible Seismic Load according to NLTH Method

	<b>Brittle</b>	<b>Ductile</b>
Max PGA	0.10 g	0.26 g

I.2 FORCE-DISPLACEMENT BEHAVIOUR

It is also of interest to look into the behaviour of the structure, in terms of forces and displacements. This is done by plotting the displacement of the top node versus the base shear which occurs at the same time moment. This is called a hysteresis plot. The hysteresis plots of signal 2 are presented in Figure I.3. The hysteresis plots of six different PGA's are presented.

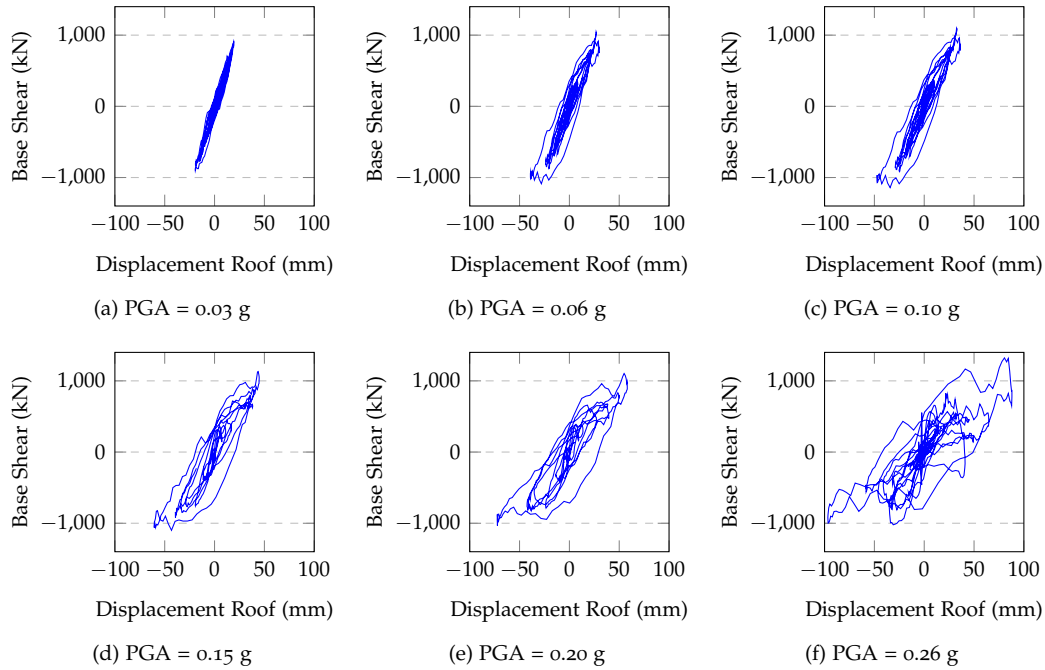


Figure I.3: Hysteresis Plots for Signal 2

The same hysteresis plots as in Figure I.3, have been made for all signals. It is possible to create capacity curves of the signals based on these graphs, by taking the maximum displacement of each hysteresis plot and the corresponding base shear for each of the scaled signals. The capacity curves which are acquired using this method are shown in Figure I.4.

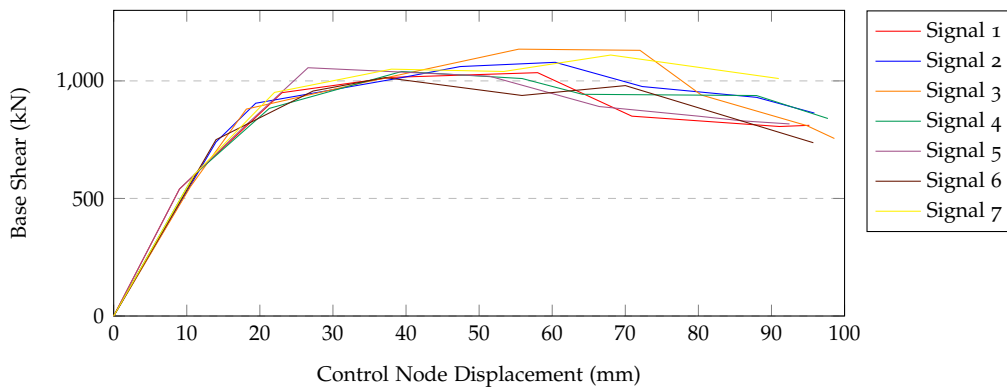


Figure I.4: Capacity Curves according NLTH Analyses

From the capacity curves can be seen that all signals show similar elastic behaviour for a relatively small seismic load. It is also clear that the plastic branch also starts for each signal round the same deformation. Degradation of the structure occurs after this point.

### 1.3 DISPLACEMENT PROFILE

The displacement profile of the structure at the time step at which the inter-story drift limit was exceeded, gives a good indication on which floor the most damage occurs. The displacement profile at this time step is shown in Figure I.5. The displacement profiles of the signals are presented by showing the normalised displacement of each floor. The normalised displacement is determined by dividing the displacement of each floor, by the displacement of the roof.

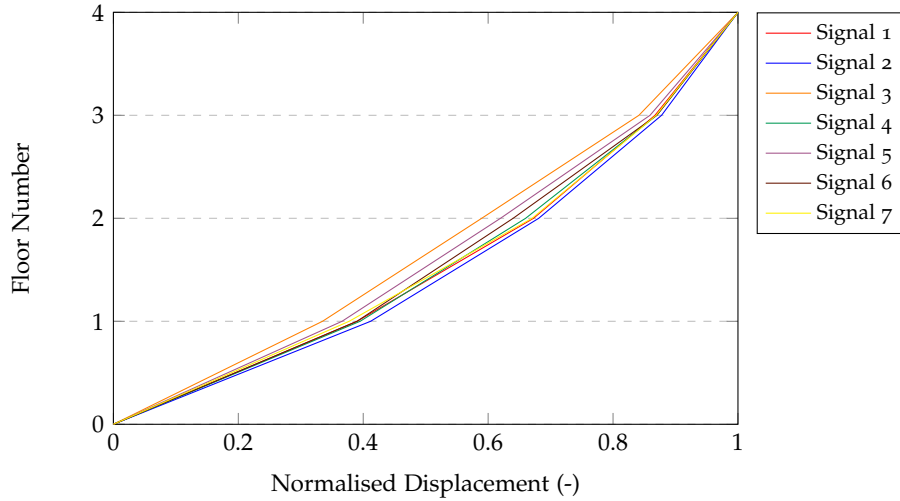


Figure I.5: Displacement Profile at Exceedance of NC Limit State Criteria

It can be seen that the displacement profile at the moment of failure is similar for all NLTH signals. Thus it is likely that a similar damage behaviour in the structure occurs for each of the signals. Another interesting aspect from the normalised displacement of the first floor is the largest for signal 2. This indicates that for this signal, the inter-story drift limits are reached as first. This can also be seen from Figure I.5, in which the inter-story drifts at the time step in which the drift limits are exceeded, of each floor per signal, are presented. This is an indication that for signal 2 the most damage of the first floor occurs, in comparison with the other signals.

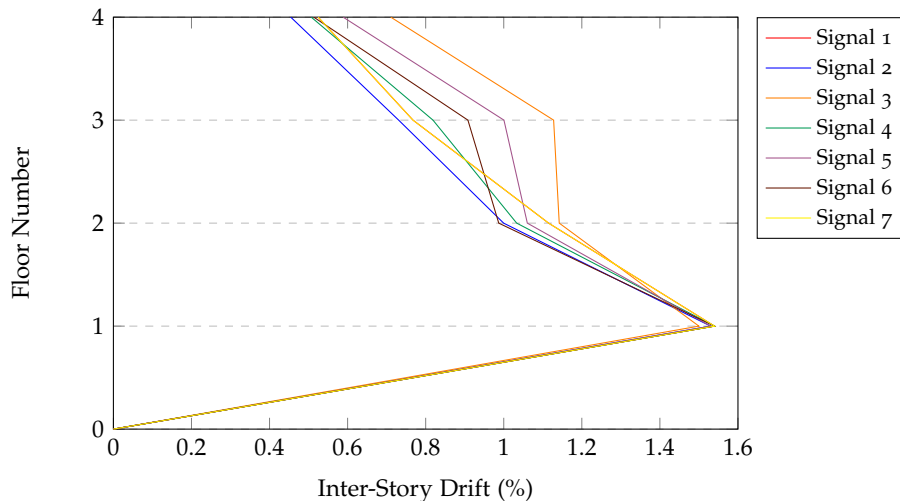


Figure I.6: Inter-Story Drifts at Exceedance of NC Limit State Criteria

I.4 DAMAGE PARAMETERS AT FAILURE

The damage parameters at the moment failure due to the governing NLTH signal, which is signal 2, are presented in this chapter. The output of DIANA which is presented are the crack widths, bed joint state parameter and head joint state parameter. A description of the masonry damage status parameters can be found in Appendix E. The output of all walls has been studied first and afterwards a selection of walls is made in which the most damage occurred at failure. The same wall numbering is used as was done in chapter 5.3. From the results of the analyses can be seen that the most damage is concentrated in walls L1, L2, L3, L4, L5 and L6. Thus only these walls will be shown in the elaboration of the damage at failure hereafter.

The damage parameters of the structure in three different time steps will be presented. The shown time steps are the moments on which the most deformations occur in the structure and the end of the time signal. These studied time steps are shown in Figure I.7.

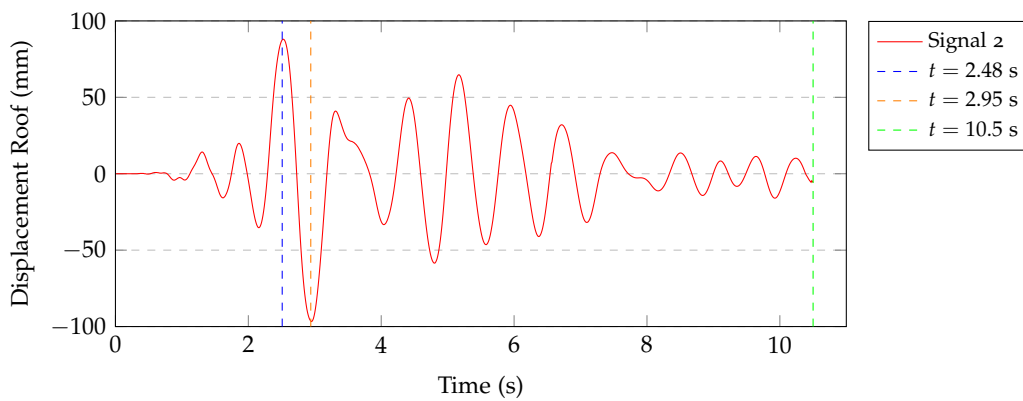


Figure I.7: Roof Displacement for Signal 2 (PGA = 0.26)

The displacement profile at these time moments gives a good indication of in which parts of the structure the most damage occurs. The normalised displacement profiles are presented in Figure I.8. The displacement profile at the end of the time signal is not presented because it not relevant.

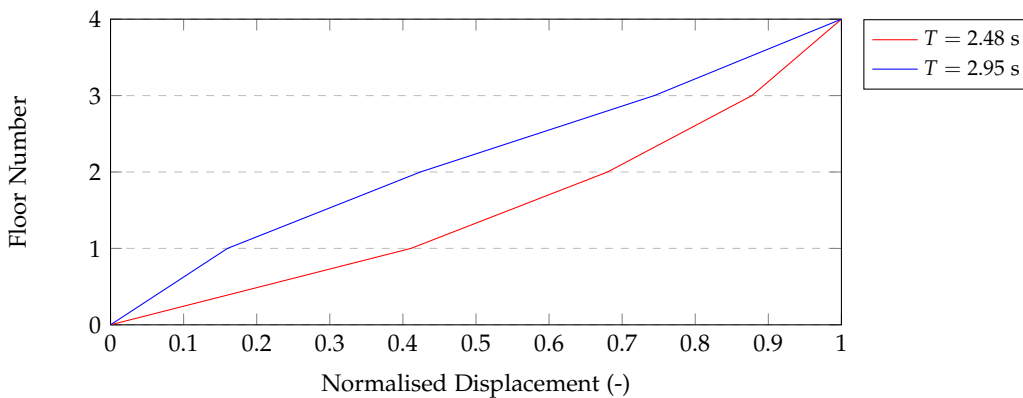


Figure I.8: Normalised Displacement Profile at Studied Time Steps

TIME STEP  $t = 2.48$  s

From the normalised displacement profile in Figure I.8 can clearly be seen that the displacements are localised on the first floor. The exceedance of the 1.5 % inter-story drift limit also occurs at this time step. Thus most damage is to be expected to occur on the first floor. This can clearly be seen when looking at the crack widths, as presented in Figure I.9 because the magnitude of the crack widths of the first floor is significantly higher compared to the other floors. The shape of the crack widths indicates that a type of shear failure occurs. This is supported by the diagonal shapes that can be found when looking at the bed and head joint status parameters. Crushing does not occur because significant crack widths in the bottom corners of the piers do not occur. When looking at the bed joint parameter can be seen that some compressive softening occurs, but the failure does not occur, because the parameter does not reach 3. Based on the fact that no clear crushing behaviour occurs and that clear diagonal cracks are developing, can be concluded that a shear dominated failure mechanism is occurring.

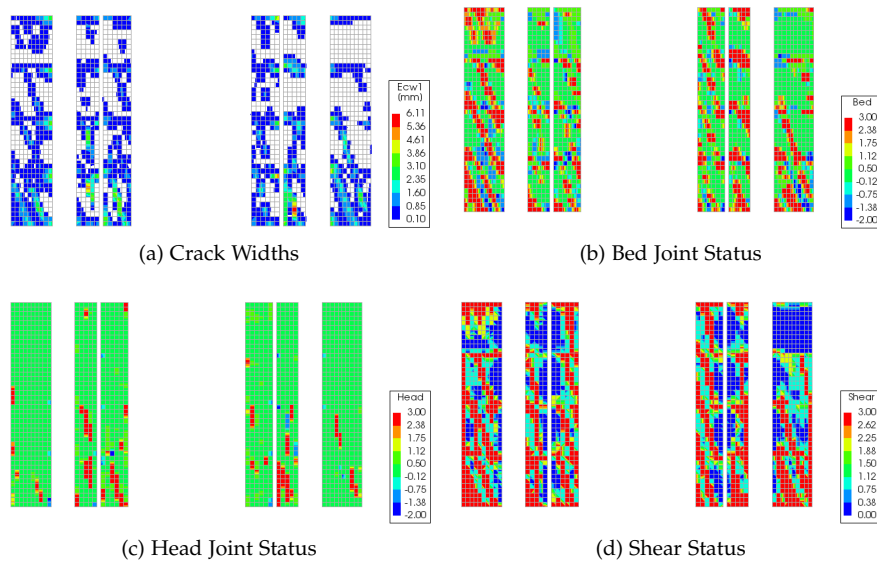


Figure I.9: Damage Parameters at Failure - Signal 2 (PGA = 0.26) -  $t = 2.48$  s

TIME STEP  $t = 2.95$  s

The highest displacement of the roof the structure occurs for time step  $t = 2.95$  s, but the inter-story drifts are lower compared to time step  $t = 2.48$  s. This is possible because the displacements are distributed more equally over all the floors. This can also be seen from the normalised displacement profile as presented in Figure I.8. Since the displacements are distributed more evenly throughout the structure, can also be expected that the damage is distributed more equally. This can be seen when looking at the crack widths throughout the structure. The magnitudes of the crack widths which occur on each floor are comparable. The type of failure behaviour has not changed with respect to time step  $t = 2.48$ , because the same diagonal patterns can be found and the bed and head joint status parameter does not reach 3, which means crushing failure.

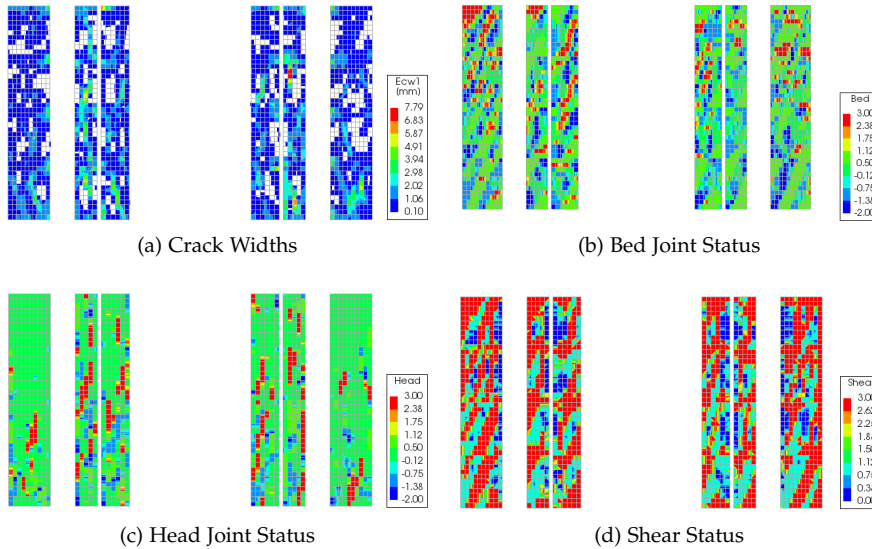


Figure I.10: Damage Parameters at Failure - Signal 2 (PGA = 0.26) -  $t = 2.95$  s

TIME STEP  $t = 10.5$  s

The crack widths at the final time step are presented in Figure I.11. The decision has been made not to present the masonry status parameters because the parameters are linked to the stress-strain curves, and the stresses and strains are almost equal to zero at this time moment because the deformations are almost equal to zero. Thus the masonry status parameters do not provide the reader with any useful information at this time step. From the crack widths can be seen that almost everywhere in the piers some cracking occurs. The significant cracks are still diagonal cracks, which can be found on all floors.

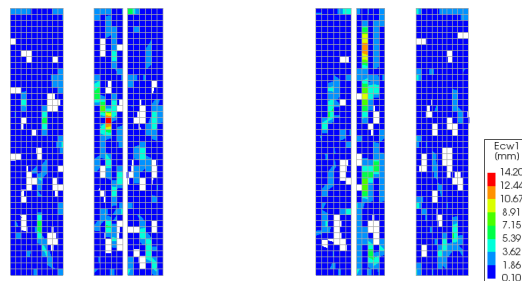


Figure I.11: Crack Widths - Signal 2 (PGA = 0.26) -  $t = 10.50$  s

## BIBLIOGRAPHY

---

- 3MURI (2018). 3MURI Manual Version 11.4.0. Technical report, S.T.A. Data, Torino, Italy.
- Angelillo, M., Lourenço, P. B., and Milani, G. (2014). *Mechanics of Masonry Structures*, volume 551 of *CISM International Centre for Mechanical Sciences*. Springer, Vienna.
- ARUP (2016). Ground Motions NPR December 2015: Spectrally-Matched Ground Motions for Site Response and Finite Element Analysis. Technical report, ARUP, Amsterdam, the Netherlands.
- ARUP and NAM (2018). Groningen Earthquakes Structural Upgrading Data Documentation Exposure Database. Technical report, ARUP and NAM, Amsterdam, the Netherlands.
- Backes, H. (1985). *On the Behavior of Masonry under Tension in the Direction of the Bed Joints*. PhD thesis, Aachen University of Technology.
- Bazzurro, B. (1978). An Ultimate Load Analysis of Laterally Loaded Brickwork Panels. *International journal of masonry construction*, 1(2):57–61.
- Bazzurro, P. (2009). Learning from earthquakes: The Mw 6.3 Abruzzo, Italy, earthquake of April 6, 2009. *EERI Special Earthquake Report*, pages 1–12.
- Borri, F. and Maria, A. D. (2012). Comportamento a Taglio delle Murature Esistenti: Esperienze e Sperimentazioni anche alla Luce del Sisma in Emilia (in Italian). Technical report, University of Perugia.
- Bourne, J. and Oates, S. (2014). An activity Rate Model of Induced Seismicity within the Groningen Field. Technical report, Nederlandse Aardolie Maatschappij B.V.
- Bruneau, M. (1994). State-of-the-Art Report on Seismic Performance of Unreinforced Masonry Buildings. *Journal of Structural Engineering*, 120(1):230–251.
- Calderini, C., Cattari, S., and Lagomarsino, S. (2008). In-plane Strength of Unreinforced Masonry Piers. *Earthquake Engineering and Structural Dynamics*, 38:243–267.
- Chopra, A. (2013). *Dynamics of Structures - Theory and Applications to Earthquake Engineering*. Pearson Education, Delft, the Netherlands, 4 edition.
- DIANA FEA BV (2017). *DIANA user manual*. DIANA FEA BV, Delft, the Netherlands, 10.2 edition.
- Dijkema, J. (2018). Pushover Analysis of Masonry Structures in Groningen - A Comparison with Incremental Dynamic Analysis. Master's thesis, Technical University of Delft.
- Dolce, M. (1991). Schematizzazione e Modellazione degli Edifici in Muratura Soggetti ad Azioni Sismiche (In Italian). *L'Industria delle Costruzioni*, 25(242):45–57.
- Drysdale, R. and Essawy, A. (2003). *Failure line design of unreinforced masonry walls subject to out-of-plane loading*. Centre for Effective Design of Structures, McMaster University.
- Ehiwario, J. and Aghamie, S. (2014). Comparative Study of Bisection, Newton-Raphson and Secant Methods of Root-Finding Problems. *IOSR Journal of Engineering*, 04(04):1–7.
- Fajfar, P. (1999). Capacity Spectrum Method Based on Inelastic Demand Spectra. *Earthquake Engineering and Structural Dynamics*, 28(28):979–993.

- Freeman, S. A. Nicoletti, J. P. and Tyrell, J. V. (1975). Evaluation of Existing Buildings for Seismic Risk - A Case Study of Puget Sound Naval Shipyard. In *Proceedings of the 1st U.S. National Conference on Earthquake Engineering*, Berkley, USA.
- Gavin, H. P. (2016). Numerical intergration in structural dynamics. In *Lecture Notes: CEE 541. Structural Dynamics*, pages 1–17, Duke University, England.
- Goodman, R., Taylor, R., and Brekke, T. (1968). A Model for the Mechanics of Jointed Rock. *Journal of the Soil Mechanics and Foundations*, 93:637–659.
- Guerrini, G., Graziotti, F., Penna, A., and Maganes, G. (2017). Improved Evaluation of Inelastic Displacement Demands for Shortperiod Masonry structures. *Earthquake Engineering and Structural Dynamics*, 46:1411–1430.
- Gupta, B. and Kunnath, S. (2000). Adaptive Spectra-Based Pushover Procedure for Seismic Evaluation of Structures. *Earthquake Spectra*, 16(2):367–391.
- Hoffmann, G. and Schubert, P. (1994). Compressive Strength of Masonry Parallel to the Bed Joints. In *Proceedings of the 10th International Brick and Block Masonry Conference*, pages 1453–1462, Calgary, Canada.
- Ingham, J. and Griffith, M. (2011). Performance of Unreinforced Masonry Structures during the 2010 Darfield (Christchurch, NZ) Earthquake. *Australian Journal of Structural Engineering*, 11(3):207–224.
- Javed, M. (2009). *Seismic Risk Assessment of Unreinforced Brick Masonry Buildings System of Northern Pakistan*. PhD thesis.
- Kiureghian, A. D. (1981). A Response Spectrum Method for Random Vibration Analysis of MDOF Systems. *Earthquake Engineering and Structural Dynamics*, 9:419–435.
- Kumar, A. (2016). Impact on the Seismic Capacity of Unreinforced Masonry Houses by varying the Geometrical Parameters of Terraced House. Master's thesis, Technical University of Delft.
- Lagomarsino, S., Penna, A., Galasco, A., and Cattari, S. (2013). TREMURI program: An Equivalent Frame Model for the Nonlinear Seismic Analysis of Masonry Buildings. *Engineering Structures*, 56:1787–1799.
- Lanting, J. (2016). Groningse Metselwerkgebouwen onder Seismische Belasting (In Dutch). Master's thesis, Eindhoven University of Technology.
- Lawrence, S. and Marshall, R. (2000). Virtual Work Design Method for Masonry Panels under Lateral Load. In *Proceedings 12th International Brick and Block Masonry Conference*, volume 2, pages 1063–1072, Madrid, Spain.
- Lourenço, P. (2017). *PhD Thesis: Computational Strategies for Masonry Structures*. PhD thesis, Technical University of Delft.
- Magenes, G. and Calvi, G. (1992). Cyclic Behaviour of Brick Masonry Walls. In *Proceedings of the 10th World Conference on Earthquake Engineering*, pages 3517–3522, Madrid, Spain.
- Mahmoud, A., Hamid, A., and Maqd, S. E. (1995). Lateral Response of Unreinforced Solid Masonry Shear Walls: an Experimental Study. In *Proceedings of the 7th Canadian Masonry Symposium*, pages 110—125, Hamilton, Canada.
- Mann, W. and Muller, H. (1980). Failure of Shear-Stressed Masonry - an Enlarged Theory, Tests and Application to Shear Walls. In *Proceedings of the International Symposium on Load bearing Brickwork*, pages 1–13, London, England.

- Messali, F. (2015). Hollow Brick Masonry Walls: In-Plane Seismic Response and Strengthening Techniques with Reinforced High-Performance Mortar Coating. *Unpublished Doctoral Dissertation*.
- Michalaki, M. (2015). Seismic Assessment of a Typical Dutch Rijtheshuis. Master's thesis, Technical University of Delft.
- Mosalam, K., Glascoe, L., and Bernier, J. (2009). Mechanical Properties of Unreinforced Brick Masonry, Section 1. Technical report, Lawrence Livermore National Security.
- Muntendam-Bos, A. and de Waal, J. (2013). Reassessment of the Probability of Higher Magnitude Earthquakes in the Groningen Gas Field. Technical report, Staatstoezicht op de Mijnen.
- Newmark, N. and Hall, W. (1973). Earthquake Spectra and Design. *Earthquake Engineering Research Institute*.
- Ngo, D. and Scordelis, A. (1967). Finite Element Analysis of Reinforced Concrete Beams. *Journal of the American Concrete Institute*, 64:152–163.
- Page, A. (1981). The Biaxial Compressive Strength of Brick Masonry. *Proceedings Institution of Civil Engineers*, 71(3):893–906.
- Page, A. (1982). An Experimental Investigation of the Biaxial Strength of Brick Masonry. In *6th International Brick and Block Masonry Conference*, pages 3–15, Rome, Italy.
- Petrovčić, S. and Kilar, V. (2013). Seismic Failure Mode Interaction for the Equivalent Frame Modeling of Unreinforced Masonry Structures. *Engineering Structures*, 54:9–22.
- Rashid, Y. (1968). Analysis of Prestressed Concrete Pressure Vessels. *Nuclear Engineering and Design*, 7:334–344.
- Rosenblueth, E. (1951). *A basis for Aseismic Design of Structures*. University of Illinois, Urbana, Urbana.
- Rosenblueth, E. and Elorduy, J. (1969). Responses of Linear Systems to Certain Transient Disturbances. In *Proceedings of the 4th World Conference on Earthquake Engineering*, pages 185–196, Santiago, Chile.
- Rots, J. and Blaauwendraad, J. (1989). Crack Models for Concrete, Discrete or Smeared? Fixed, Multi-Directional or Rotating? *Heron*, 34:1–59.
- Schreppers, G., Garofano, A., Messali, F., and Rots, J. (2017). DIANA Validation Report for Masonry Modelling. Technical report, DIANA FEA report 2016-DIANA-R1601.
- Scrivener, J. (1993). Masonry structures - Earthquake resistant Design and Construction. In *Proceedings Earthquake Engineering and Disaster Reduction Seminar*, pages 39–44, Melbourne, Australia.
- Shakeri, K., Shayanfar, M., and Mohebbi, M. A. (2008). A Spectra-Based Multi Modal Adaptive Pushover Procedure for Seismic Assessment of Buildings. *The 14th World Conference on Earthquake Engineering October 12-17 2008 Beijing China*.
- Siano, R., Camata, G., Sepe, V., Spacone, E., Roca, P., and Pelà, L. (2017). Finite Elements vs. Equivalent Frame Models for URM walls In-Plane Behaviour. *16th World Conference on Earthquake Engineering 16WCEE 2017*, pages 1–11.
- Tena-Colunga, A. and Abrams, D. (1996). Seismic Behavior of Structures with Flexible Diaphragms. *Journal of Structural Engineering*, 122(4):439–445.

- Timur, T. (2017). Opencourseware, lecture slides, introduction to seismic essentials in groningen: Chapter 3.3 response spectrum. Technical report, Delft University of Technology.
- Tsouvalas, A. (2017a). Seismic analysis of complex structures. Lecture Notes: CIE5260 Structural Response to Earthquakes. Technical University of Delft, the Netherlands.
- Tsouvalas, A. (2017b). Seismic response of simple structures. Lecture Notes: CIE5260 Structural Response to Earthquakes. Technical University of Delft, the Netherlands.
- Turnšek, V. and Čačovič, F. (1970). Some Experimental Results on the Strength of Brick Masonry Walls. In *Proceedings of the 2nd International Brick Masonry Conference*, pages 149–156, Stoke-on-Trent, England.
- Vaculik, J. (2012). *PhD Thesis: Unreinforced Masonry Walls Subjected to Out-of-Plane Seismic Actions*. PhD thesis.
- van der Pluijm, R. (1992). Material Properties of Masonry and its Components under Tension and Shear. In *Proceedings of the 6th Canadian Masonry Symposium*, pages 675–686, Saskatoon, Canada.
- van der Pluijm, R. (1993). Shear Behavior in Bed Joints. In *Proceedings of the 6th North American Masonry Conference*, pages 125–136, Philadelphia, USA.
- VIIA (2017a). NLTH-analyse Geotechniek met DIANA (In Dutch). Technical report, VIIA, Groningen, the Netherlands.
- VIIA (2017b). Uitgangspuntenrapport NLTH-Analyse (In Dutch). Technical report, VIIA, Groningen, the Netherlands.
- VIIA (2018). Failure Mechanism Determination of Masonry Walls. Technical report, VIIA, Groningen, the Netherlands.
- Vrouwenvelder, A. (2016). Lecture Notes: CIE5145 – Random Vibrations. Lecture Notes. Technical University of Delft, the Netherlands.
- Wesche, K. and Ilantzis, A. (1980). General Recommendations for Methods of Testing Load Bearing Walls. *Materials and Structures*, 13(78):433–445.
- Yi, T., Moon, F., and Kahn, L. (2006). Lateral Load Tests on a Two-Story Unreinforced Masonry Building. *Journal of Structural Engineering ASCE*, 132(5):643–652.

